THE DESIGN AND CHARACTERIZATION OF DNA-BASED VIRAL DIAGNOSTICS

By

Jonas W. Perez

Dissertation

Submitted to the Faculty of the

Graduate School of Vanderbilt University

in partial fulfillment of the requirements

for the degree of

DOCTOR OF PHILOSOPHY

in

Chemistry

December, 2010

Nashville, Tennessee

Approved:

Dr. David W. Wright

Dr. Charles M. Lukehart

Dr. Gary A. Sulikowski

Dr. Frederick R. Haselton

To my family, who have always been supportive of all I have done

and

To my amazing wife, my best friend

ACKNOWLEDGEMENTS

I would like to thank the National Institutes of Health and the Vanderbilt University Discovery Grant program for providing the financial resources for this research. Additionally, I would like to thank the Chemistry-Biology Interface training grant for its support. I am grateful to my ARM Committee for the guidance they have provided throughout my years here. I especially want to thank Dr. Haselton and my mentor Dr. David Wright his guidance, assistance, leadership and all of the other things he has provided these last 5 years.

I would like to express my appreciation to the entire Wright group, both past and present for the camaraderie. John, thanks for helping to keep me motivated to get in the gym, some days it helped me keep my sanity. Reese, I'll thank you twice, thank you and thank you, since you came back to Vandy and we had a lot of fun because you did. Dr. Elizabeth Bentzen, thanks for everything, especially the mentoring that first semester. Dr. Melissa Carter, what can I say, even during this time of dissertation writing you have been there to help and proof-read. My brother, who moved to Nashville with me, made my first year wonderful and I am so grateful for our entire relationship. Sarah, welcome to the family! Of course, my parents who have never once doubted what I could accomplish. And most of all, my wife, I cannot thank you enough!

TABLE OF CONTENTS

LIST OF TABLES

LIST OF FIGURES

CHAPTER I

INTRODUCTION

The Discovery of Viruses

Viruses were first discovered in 1898 when Martinus Beijerinck showed that a particular infection of tobacco plants could be transmitted even when using filtered and bacteria-free media.[1, 2] According to the germ theory of disease at that time, all infectious agents could be removed with filtration.[3] Further, all infectious agent could be propagated on an appropriate nutrient medium.[3] Both of these principles were found to be untrue for the infectious agent Beijerinck was working with; which later came to be known as tobacco mosaic virus (TMV).[1, 2] In 1939, Gustav Kausche and Helmut Ruska showed that TMV could be crystallized and analyzed via electron microscopy.[4] Up until this point, viruses had not been imaged because they were too small to see using an optical microscope.

These infectious agents were interesting for a number of reasons. First, their extremely small size, ~300 nm in length and 17 nm in diameter, made it possible for the virus to pass through filters that other infectious agents, such as bacteria, could not.[5] Second, the fact that the virus required a host to propagate precluded it from being cultured strictly on a nutrient medium.[2] Finally, even after crystallization, the agents were still infectious.[6] Although these attributes confounded scientists of the day, modern techniques have allowed for a much greater understanding of the intricacies of viruses.

One common attribute of viruses is their need of a host to proliferate.[7] Viruses need a host to proliferate because they lack their own metabolism and therefore, are not considered living organisms.[8] This concept is further emphasized by the fact that virions can multiply by spontaneously assembling within host cells instead of through cell division.[9] However, it is interesting to note that like living organisms, virus do possess genes and evolve by natural selection.[10]

The Anatomy of a Virion

A virus particle, known as a virion, consists of a minimum of two parts.[7] The first is genetic material, which is composed of DNA or RNA. The genetic material acts as a blueprint to encode information about the proteins associated with the virus. Even at the level of genetic material, a large amount of diversity can be observed. The viral genome can be single-stranded DNA (ssDNA), double-stranded DNA (ds-DNA), or RNA. If the genome is ssDNA or RNA, it can be positive-sense or negative-sense. RNA genome are often further divided in segmented and nonsegmented genomes. The second part of a virion is the protein coat. The protein coat serves as protection for the genetic material. It is the formation of the protective protein coat that dictates the structure of the virus, which can range from simple helical or icosahedral structures to much more complex structures.[11, 12] Often times, in addition to protection of the genetic material, the proteins associated with the virus will serve additional functions. Some proteins can mediate cell fusion or cell attachment; others can serve as a viral polymerase once the virus is inside a host cell.[13] Some viruses are characterized by having a third part, a lipid envelope which

surrounds the protein coat.[7] The lipid coat is obtained from one of host cell's membranes and is typically interlaced with viral proteins. All of these factors contribute to the diverse morphologies observed in viruses (**Figure 1**).

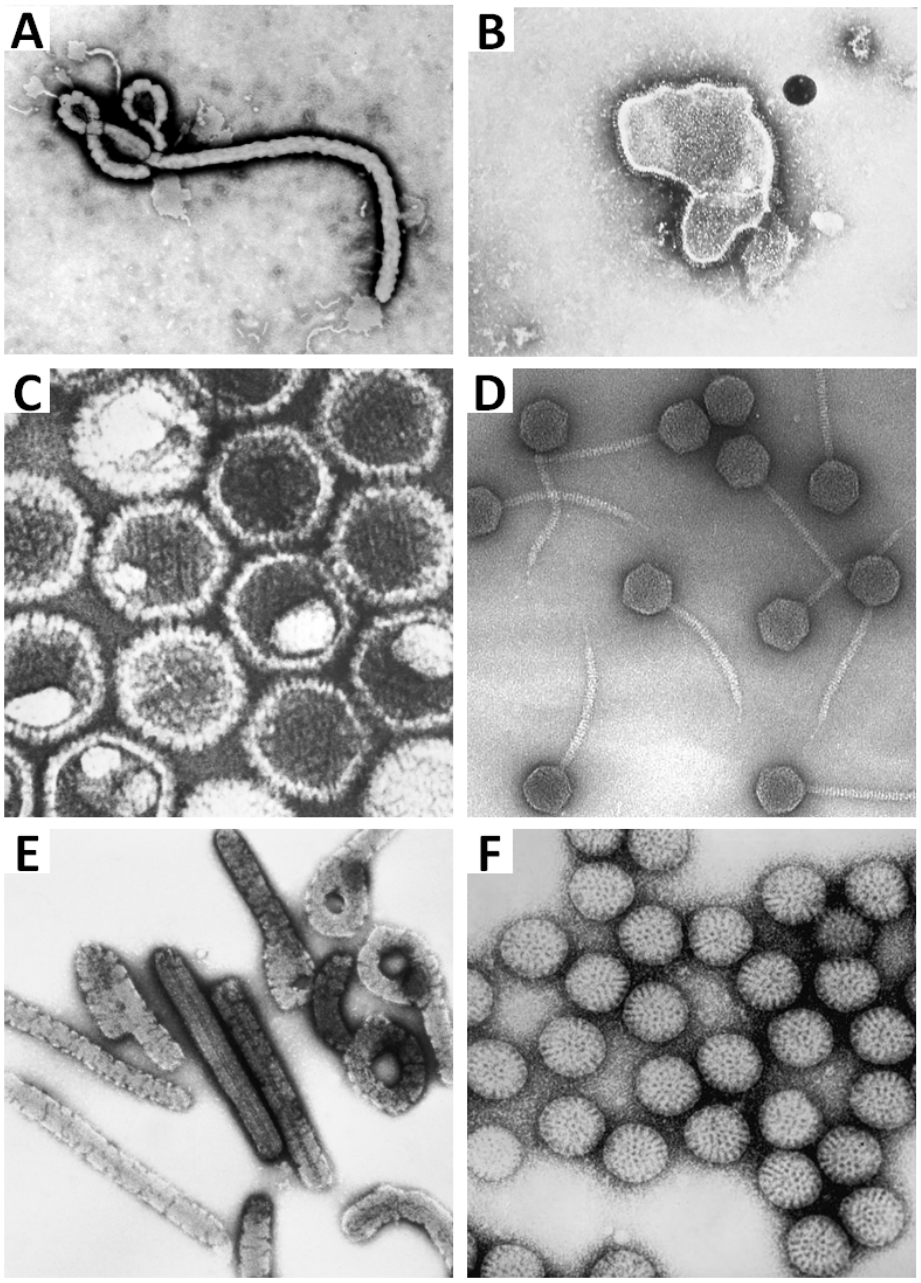

Figure 1. Electron micrographs of different viruses to illustrate the diverse morphologies of viruses. A) Ebolavirus. B) Respiratory Syncytial Virus. C) Herpes Simplex Virus. D) Bacteriophage T7. E) Marburg Virus. F) Rotavirus. Images are public domain and courtesy of the Public Health Image Library.

Respiratory Syncytial Virus

Currently, there are over 2000 recognized species of viruses.[14] One common virus in infants, respiratory syncytial virus (RSV), infects nearly all children by the age of three.[15] RSV was first isolated in 1956 from a chimpanzee presenting a common cold-like illness.[16] Soon after, the virus was found in infants with respiratory illness, and now it is recognized as the leading cause of lower respiratory tract infections in infants and young children.[17, 18]

RSV is classified in the family *Paramyxoviridae*, order *Mononegavirales*.[13] It is an enveloped virus with a nonsegmented negative-strand RNA genome. The 15.2 kilobase genome of RSV encodes 11 identified proteins.[13] Three of the genes encode transmembrane surface glycoproteins, the fusion protein (F), attachment protein (G) and small hydrophobic protein (SH), which coat the lipid envelop of the virus (**Figure 2**).[13] The F protein facilitates viral entry into a potential host cell through fusion of the viral envelop with the plasma membrane of the host cell.[19, 20] The G protein serves as the major attachment protein, and although it is not required for virulence, it does increase infectivity.[21, 22] The direct role of the SH protein in RSV infection is still unclear.[13] Four of the other genes encode the five proteins that make up the nucleocapsid/polymerase complex. The nucleocapsid/polymerase complex is composed of the nucleoprotein (N), large polymerase subunit (L), phosphoprotein (P), M2-1 and M2-2 cofactors.[13, 23] The N protein encapsidates genomic RNA to form an RNase-resistant nucleocapsid.[13] The L protein serves as the RNA polymerase for replication and transcription.[24, 25] The P protein serves as a chaperone for soluble N protein as well as positions the L protein on

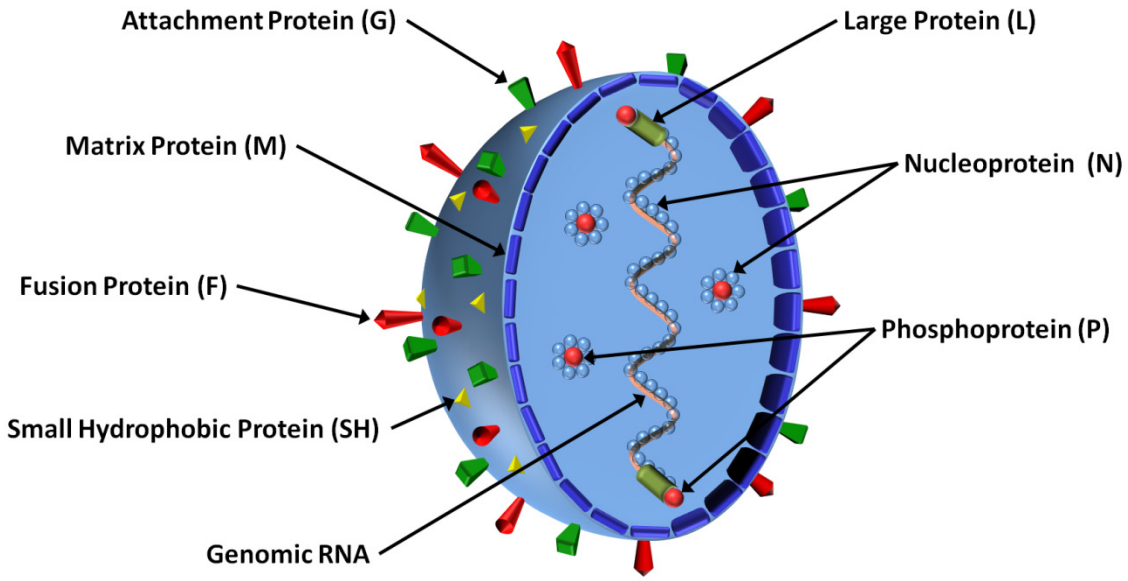

Figure 2. Viral structure of respiratory syncytial virus. The structure shows 1) the location of the transmembrane surface glycoproteins (F, G and SH) interlaced in the lipid bilayer envelope of the virion, 2) the location of the matrix protein (M) associated with the interior of the lipid bilayer, 3) the phosphoprotein (P) associated with soluble N protein and positioning the L protein on the viral RNA, 4) the large protein (L) complexed with both P protein and viral RNA, and 5) the nucleoprotein (N) bound to viral RNA forming an RNase-resistant nucleocapsid.

the RNA template.[13, 24] M2-1 serves as a transcription antitermination factor while M2-2 acts to regulate RNA synthesis.[24, 26-28] A ninth encoded protein, the matrix protein (M), mediates the association of the viral nucleocapsid with the lipid envelop.[13] The remaining two proteins, nonstructural proteins one and two (NS1 and NS2), are not believed to have a significant role in virus assembly and their specific roles are still undefined.[13] All of these features of the virus can serve as potential biomarkers of an infection.

Detecting a Viral Infection: Conventional Diagnostics

Currently, there is no approved vaccine for RSV, and treatment options are limited.[29-31] However, progress in antiviral therapeutics could offer a promising treatment option if the virus can first be accurately diagnosed. In addition to effective treatment, diagnosis is important for patient placement to limit nosocomial transmission.[32] Traditionally, viral infections have been detected using a number of means including cell culture, serology, antigen detection and nucleic acid detection.[33]

Cell culture techniques of virus detection date back to 1948 when the first description of viral isolation in cell culture was described by Thomas Weller and John Enders.[34] This technique involves the growth of a virus in cell cultures and the detection of the virus through morphologic changes in cells as a result of the infection, also known as the cytopathic effect (CPE) of the virus (**Figure 3**).[35] One distinct advantage of viral

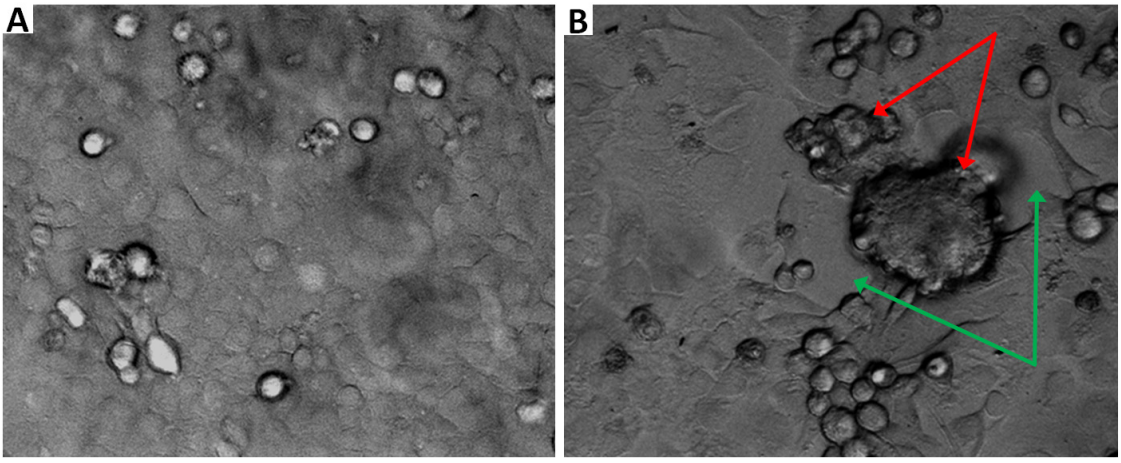

Figure 3. Cytopathic effects of RSV on HEp-2 cells. A) A confluent monolayer of uninfected HEp-2 cells. B) HEp-2 cells 60 hours post infection. Post RSV infection, large multinucleated cell-like structures (red arrows) termed syncytia are present as a result cell to cell fusion by F protein expressed on the surface of infected cells. Also, post infection holes in the monolayer (green arrows) are present as a result of cell death.

culture over other diagnostics is that the technique provides a viable isolate that can be used for further characterization. However, the utilization of viral culture techniques as diagnostics is diminishing as it comes with a number of drawbacks. First, no one cell type can support the growth of all viruses, so multiple cells lines must be kept on hand and unknown viruses must be tested in a variety of cell lines.[33] Second, detection via CPE can be slow and can take upwards of 3 weeks for some viruses to induce morphologic changes in the cells and requires expertise to evaluate.[33] Finally, viral culture places increased weight on specimen handling and transport as the specimen must contain viable virus in order for the technique to work.[33]

The drawbacks of viral culture have led to its gradual replacement by antigen detection techniques. Antigen detection utilizes specific antibodies to detect viral specific proteins to identify the presence of an infection.[36] These methods are particularly useful for viruses that are difficult to culture or grow slowly in culture.[37, 38] In addition to the increased flexibility in pre-assay handling because the virus does not need to be viable, direct antigen methods are typically much faster than viral culture techniques. Furthermore, the number of antigens per virion provides multiple targets per virion and gives an increase in the initial target concentration when compared to viral culture. The most common antigen detection techniques are fluorescent antibody (FA) staining and enzyme immunoassays (EIA).

Fluorescent antibody staining was first described by Liu in 1956 for the detection of influenza.[39] However, it wasn't until specific monoclonal antibodies became commercially available that the technique became widely used in clinical labs.[34] FA staining involves the mounting of specimen cells to a glass slide. The cells are then fixed

and blocked. Finally, the cells are labeled with virus specific antibodies conjugated to a fluorophore.[36] The slide is then viewed under a fluorescence microscope and the presence of fluorescent staining indicates the presence of an infection. FA staining allows multiplexed detection using different specific antibodies labeled with different fluorophores and the appropriate excitation/emission filters.

Enzyme immunoassays were developed as a derivative of radioimmunoassays (RIA). First published by Rosalyn Yalow and Solomon Berson in 1960, RIAs required the use of radioactively-labeled antibodies to detect antigen.[40] Later, EIA was developed to address the safety concerns of working with radioactive compounds by utilizing enzymes and a colorimetric change instead. In 1971, two groups: 1. Peter Perlmann and Eva Engvall, and 2. Anton Schuurs and Bauke van Weemen independently developed methods on EIA, or as Perlmann and Engvall termed them, enzyme-linked immunosorbent assays (ELISA).[41, 42]

A "sandwich" ELISA is the typical EIA used to detect the presence of virus in infected cells (**Figure 4**). In a sandwich ELISA, a protein binding substrate is coated with antibodies specific to the virus of interest. The substrate is then blocked to displace non-specific interactions and then incubated with the specimen. The capture antibodies will bind to antigen in the sample and prevent the antigen from being washed away on subsequent washing steps. Finally, the captured virus is incubated with a second antibody that is conjugated to an enzyme; often times horseradish peroxidase (HRP) is used as the enzyme.[43] If virus is present in the sample, the second antibody will form a "sandwich" complex with the antigen and the capture antibody. However, if virus is not present in the sample, the second antibody, along with the coupled enzyme, will be

washed away. Upon addition of a colorimetric substrate, a color change will be observed if the second antibody is still present.

Using an ELISA to detect viruses has a number of strengths. First, the colorimetric signal can be detected using a spectrophotometer, making its interpretation more objective than monitoring CPE. Second, the use of protein binding microtiter plates allows for automation and parallel analysis of many samples at once. Finally, analysis is quick and can be accomplished in a matter of hours instead of days like viral culture. However, ELISA, like many traditional direct antigen detection methods, suffers from a lack of sensitivity resulting in a high false negative rate.

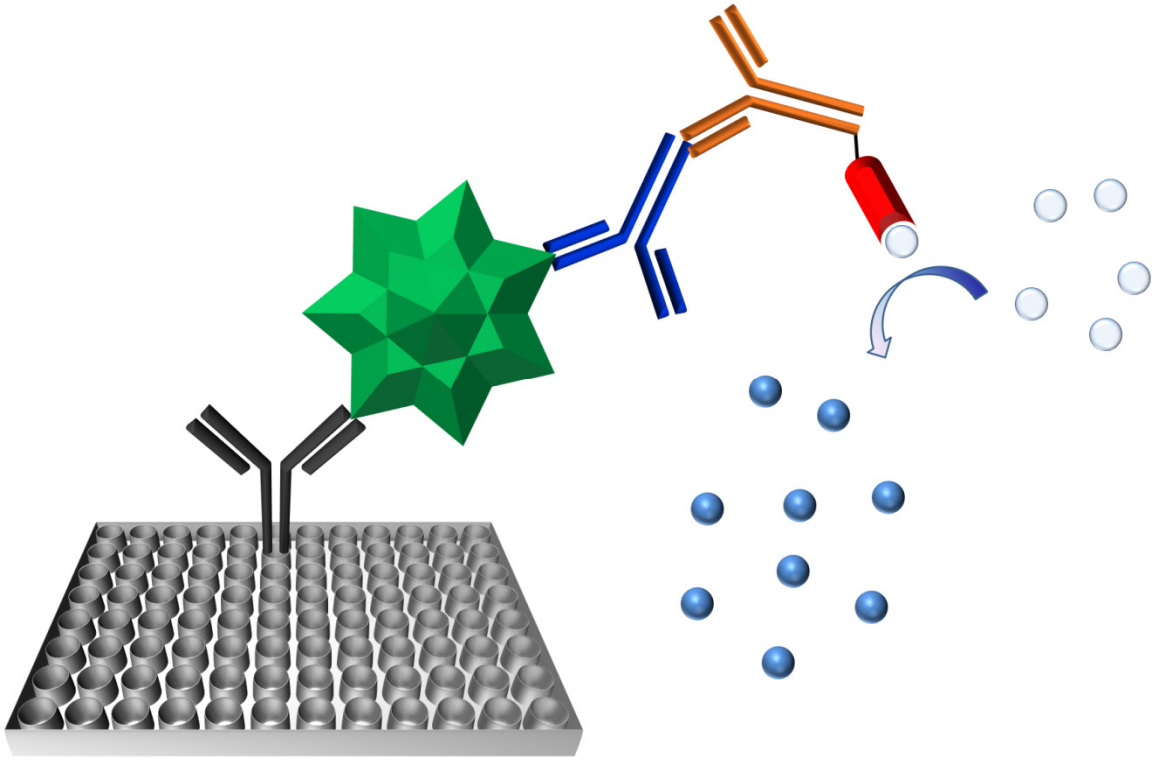

Figure 4. Detecting viruses with a sandwich ELISA. In a sandwich ELISA, capture antibodies (black) are first bound to a microtiter plates. The sample of interest is then incubated in the microtiter plate to allow capture of any antigen (green). Following washing and blocking, primary antibody (blue) is added to form a "sandwich" complex with antigen and capture antibodies. An enzyme linked, secondary antibody (orange) is then added to label any formed sandwich complexes. A colorimetric substrate (white) is then added to detect the presence of the enzyme (light blue), and in turn antigen.

A more recent viral diagnostic is the use of nucleic acid detection. The development of the polymerase chain reaction (PCR) in 1983 by Kary Mullis, allowed nucleic acid sequences to be amplified, increasing the number of copies several orders of magnitude.[44] The technique was extended to the detection of diseases by Randall Saiki in 1985.[45] Nucleic acid diagnostics were expanded with the development of reverse transcriptase PCR (RT-PCR), which allowed any virus to be detected using nucleic acid detection.[33] RT-PCR allows for the detection of RNA viruses by first reverse transcribing their genomes or mRNA into cDNA which is subsequently amplified and detected. The use of real-time thermocyclers has further solidified the use of nucleic acid detection as a clinical diagnostic tool. Currently, PCR-based diagnostics remain the gold standard for sensitive detection of virus. The amplification power of PCR allows for a much lower limit of detection than traditional direct antigen diagnostics. However, nucleic acid diagnostics are not without their drawbacks. Because of the inherent amplification potential of these diagnostics, even small amounts of cross-contamination can result in false positives. Additionally, lysis of the cell to release viral genetic material also releases DNases and RNases which can degrade the viral DNA or RNA that is being detected. This places increased attention on pre-assay handling and storage as compared to direct antigen diagnostics.

Serology has also been utilized to diagnose a viral infection. Serological methods detect specific antiviral antibodies in order to detect the presence of an infection.[46] These methods provide a different level of information than the previously discussed methods. An immunological response is what is actually being detected, and although it is informative to know if an immunological response is present, it does not tell the whole

story of the infection.[47] Often times, the immunological response lags behind the initial infection so that there is an inherent window when a serological method would give a false-negative because the immunological response has not begun. Additionally, serological results can be confusing when dealing with chronic infections, such as RSV, where residual antibodies tend to linger after the infection has passed.

Detecting a Viral Infection: Modern Diagnostics

Although techniques for detecting viral infections have greatly improved over the last 60 years, there are still a number of shortcomings with conventional diagnostics. No single technique can meet all the criteria of being rapid, sensitive, specific and simple. In the interest of continuing to improve diagnostics, a number of modern techniques have been developed which offer a novel approach to detection.[48] These new techniques range from the use of atomic force microscopes (AFM) to the use of magnetic nanoparticle and fluorescent semiconductor quantum dots.

AFM has not only been used to visualize viruses, but more recently it has been used to detect them (**Figure 5**).[49-51] AFM measures the deflections from a cantilever tip that scans a given surface.[52] As the height of the surface changes, the amplitude of the oscillations of the tip also changes. These changes are then detected by a laser that is deflected off of the tip to a photodiode detector. In these experiments, an array of antibodies specific to different viruses was printed onto a protein binding substrate. The printing process provided spatial control of where each type of antibody was placed. The substrate could then be incubated with cell lysate. In the presence of an infection, antigen

would be captured by the specific antibody along the array. As the AFM tip taps along the surface, binding of antigen can be detected by an increase in the height of the surface. This technique provided a number of benefits as a viral diagnostic. Using the AFM tip itself as a detector made the assay completely label-free. The use of an array of antibodies allowed for the detection of multiple viruses at once. Additionally, the change in height provides a definitive diagnosis. It was also shown that the sample matrix showed very little interference with the final result. However, the limit of detection of

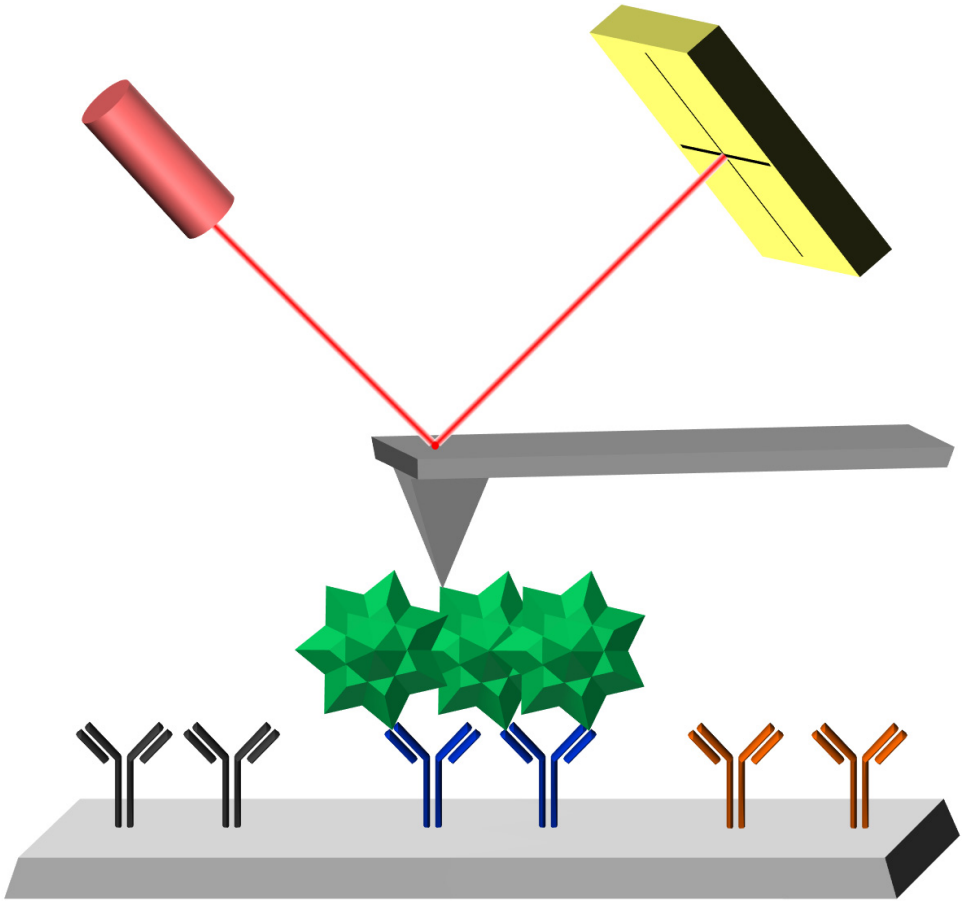

Figure 5. Immunocapture AFM. The "ViriChip," which contained an array of different specific antibodies, is incubated with the sample of interest. In the presence of virus, antibodies specific to that virus will bind antigen. The array is then analyzed via AFM. As the cantilever (dark gray), taps along the surface of the array, a photodiode detector (yellow) records the oscillations of a laser (red) that is being deflected by the cantilever. Binding of antigen causes a change in the amplitude of the cantilevers oscillation which is then detected by the photodiode detector as a change in the oscillation of the laser.

AFM diagnostic was quite high (10^6 – 10^7 $TCID_{50}$/mL), making it no more sensitive than conventional direct antigen diagnostics.[48] Without an increase in sensitivity, the need for specialized equipment and trained personnel outweighs the benefits of the AFM diagnostic.

Another modern diagnostic that has been recently reported is the use of functionalized magnetic nanoparticles to detect viruses (**Figure 6**). Magnetic nanoparticles can enhance the T_2 relaxation times of surrounding water molecules by de-phasing the spin of the protons in water molecules.[53] Magnetic resonance imaging (MRI) can detect these changes in relaxation times. By attaching virus specific antibodies to the magnetic nanoparticles, it is possible to form assemblies of nanoparticle-virus complexes.[54] These assembles can then be detected to indicate the presence of a virus. It

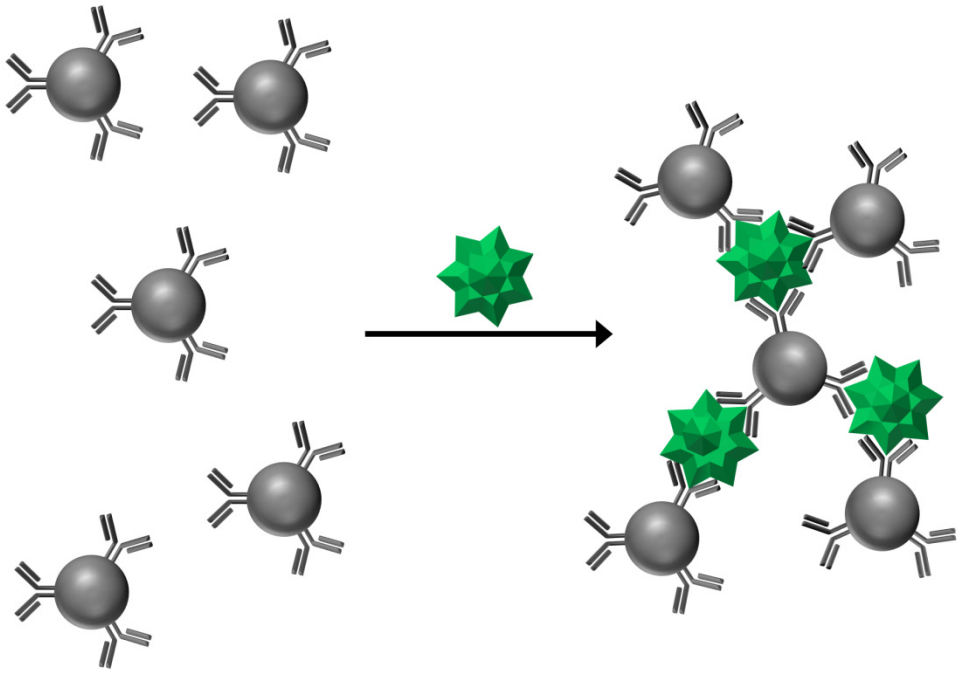

Figure 6. Viral-induced assemblies of antibody functionalized magnetic nanoparticles. In the presence of virus, antibody functionalized magnetic nanoparticles bind antigen and form larger nanoparticle-virus complexes. The formation of these complexes can then be detected via MRI.

has been shown that by using a MRI, it is possible to detect as few as five virus particles per 10 μL.[48] In the presence of virus, an initial bimodal population distribution exists, corresponding to the magnetic nanoparticles (46 nm) and the virus (100 nm). After 30 minutes, however, the population representing the virus disappears and is replaced by a larger population (494 nm) representing the nanoparticle-virus complex.[48] The use of magnetic nanoparticles provides both sensitive and rapid detection of virus. Unfortunately, these attributes are offset by the need for expensive equipment like a MRI and the difficulty of multiplexed detection.

Recently, fluorescent semiconductor nanocrystals (QD) have been used to improve traditional FA staining (**Figure 7**).[55] QDs offer a number of advantages over

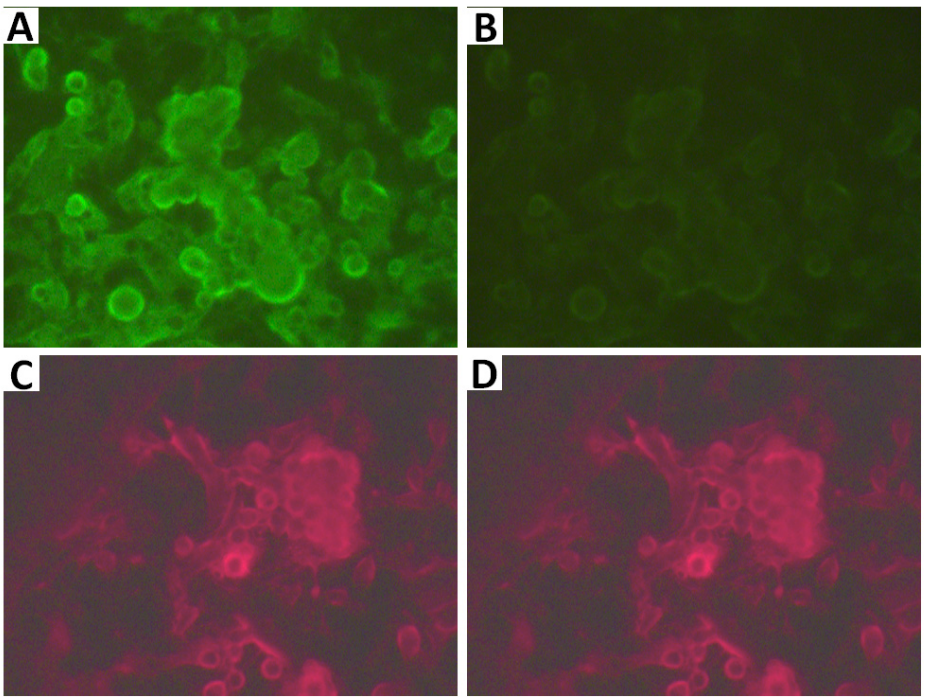

Figure 7. Improved photostability of QDot FA staining. RSV F protein labeled with A) Fluorescein conjugated secondary antibody and C) biotin conjugated secondary followed by streptavidin 605 Qdots. After 1 minute of continuous illumination, B) Fluorescein labeled sample show extensive photobleaching, while D) QDot labeled samples show no change in intensity.

standard organic fluorophores: 1. QDs are extremely bright, offering increased sensitivity, 2. QDs have better photostability than organic fluorophores, and 3. QDs have a broad absorption and narrow emission spectra to allow for multiplexed detection. The use of QDs improved the limit of detection of FA staining and allowed for the detection of as few as 35 PFU/well only 24 hours after infection when using a plate reader to detect fluorescence.[48] Using an epifluorescence microscope, these same samples could be detected as early as one hour post infection.[48] It is clear that simply changing FA staining protocols to utilize QDs instead of organic fluorophores improved FA detection with little to no additional cost.

Conclusions

Although viral diagnostics continue to improve, it is clear that an ideal diagnostic does not yet exist. As new technologies become available, they need to be integrated into diagnostics to continue to improve upon existing diagnostics while completely new approaches should be explored also. Improved diagnostics will not only help physicians in their course of treatment, but also help encourage the development of new antivirals. If it is possible to accurately and quickly diagnose a virus, the motivation to develop new therapeutics for that virus will increase.

Bibliography

1. Dimmock, N. J., Easton, A. J. and Leppard, K., *Introduction to Modern Virology*, 6th edn., Blackwell Publishing, Malden, 2007.

2. Beijerinck, M. W., "Ueber ein contagium vivum fluidum als Ursache der Fleckenkrankheit der Tabaksblatter", *Verhandelingen der Koninklyke academie van Wettenschappen te Amsterdam*, 1898, **65**, 33-52. Translated into English as *Phytopathological Classics No.* 37. American Phytopathological Society Press, St. Paul, 1942.

3. Ewald, P. W., *Evolution of Infectious Disease*, Oxford University Press, New York, 1994.

4. Kausche, G. A., Pfankuch, E. and Ruska, H., "Die Sichtbarmachung von pflanzlichem Virus im Übermikroskop", *Naturwissenschaften*, 1939, **27**, 292-299.

5. Hidaka, Z. and Murano, H., "Determination of Size of the Small Particle compared with the Width of the Tobacco Mosaic Virus (TMV) in Electron Microscopy", *J. Electron Microsc.*, 1957, **5**, 33-38.

6. Zaitlin, M., in *Discoveries in Plant Biology*, eds. S. D. Kung and S. F. Yang, World Publishing, Hong Kong, 1998, pp. 105-110.

7. Collier, L., Balows, A. and Sussman, M., in *Topley and Wilson's Microbiology and Microbial Infections*, eds. B. Mahy and L. Collier, Hodder Arnold Publishing, London, 9th edn., 1998, vol. 1.

8. Rybicki, E. P., "The classification of organisms at the edge of life, or problems with virus systematics", *S. Afr. J. Sci.*, 1990, **86**, 182-186.

9. Roberts, B. E., Paterson, B. M. and Sperling, R., "The cell-free synthesis and assembly of viral specific polypeptides into TMV particles", *Virology*, 1974, **59**, 307-313.

10. Holmes, E. C., "Viral Evolution in the Genomic Age", *Pub. Lib. Sci. Biol.*, 2007, **5**, e278.

11. Caspar, D. L. and Klug, A., "Physical principles in the construction of regular viruses", *Cold Spring Harb. Symp. Quant. Biol.*, 1962, **27**, 1-24.

12. Crick, F. H. and Watson, J. D., "Structure of small viruses", *Nature*, 1956, **177**, 473-475.

13. Collins, P. L., Chanock, R. M. and Murphy, B. R., in *Fields Virology*, ed. D. M. Knipe, Lippincott Williams & Wilkins, Philadelphia, 4th edn., 2001, vol. 1, pp. 1443-1486.

14. Fauquet, C. M. and Fargette, D., "International Committee on Taxonomy of Viruses and the 3,142 unassigned species", *Virol. J.*, 2005, **2**, 1-10.

15. Glezen, W. P., Taber, L. H., Frank, A. L. and Kasel, J. A., "Risk of primary infection and reinfection with respiratory syncytial virus", *Am. J. Dis. Child.*, 1986, **140**, 543-546.

16. Morris, J. A., Blount, R. E. and Savage, R. E., "Recovery of cytopathic agent from chimpanzees with coryza", *Proc. Soc. Exp. Biol. Med.*, 1956, **92**, 544-550.

17. Chanock, R. M., Roizman, B. and Myers, R., "Recovery from infants with respiratory illness of a virus related to chimpanzee coryza agent (CCA). Isolation, properties and characterization", *Am. J. Hyg.*, 1957, **66**, 281-290.

18. Davidson, T., in *Gale Encyclopedia of Medicine*, eds. D. Olendorf, C. Jeryan, K. Boydon and M. K. Fyke, Gale Group, Detriot, MI, 1999, vol. 4, pp. 2478-2480.

19. Zhao, X., Singh, M., Malashkevich, V. N. and Kim, P. S., "Structural characterization of the human respiratory syncytial virus fusion protein core", *Proc. Natl. Acad. Sci. USA*, 2000, **97**, 14172-14177.

20. Walsh, E. E. and Hruska, J., "Monoclonal antibodies to respiratory syncytial virus proteins: Identification of the fusion protein", *J. Virol.*, 1983, **47**, 171-177.

21. Karron, R. A., Buonagurio, D. A., Georgiu, A. F., Whitehead, S. S., Adamus, J. E., Clements-Mann, M. L., Harris, D. O., Randolph, V. B., Udem, S. A., Murphy, B. R. and Sidhu, M. S., "Respiratory syncytial virus (RSV) SH and G proteins are not essential for viral replication in vitro: Clinical evaluation and molecular characterization of a cold-passaged, attenuated RSV subgroup B mutant", *Proc. Natl. Acad. Sci. USA*, 1997, **94**, 13961-13966.

22. Levine, S., Klaiber-Franco, R. and Paradiso, P. R., "Demonstration that glycoprotein G is the attachment protein of respiratory syncytial virus", *J. Gen. Virol.*, 1987, 2521-2524.

23. Tran, T. L., Castagne, N., Bhella, D., Varela, P. F., Bernard, J., Chilmonczyk, S., Berkenkamp, S., Benhamo, V., Grznarova, K., Grosclaude, J., Nespoulos, C., Rey, F. A. and Eleouet, J. F., "The nine C-terminal amino acids of the respiratory syncytial virus protein P are necessary and sufficient for binding to ribonucleoprotein complexes in which six ribonucleotides are contacted per N protein protomer", *J. Gen. Virol.*, 2007, **88**, 196-206.

24. Cowton, V. M., McGivern, D. R. and Fearns, R., "Unravelling the complexities of respiratory syncytial virus RNA synthesis", *J. Gen. Virol.*, 2006, **87**, 1805-1821.

25. Grosfeld, H., Hill, M. G. and Collins, P. L., "RNA replication by respiratory syncytial virus (RSV) is directed by the N, P, and L proteins; transcription also occurs under these conditions but requires RSV superinfection for efficient synthesis of full-length mRNA", *J. Virol.*, 1995, **69**, 5677-5686.

26. Fearns, R. and Collins, P. L., "Role of the M2-1 transcription antitermination protein of respiratory syncytial virus in sequential transcription", *J. Virol.*, 1999, **73**, 5852-5864.

27. Hardy, R. W., Harmon, S. B. and Wertz, G. W., "Diverse gene junctions of respiratory syncytial virus modulate the efficiency of transcription termination and respond differently to M2-mediated antitermination", *J. Virol.*, 1999, **73**, 170-176.

28. Hardy, R. W. and Wertz, G. W., "The product of the respiratory syncytial virus M2 gene ORF1 enhances readthrough of intergenic junctions during viral transcription", *J. Virol.*, 1998, **72**, 520-526.

29. Kaur, J., Tang, R. S., Spaete, R. R. and Schickli, J. H., "Optimization of plasmid-only rescue of highly attenuated and temperature-sensitive respiratory syncytial virus (RSV) vaccine candidates for human trials", *J. Virol. Methods*, 2008, **153**, 196-202.

30. Hall, C. B., "Respiratory Syncytial Virus and Parainfluenza Virus", *New Engl. J. Med.*, 2001, **344**, 1917-1928.

31. "Prevention of Respiratory Syncytial Virus Infections: Indications for the Use of Palivizumab and Update on the Use of RSV-IGIV", *Pediatrics*, 1998, **102**, 1211-1216.

32. Keith, K., Rita, L., Robert, S. H., Evans, W., Stanley, B. and Bruce, H., "Screening for respiratory syncytial virus and assignment to a cohort at admission to reduce nosocomial transmission", *J. Pediatr.*, 1990, **116**, 894-898.

33. Storch, G. A., "Diagnostic Virology", *Clin. Infect. Dis.*, 2000, **31**, 739-751.

34. Weller, T. H. and Enders, J. F., "Production of hemagglutinin by mumps and influenza A viruses in suspended cull tissue cultures", *Proc. Soc. Exp. Biol. Med.*, 1948, **69**, 124-128.

35. Leland, D. S., in *Laboratory diagnosis of viral infections*, eds. E. H. Lennette and T. F. Smith, Marcel Dekker, New York, 3rd edn., 1999.

36. Forghani, B., in *Laboratory diagnosis of viral infections*, eds. E. H. Lennette and T. F. Smith, Marcel Dekker, New York, 3rd edn., 1999.

37. Schmidt, N. J., in *Medical Virology*, eds. L. M. Maza and E. M. Peterson, Elsevier, New York, 1981, pp. 1-33.

38. Forghani, B. and Hagens, S., in *Diagnostic Procedures for Viral, Rickettsial, and Chlamydial Infections*, eds. E. H. Lennette, D. A. Lennette and E. T. Lennette, American Public Health Association, Washington, 7th edn., 1995, pp. 79-96.

39. Liu, C., "Rapid diagnosis of juman influenza infection from nasal smears by means of fluorescein-labeled antibody", *Proc. Soc. Exp. Biol. Med.*, 1956, **92**, 883-887.

40. Yalow, R. S. and Berson, S. A., "Immunoassay of endogenous plasma insulin in man", *J. Clin. Invest.*, 1960, **39**, 1157-1175.

41. Engvall, E. and Perlman, P., "Enzyme-linked immunosorbent assay (ELISA). Quantitative assay of immunoglobulin G", *Immunochemistry*, 1971, **8**, 871–874.

42. Van Weemen, B. K. and Schuurs, A. H., "Immunoassay using antigen-enzyme conjugates", *FEBS Lett.*, 1971, **15**, 232-236.

43. Crowther, J. R., *The ELISA Guidebook*, 2nd edn., Humana Press, Totowa, NJ, 2001.

44. Rabinow, P., *Making PCR: A Story of Biotechnology*, University of Chicago Press, Chicago, 1996.

45. Saiki, R. K., Scharf, S., Faloona, F., Mullis, K. B., Horn, G. T., Erlich, H. A. and Arnheim, N., "Enzymatic amplification of beta-globin genomic sequences and restriction site analysis for diagnosis of sickle cell anemia", *Science*, 1985, **230**, 1350-1354.

46. Ryan, K. J. and Ray, G. C., *Sherris Medical Microbiology : An Introduction to Infectious Diseases*, 4th edn., McGraw-Hill Medical, New York, 2003.

47. Baron, S., in *Medical Microbiology*, University of Texas Medical Branch, Galveston, 4th edn., 1996.

48. Bentzen, E. L., Wright, D. W. and Crowe, J. E., "Nanoscale tools for rapid and sensitive diagnosis of viruses", *Future Virol.*, 2006, **1**, 769-781.

49. Kuznetsov, Y. G., Malkin, A. J., Lucas, R. W., Plomp, M. and McPherson, A., "Imaging of viruses by atomic force microscopy", *J. Gen. Virol.*, 2001, **82**, 2025-2034.

50. Nettikadan, S. R., Johnson, J. C., Vengasandra, S. G., Muys, J. and Henderson, E., "ViriChip: a solid phase assay for detection and identification of viruses by atomic force microscopy", *Nanotechnology*, 2004, **15**, 383.

51. Nettikadan, S. R., Johnson, J. C., Mosher, C. and Henderson, E., "Virus particle detection by solid phase immunocapture and atomic force microscopy", *Biochem. Biophys. Res. Commun.*, 2003, **311**, 540-545.

52. Binnig, G. and Quate, C. F., "Atomic force microscope", *Phys. Rev. Lett.*, 1986, **56**, 930-933.

53. Perez, J. M., Josephson, L., O'Loughlin, T., Hogemann, D. and Weissleder, R., "Magnetic relaxation switches capable of sensing molecular interactions", *Nat. Biotechnol.*, 2002, **20**, 816-820.

54. Perez, J. M., Simeone, F. J., Saeki, Y., Josephson, L. and Weissleder, R., "Viral-Induced Self-Assembly of Magnetic Nanoparticles Allows the Detection of Viral Particles in Biological Media", *J. Am. Chem. Soc.*, 2003, **125**, 10192-10193.

55. Bentzen, E. L., House, F., Utley, T. J., Crowe, J. E. and Wright, D. W., "Progression of Respiratory Syncytial Virus Infection Monitored by Fluorescent Quantum Dot Probes", *Nano Lett.*, 2005, **5**, 591-595.

CHAPTER II

VIRAL DETECTION USING DNA FUNCTIONALIZED GOLD FILAMENTS[1]

Respiratory viral infections are among the leading causes of medical care in the United States. The most common respiratory viruses in humans are influenza virus, parainfluenza, metapneumavirus and respiratory syncytial virus (RSV).[2, 3] RSV, a paramyxovirus, is the leading cause of lower respiratory tract infections in infants and young children and results in an estimated 90,000 hospitalizations annually in children under five years of age.[4-6] Worldwide, RSV is the cause of death of over 1 million children per year.[7] Furthermore, RSV is problematic for elderly and immuno-compromised populations.[8, 9]

Recently, antivirals have been made available for treatment of RSV, but they are only effective when given in the early stages of infection, creating a need for early-stage diagnostics.[10, 11] The importance of these diagnostic tests is further emphasized by the fact that there is no approved vaccine for RSV.[12] Rapid, simple and accurate diagnostic tests for early respiratory virus infections would give physicians additional information and help avoid the use of unnecessary antibiotics which has led to soaring rates of antibiotic resistance in the U.S.[13-16]

Although a number of diagnostic alternatives exist, none of them are fast, easy and sensitive enough to be an attractive option in a clinical setting. Viral infections are typically detected in clinical diagnostic labs using cell cultures, serology, or direct antigen detection, but each has a significant drawback. Cell cultures usually require

expertise and extended observation time of up to ten days. Serological methods, which detect antibodies in response to a viral infection, are difficult to interpret when diagnosing repetitive or chronic viral infections such as RSV. Direct antigen detection, such as immunofluorescence, requires technical expertise in using a fluorescence microscope and is far from a simple diagnostic.[17, 18] Alternatively, PCR and immuno-PCR have proven to be very sensitive diagnostics; however, they require technical expertise and often suffer from high false positive rates due to DNA contamination.[19-21]

From the clinical perspective, one of the most attractive features of a recently published antibody-based virus detection technology approach is the simplicity of sample processing. This filament-based antibody recognition assay (FARA) utilizes an ELISA-like sandwich detection strategy that employs antibodies immobilized on a moveable polyester filament to capture antigen.[22-24] The filament is then pulled through a series of capillary tubes to achieve assay processing and detection. Although FARA allows for rapid processing and detection, to date its sensitivity is comparable to ELISA, with a lower limit of detection of ~1.7 x 10^7 virus particles.[22]

In this work, the filament-based design is modified to incorporate the use of a gold-clad filament as a fluorescence quencher for molecular beacon hairpin structures coupled along the construct at known locations. Molecular beacon detection strategies have proven very successful for identifying a variety of DNA targets, ranging from pathogens[25] and cancer cells[26, 27] to single nucleotide polymorphisms.[28] Molecular beacons are composed of single stranded DNA designed with 5′ and 3′ ends that are complementary to each other, ensuring that the beacon remains in a hairpin

conformation in the absence of target DNA. One end of the beacon is functionalized with a fluorophore and the other with a quencher. While the beacon is in a hairpin conformation, the fluorophore is spatially close to the quencher and fluorescence is not observed, rendering the beacon in a "dark" state. In the presence of target DNA, however, the target anneals to the beacon, and the hairpin opens. As a result, the two ends of the beacon are spatially separated, eliminating quenching, resulting in a "bright" signal state. As shown in this report, the combination of molecular beacons with filament processing retains the simple and rapid processing design and improves the lower level of detection significantly.

Experimental

DNA Preparation and Immobilization on Filaments. RSV hairpin DNA was purchased from Biosearch Technologies, the sequence of which can be found in **Table 1** (RSV Probe) and is discussed in Results and Discussion. Gold-plated tungsten filament (100 μm diameter) was purchased from Luma Metall Fine Wire Products (Kalmar, Sweden). 6-Mercapto-1-hexanol was purchased from Aldrich chemical company. All H_2O used was Gibco ultraPURE DNAse RNAse Free. The buffer used was 10 mM phosphate buffer with 0.3 M NaCl, pH 7.0 (PB).

Thiolated probe DNA sequences were received as disulfides and were activated by cleaving the disulfide bond. Cleavage was performed in 100 mM dithiothreitol (DTT), 0.1 M phosphate buffer, pH 8.3. After 0.5 hr, thiolated DNA was purified using

Table 1. Oligonucleotide sequences used in filament studies. The underlined regions of the sequence indicate the "stem" which keeps the hairpin closed in the absence of target RNA. CAL indicates the position of a CAL Fluor Red 590 dye which is a TAMRA equivalent.

Name	Sequence 5′ → 3′
RSV Probe	[C6Thiol]TTTTTTTTTTCGACGAAAAATGGGGCAAATACGTCG[CAL]
RSV Target	TTTTTTATTTGCCCCATTTTTTTTTT
FemA Target	ACGCTCACTATGAGTTAAAGCTTGCTGAAGGTTATGA
RSV Primer1	GCTCTTAGCAAAGTCAAGTTGAATGA
RSV Primer2	TGCTCCGTTGGATGGTGTATT
GAPDH Primer1	GGTGGTCTCCTCTGACTTC
GAPDH Primer2	CTCTTCCTCTTGTGCTCTTG
Linear Capture Probe	[C6Thiol]TTTTTTTTTTTTTTTCTGTGTAAGCTTTGTCTT[Quasar 670]
Linear Target	[TAMRA]AAGACAAAGCTTACACAG
Biotin Capture Probe	[C6Thiol]TTTAAAAATGGGGCAAATA
Biotin Target	[C6Biotin] TATTTGCCCCATTTTT

Millipore Microcon YM-3 spin filters. The purified DNA was diluted to 30 μM in H_2O and stored in small aliquots at -80 °C.

Gold-plated filaments were cleaned by thorough rinsing in PB. The cleaned gold filament was incubated overnight at room temperature in a solution of PB containing 1 μM of activated DNA and 10 μM mercaptohexanol. After a minimum of 8 hr, the filaments were removed from the DNA solution and rinsed with PB. The filaments were then stored at 4˚C in PB until use.

RSV Infection of HEp-2 Cells. Uninfected HEp-2 cells were incubated at 37˚C with 5% CO_2 and grown to 80% confluency in OPTI-MEM media containing 2% fetal bovine serum, 200 mM L-glutamine, 250 μg/ml of amphotericin-B and 10 mg/ml gentamicin (c/OPTI-MEM/2%). Quick thawed virus diluted in c/OPTI-MEM/2% was used to infect 80% confluent HEp-2 cultures. Following infection, flasks were incubated at 37°C, 5% CO2 for 4 days.

Titer of Infected Cells. An aliquot of infected cells was suspended in 1 mL c/OPTI-MEM/2% and used to determine the titer of the virus. The 1 ml of stock was then frozen using a slurry of ethanol and dry ice. After freezing, the supernatant was thawed in a 37°C water bath. The freeze/thaw cycle was repeated three times to maximize the release of virus particles from the cell wall. After the third cycle, the supernatant was separated and used to infect three columns (18 wells) of a 24-well microtiter plate. Each successive row of the column was infected with a 10-fold serial dilution of the stock. After infection, the cells were incubated for 1 hr at 37°C and 5% CO_2. The cells were then overlaid with 1 mL of media containing 0.75% (w/v) methylcellulose and incubated for 4 days at 37°C and 5% CO_2.

After incubation, the cells were fixed with cold 80% methanol and stored at 4°C for at least 1 hr. Cells were blocked with 2% BSA in Dulbeccos' PBS (Mg^{2+} and Ca^{2+} free) for 1 hr. After blocking, the cells were incubated for 30 min at room temperature with a 1:1000 dilution of anti-RSV F protein antibodies (final concentration of 20 µg/mL). The cells were then washed with PBS and incubated in a 1:1000 dilution of secondary antibody (goat anti-mouse horseradish peroxidase (HRP) conjugate, Santa Cruz Biotechnology) for 1 hr. Excess antibody was removed by rinsing with PBS. The HRP was then developed with a TrueBlue peroxidase precipitating substrate (KPL Protein Research Products) which rendered a colored dot. The dots were then counted to quantify the amount of plaque forming units (PFU).

RNA Isolation from HEp-2 Cells. Four days post-infection (for infected cells) or at 100% confluency (for uninfected cells), the cells were washed two times with PBS and then scraped from the flasks. The scraped cells were centrifuged at 1500 x g for five min

to pellet the cells. The supernatant was removed and RNA was extracted in approximately 30 min using a 5-Prime PerfectPure RNA Cell and Tissue kit. Cells were lysed in lysis buffer and passed 10 times through a 22 gauge needle. The cell lysate was passed through a spin filter to bind nucleic acids. The filter was washed, treated with DNase and washed two more times. Finally, the extracted RNA was eluted from the filter with H_2O, and the concentration was obtained via UV-Vis Spectroscopy.

RSV N-Gene RNA Standard. *E. coli* transformed with the RSV N-gene cloned into a pcDNA3.1(-) vector was received from the Crowe Lab. *E. coli* was grown overnight in Miller's LB Broth at 37°C on a rotating rack. The next day, growth was confirmed by the turbidity of the broth and the plasmid was extracted using a Qiagen Spin Miniprep Kit. The concentration of extracted plasmid DNA was then calculated using UV-Vis spectroscopy. The purified plasmid was linearized using a *Pvu I* restriction enzyme and linearization was confirmed by running both pre- and post-linearized plasmids on a 1% agarose gel. Linearized plasmid was purified using ethanol precipitation. The purified plasmid was then transcribed into RNA using a T7 MEGAscript transcription kit. Appropriate RNA length was confirmed on a denaturing Agarose-Formaldehyde gel. The N-gene RNA was then quantified using UV-Vis spectroscopy, separated into aliquots, and stored at -80°C.

Viral RNA Hydrolysis. Hydrolysis was performed by adding an equal volume of H_2O to extracted RNA, followed by the addition of two volumes of carbonate buffer (pH 10.2). The RNA was then incubated at 65°C for up to 60 min, depending on the amount of desired hydrolysis. In this experiment, samples were incubated for 0, 1, 5, 15, 30 and 60 min. After incubation, the hydrolysis was stopped with neutralization buffer (3 M

sodium acetate, 1% (v/v) acetic acid; pH 6.0). Following neutralization, the hydrolyzed RNA was ethanol precipitated and finally, resuspended in H_2O and stored at -85°C. To verify hydrolysis, the hydrolyzed samples were run on an Agilent 2100 Bioanalyzer, and the resulting electropherograms were examined.

RNA Capture and Detection. Gold-clad filaments were functionalized, as described above, with molecular beacon style capture DNA. The functionalized filament was then incubated for 2 hrs at room temperature in PB containing 3 ng/μL of total RNA extracted from RSV-infected and uninfected cells. Following capture of the target RNA, the filament was washed for 1 min in 2X sodium citrate/sodium chloride (SSC), 1X SSC, 0.1X SSC and finally in PB. The filament was then mounted on a glass slide and imaged. Fluorescence measurements of the filament were performed on an Axon Instruments GenePix 4000B microarray scanner. The scanner is equipped with excitation lasers of 532 nm (green) and 635 nm (red), and 575DF35 and 670DF40 emission filters. Fluorescence was quantified using GenePix software. Regions of interest (ROI) were created along the entire length of the filaments, and the ROIs were averaged to obtain the average fluorescence along the filament.

Biotin-Streptavidin Amplification. In a typical experiment, a 100 μm diameter gold filament was incubated overnight at room temperature in a solution of 10 mM phosphate buffer, pH 7.0 and 0.3 M NaCl (PB) containing 1 μM of activated DNA to couple the capture DNA to the filament. Following DNA coupling the filament was washed for 5 minutes in phosphate buffered saline (PBS). The filament was then incubated for 3 hours at room temperature in PB containing target DNA, which was the Watson-Crick complement of the capture strand functionalized with a 5′ Biotin.

Following capture of the target DNA, the filament was washed in 2X SSC, 1X SSC, 0.1X SSC and finally in PB. The filament was then incubated for 1 hour in PBS containing 1 nM streptavidin-Qdots, followed by washing in PBS for 5 minutes. After the initial labeling, the filament was incubated for a 2nd hour in PBS containing 1 nM biotin-Qdots, followed by washing in PBS for 5 minutes. Finally, the filament was incubated once again in 1 nM streptavidin-Qdots for 1 hour, followed by washing in PBS for 5 minutes. The filament was then mounted on a glass slide and imaged.

Real-Time RT-PCR for PFU Quantitation of RNA Samples. Real-time RT-PCR was performed using a SmartCycler II thermal cycler system (Cepheid, Sunnyvale, CA). Reactions were done in a 25 μL volume with 12.5 μL of 2X One-Step qRT-PCR Buffer plus SYBR (Clontech), 0.5 μL of 50X QTaq DNA Polymerase Mix (Clontech), 0.4 μL of 60X qRT Mix (Clontech), 200 nM left and right primers (RSV or GAPDH primers, **Table 1**), and H_2O. The protocol consisted of RT followed by a three-step PCR. RT was performed at 48°C for 20 min followed by an initial QTaq DNA polymerase activation step of 95°C for 3 min and 40 cycles at 95°C for 15 sec to denature, 60°C for 60 sec to anneal and extend, and 72°C for 15 sec to detect fluorescence.

ELISA. A standard indirect sandwich ELISA was performed.[29] A stock solution of RSV infected HEp-2 cell lysate ($3.0x10^4$ PFU/mL) was serially diluted 1:2 and used to determine the lower limit of detection. To allow capture antibodies to bind to the Immulon 2HB microtiter plate, 100 μL of 2 μg/mL F-mix (an equal mixture of two anti-RSV fusion protein antibodies, clones 1269 and 1214) was added to three rows of the 96-well plate and placed in a humidified box at room temperature for 1 hr. After 1 hr, the wells were rinsed three times with PBS and blocked with 2% BSA for 10 min. After

blocking, BSA was removed from the wells and 100 μL of infected cell lysate stock was placed in the three rows of column 1 and serial dilutions in columns 2 through 11, leaving column 12 for PBS. The plate was then placed back in a humidified box at room temperature for 1 hr. Following antigen binding, the wells were rinsed three times with PBS and 100 μL of 10 μg/mL of primary antibody (Synagis, humanized monoclonal antibody, MedImmune Inc.) was added to each well. The plate was placed in a humidified box at room temperature for 1 hr. The wells were then rinsed three times with PBS and 100 μL of secondary antibody (1:1000 dilution of goat anti-human HRP conjugated, Pierce) was added to each well. After 1 hr in a humidified box at room temperature, the wells were rinsed five times with PBS. Next, 100 μL of substrate (Tetramethylbenzidine, Pierce) was added to each well and the enzymatic reaction was allowed to proceed for 10 min, after which it was quenched with 100 μL 2 M H_2SO_4. Finally, absorbance at 450 nm was measured using a Bio-Tek Synergy HT microplate reader.

Results and Discussion

The following viral detection design utilizes a molecular beacon-style hairpin DNA covalently coupled to a moveable gold-clad filament (**Figure 8**). This allows the viral probes attached to the filament to be easily added to and removed from processing solutions. In adapting molecular beacons for use with the simple processing offered by FARA, the quenching function is performed by the gold-clad filament itself. Studies have shown that fluorophores in close proximity to metal

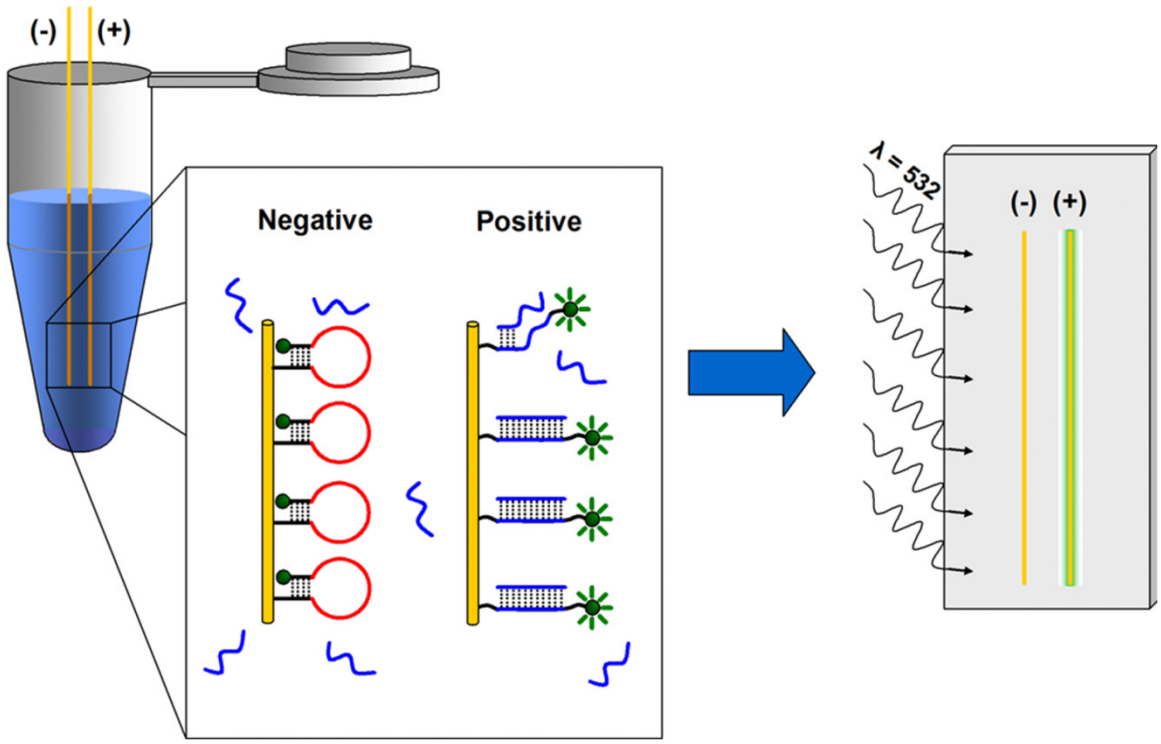

Figure 8. Illustration of the filament-based assay method. In an analyte solution, a conformational change is observed when the molecular beacon style probe DNA binds target DNA/RNA. In the closed conformation (negative), the fluorophore is in close proximity to the gold surface and is quenched. Upon binding the target (positive), the fluorophore becomes spatially separated from the gold surface. After binding the target, the filaments are rinsed and mounted to a glass slide for imaging. Upon excitation at the desired wavelength (532 nm), fluorophores that have bound target and are in an open conformation will exhibit a distinct fluorescence signal (575nm).

surfaces can experience changes in emission intensity.[30, 31] Specifically, metal surfaces have been shown to quench a beacon while it is in a hairpin conformation.[32-35] This quenching effect is typically only observed at fluorophore to metal distances of ≤ 5-10 nm which is on the scale of Förster energy transfer processes.[31, 35] By using a metal filament for probe DNA attachment, the metal filament can be used as a quencher for the beacon in the closed state.

DNA Coupling to Gold Filaments. The first step in the successful development of this new diagnostic approach was to examine the appropriate coupling conditions for covalent attachment of DNA to the gold filament. These

studies utilized a short linear 55-mer oligonucleotide functionalized with a 5′ thiol and a 3′ fluorescent dye (Linear Capture Probe, **Table 1**). In order to determine the optimum time for coupling, a series of experiments were perform exposing 50 μm diameter gold-plated tungsten filaments to activated DNA for 1 to 16 hr. The images from the time-dependence study (**Figure 9**) revealed significant coupling as early as 4 hr. At 4 hr, 78% of the maximum fluorescence was obtained and after 8 hr, ≥90% of maximum fluorescence was obtained. Using this information, 8 hr was chosen as a minimum time to facilitate optimal coverage of filament in subsequent experiments.

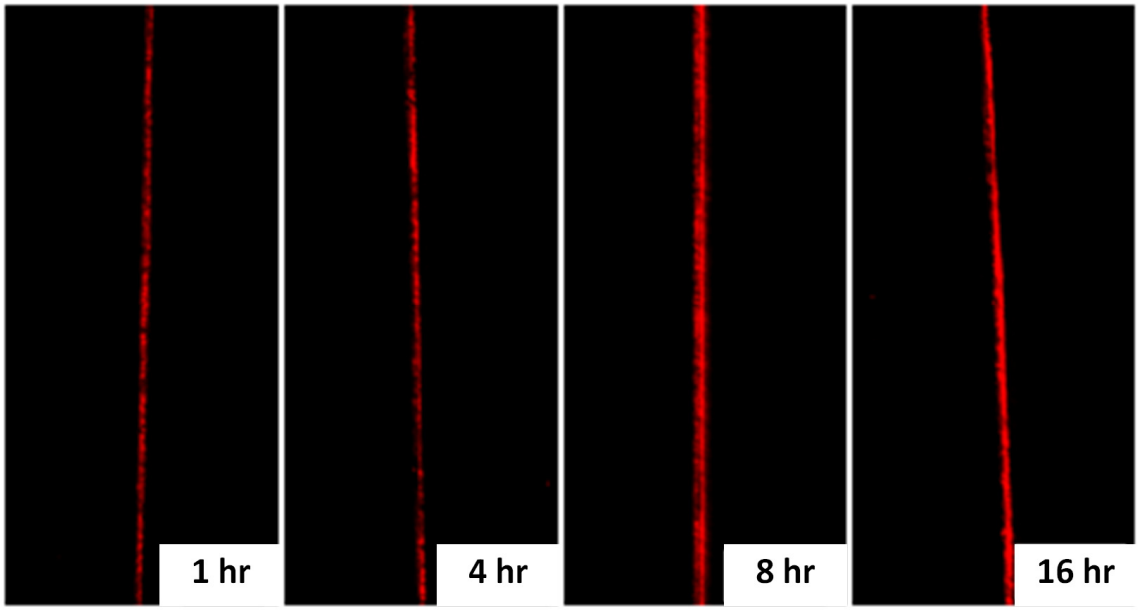

Figure 9. Time dependence of coupling. Fluorescence scan of gold-plated filaments with Quasar 670-tagged capture DNA. All wire were coupled using a solution of 5 μM capture DNA with differing coupling times, ranging from 1 hour to 16 hours. The greatest coupling occurs after 16 hours, but sufficient coupling has occurred after 4 hours.

In order to show that the coupling of DNA to the filament did not prevent hybridization of complementary DNA in solution, two types of DNA were employed. The capture DNA was functionalized with a 5′ thiol and a 3′ Quasar (670 nm) dye

(Linear Capture Probe, **Table 1**). The second strand, target DNA, was complementary to the capture DNA and functionalized with a 5′ Tamra (575 nm) dye (Linear Target, **Table 1**). In this experiment (**Figure 10**), the right two regions of the gold filament were exposed only to target DNA. As a result, no capture DNA was present, and the target DNA was washed away yielding no fluorescence. The middle two regions were exposed

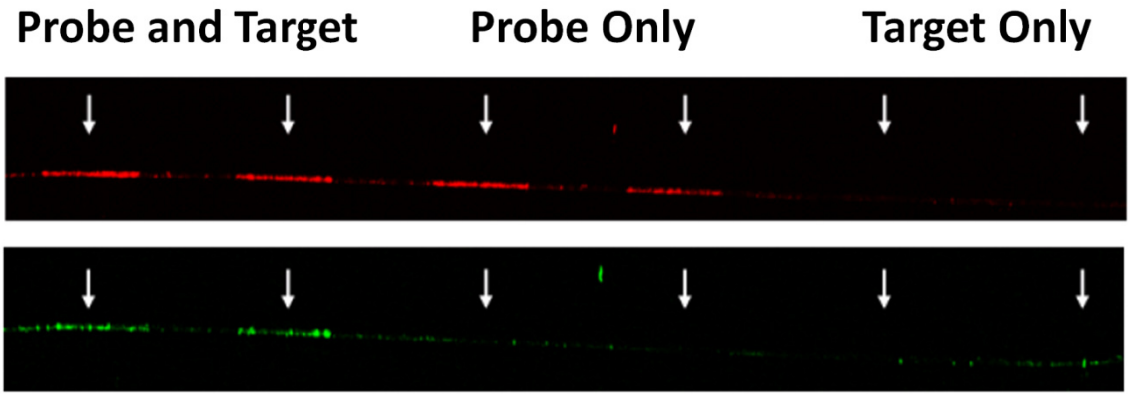

Figure 10. Fluorescence scans of the same gold wire using the Cy5 (top) and Cy3 (bottom) channels of a microarray scanner. The capture probe coupled to the wire was labeled with Quasar 670. The hybridized target was labeled with Tamra. After coupling the probe to the wire and hybridization with target DNA, both red and green fluorescence are visible (left pair of bands). If coupling is not followed be hybridization, no target DNA is present (middle pair of bands). Without the coupled capture probe, target DNA does not nonspecifically bind (right pair of bands).

only to capture DNA. The red fluorescence was a result of Quasar (670 nm) dye present on the capture DNA which bound to the gold filament via the 5′ thiol and was not washed away. The left two regions were exposed first to capture DNA followed by exposure to target DNA. The result was both red fluorescence from the capture DNA and green fluorescence from the target DNA which has hybridized to the capture DNA. These results were significant for two reasons. First, they showed that the capture DNA was still functional post-coupling. Second they revealed that non-thiolated DNA does not

bind to the gold filament, instead it is washed away unless it is hybridized to a thiol-coupled strand.

Biotin-Streptavidin Signal Amplification. Although the ultimate goal of this work was to utilize molecular beacon structures on gold filaments, the use of linear DNA does allow for unique amplification strategies. One promising amplification method was based on the exposure of hybridized DNA containing a 5′ biotin to successive rounds of streptavidin quantum dots and biotin quantum dots (**Figure 11**). In a test of this approach, a filament functionalized with capture DNA (Biotin Capture Probe, **Table 1**) was incubated with biotinylated target DNA (Biotin Target, **Table 1**) for 3 hours at room

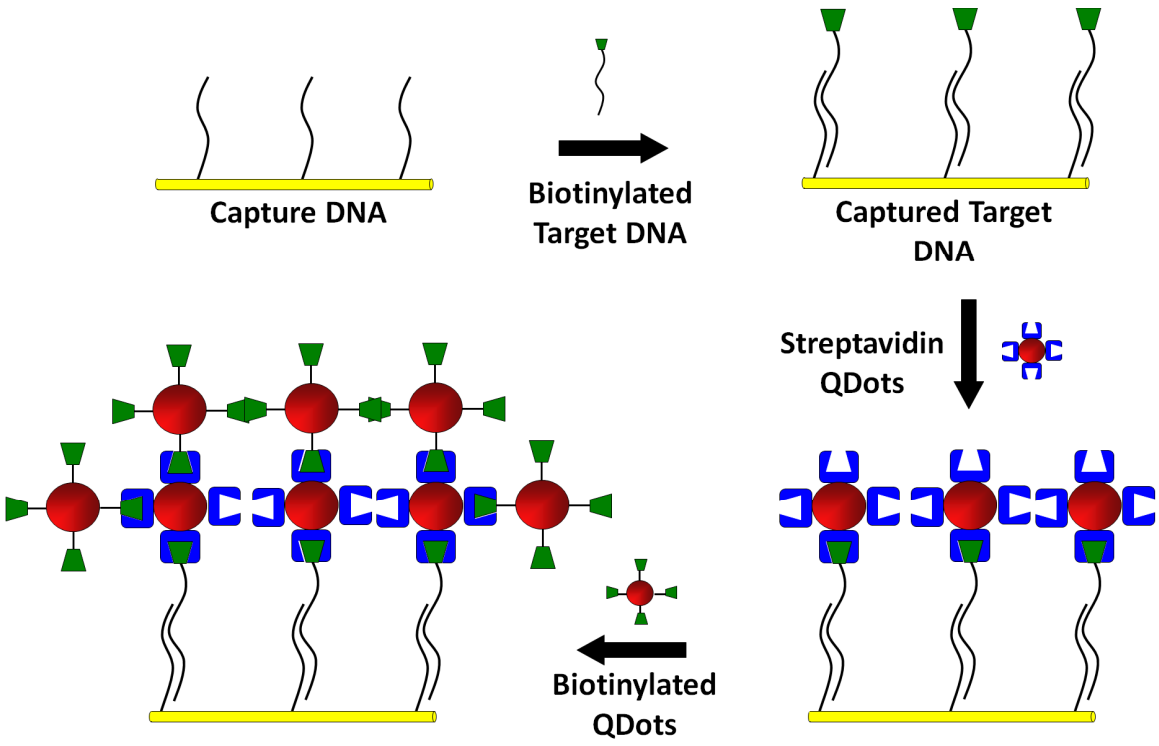

Figure 11. Illustration of Biotin-Streptavidin amplification. After the capture of biotinylated target DNA, the filament is incubated with streptavidin Qdots. After washing, the filament is then incubated in biotinylated Qdots. This process can be repeated multiple times for additional amplification.

temperature. Following capture of the target DNA, the filament was washed and then incubated in PBS containing streptavidin-Qdots. After the initial labeling, the filament was washed and then incubated in PBS containing biotin-Qdots. Finally, the filament was washed and then incubated once again in streptavidin-Qdots. The filament was then washed, mounted on a glass slide and imaged. The resulting amplification of binding signal using biotin and streptavidin quantum dots can be seen in **Figure 12**. The average fluorescence of the three wires was 400 (left wire, not visible), 2400 (center), and 5800 (right) relative fluorescence units, suggesting that successive rounds of incubation in Qdots does result in signal amplification.

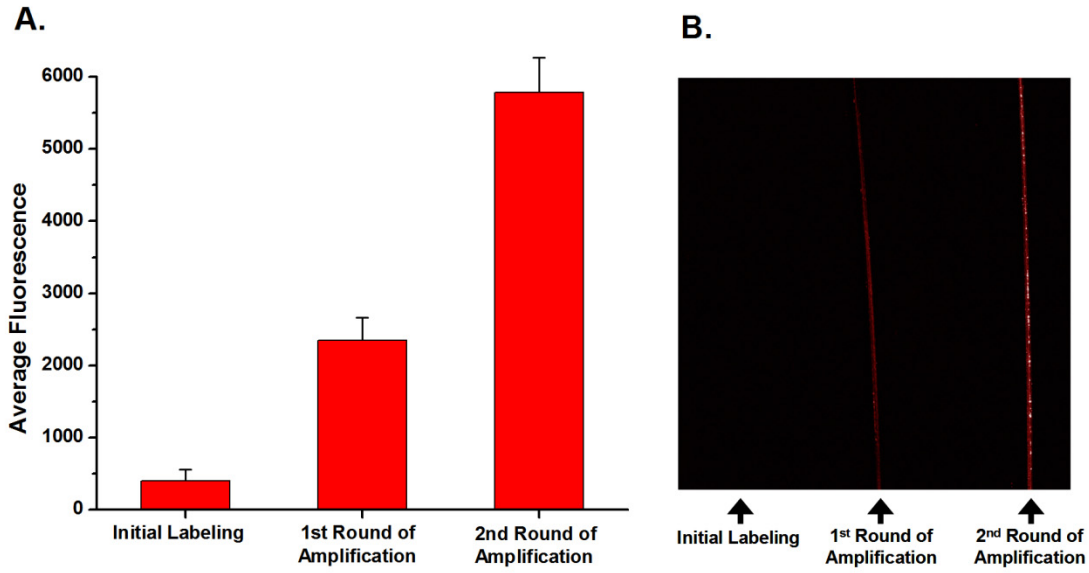

Figure 12. Amplification of binding signal using biotin and streptavidin quantum dots. A) The average fluorescence of the three wires. B) The difference in fluorescence is also clearly visible in fluorescence scan.

Hairpin DNA Design. The sequence of hairpin DNA used in this study to target RSV viral RNA is shown in **Figure 13**. The RSV specific probe is designed so

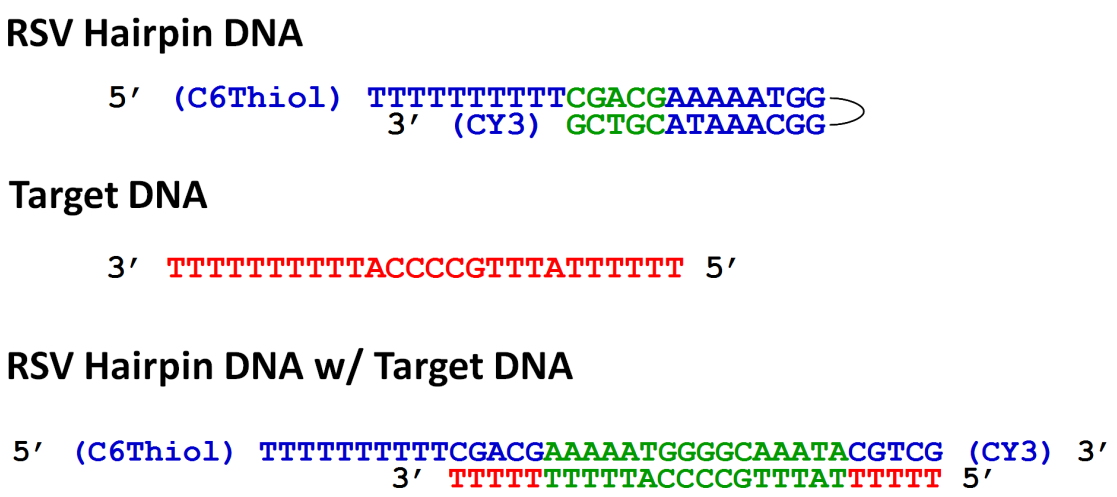

Figure 13. RSV Probe DNA's hairpin and linear conformations. In the absence of target DNA, RSV probe DNA is in a hairpin conformation (top), bring both the 5′ and the 3′ ends in close proximity to one another. However, the presence of target DNA disrupts the hairpin conformation (bottom).

that the initial loop region targets a gene end-intergenic start sequence which has three exact repeats and six almost-exact repeats with various numbers of nucleotide mismatches throughout the RSV genome.[36, 37] Similar intergenic repeats are common in other RNA viruses,[38] suggesting that the approach may be generalized to the study of other viruses. Successfully used in antisense and small interfering RNA experiments,[37-39] this site was considered the most accessible and therefore, a prime site for oligonucleotide binding and probe targeting. As shown in **Figure 13**, this RSV specific sequence is then flanked by five base stem regions that hold the DNA in a closed conformation in the absence of RSV RNA. The 5′ end of the hairpin is further functionalized with a 10-base poly-T linker. Of the four possible nucleotides, thymines are the least reactive with gold surfaces.[40] This sequence promotes favorable orientation and binding of the DNA through the 5′ thiol with minimal adsorption to the surface. Additionally, the 3′ end of the hairpin is functionalized

with a TAMRA equivalent dye to facilitate detection. Prior to RNA binding, the stem region of the probe ensures that the DNA maintains a hairpin conformation. Upon binding of viral RNA, the probe undergoes a conformational change that increases the distance between the fluorophore and the gold-clad filament which results in an increased fluorescence signal (**Figure 8**).

Effect of Probe Density on Signal-to-Noise. Initial studies indicated that the gold surface quenches the 3′ hairpin fluorophore when the hairpin is in a closed state and that this quenching is dependent on probe density at the gold surface. Gold-clad filaments were functionalized with various molar ratios (1:0 to 1:20) of RSV probe DNA and mercaptohexanol. The mercaptohexanol competes with the probe DNA for binding at the gold surface, separating DNA beacons at higher molar ratios of mercaptohexanol. After being functionalized, half of the filaments were imaged to gather information about the dark state at each of the molar ratios. The other half of the filaments were incubated with 100 nM RSV target DNA to open the hairpin probes and then imaged for information about the bright state at each of the molar ratios. Fluorescence data from both the dark and bright states was then used to calculate the signal-to-noise ratio for each of the conditions (**Figure 14**). These results were then used to optimize the probe density along the filament for all subsequent experiments.

At low concentrations of mercaptohexanol (1:0, 1:2 and 1:5), the signal-to-noise is low due to the lack of quenching in the dark state. At these concentrations, the monolayer is principally composed of probe DNA. At this attachment density, the DNA strands are too close together to fold into the hairpin conformation, thus resulting in substantial fluorescence in the dark state. In higher mercaptohexanol concentrations

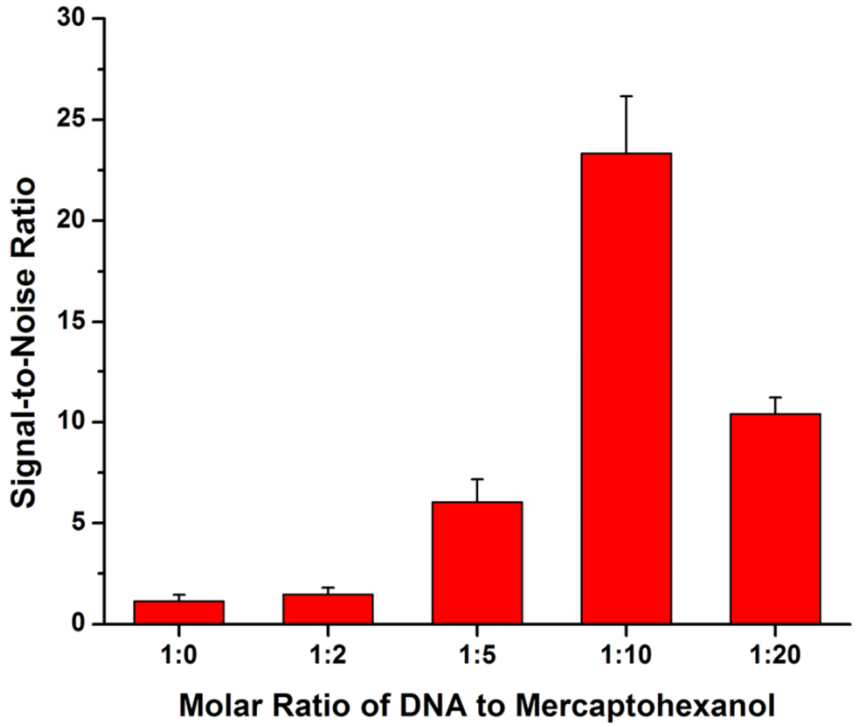

Figure 14. Effect of probe spacing on fluorescence. Comparison of the signal–to-noise ratio of filaments functionalized with mixed monolayers of RSV probe DNA and mercaptohexanol.

(1:10), the DNA strands have sufficient room to fold into the hairpin conformation, resulting in adequate quenching and a substantially higher signal-to-noise ratio. At the highest mercaptohexanol concentration tested (1:20), the noise no longer decreased as the DNA had sufficient room to adopt the hairpin conformation. Additionally, the signal-to-noise ratio was reduced due to a lower density of probe DNA on the gold surface.

Specificity of Filament-Based Detection. The specificity of the RSV-targeted filament was examined against positive (RSV) and negative (femA) control complements (**Table 1**). RSV target DNA is the synthetic DNA equivalent of the RSV RNA targeted by the RSV probe. The femA sequence, a portion of the *femA* gene[33] which encodes a

protein whose expression is necessary for methicillin resistance in *Staphylococcus aureus,* was selected to be a biologically significant probe with a similar GC content to that of the RSV target.

As **Figure 15** illustrates, hairpin opening due to target capture was highly dependent on the sequence of the target DNA in solution. To test this, filaments functionalized with RSV specific probe DNA were incubated with various concentrations of either RSV target DNA or femA target DNA (**Table 1**), ranging

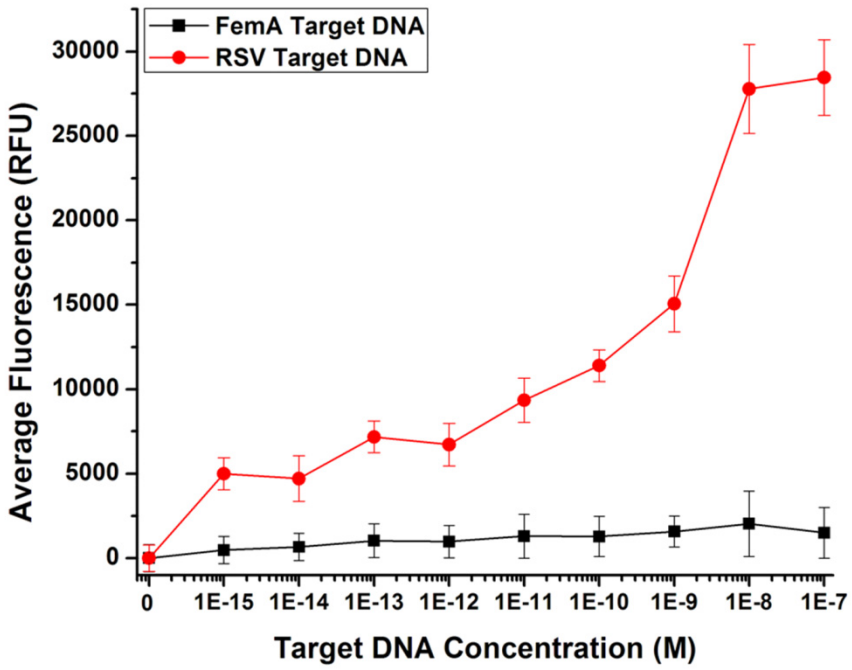

Figure 15. Specificity of probe functionalized filaments. Comparison of filament-functionalized RSV probes in the presence of increasing concentrations of RSV target DNA and nonspecific *femA* target DNA.

from 1 fM to 100 nM. At femtomolar concentrations of femA target DNA, the filaments functionalized with RSV probes remain primarily in the dark state. At high

nanomolar concentrations of femA, probes begin to open slightly, but this signal is still below a 5σ limit of detection and significantly less than the signal generated by the RSV probes at 1 fM RSV target DNA. It is apparent that concentrations greater than 100 nM femA target DNA, can force nonspecific interactions; however, across the range of concentrations tested, the signal was significantly higher in RSV target DNA than in the nonspecific femA target DNA.

Detection of Viral RNA. As expected, RSV-targeted filaments detect viral RNA isolated from infected cells. This was demonstrated using functionalized gold-clad filaments incubated in capillaries with 20 uL of RNA (3 ng/μL) from either uninfected or RSV infected HEp-2 cells. As seen in **Figure 16**, the filament-coupled DNA probes have two states: a dark state corresponding to a probe that remains in a closed conformation

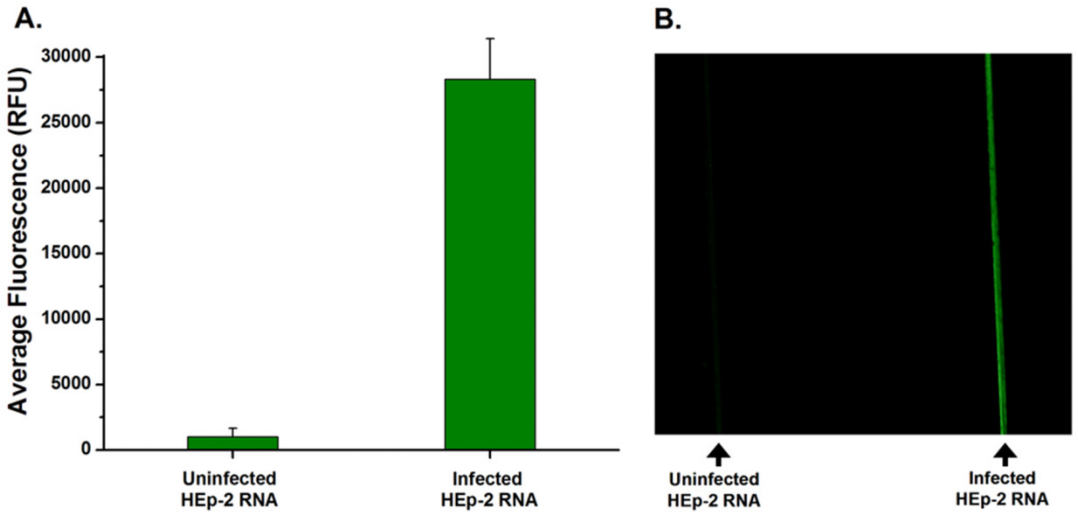

Figure 16. Response of probe DNA upon target binding. A) The average fluorescence along filaments functionalized with RSV probe DNA that have been exposed to lysates from either uninfected HEp-2 cells (left) or RSV infected cells (right). B) An image of these same filaments.

and a bright state corresponding to a probe that has captured viral RNA. The high quenching efficiency for the closed state allows for ease of detection when comparing uninfected cells (1,006 RFU) to RSV-infected cells (28,325 RFU). Using the average fluorescence values along the entire length of the filaments, the quenching efficiency of the gold filament for probe DNA in a hairpin conformation was found to be ~97%.

Optimum Length of Target RNA. The genomic sequence targeted was selected because it is not only specific to RSV but also repeated throughout the genome. Therefore, hydrolyzing the RSV into smaller fragments would make the repeated sites more available for capture by probe DNA and improve capture efficiency.[41] As expected, the changes in the RNA lengths confirm an increase in hydrolysis over time when measured by an Agilent bioanalyzer (**Figure 17A**). Signal increased to 2.5-fold of

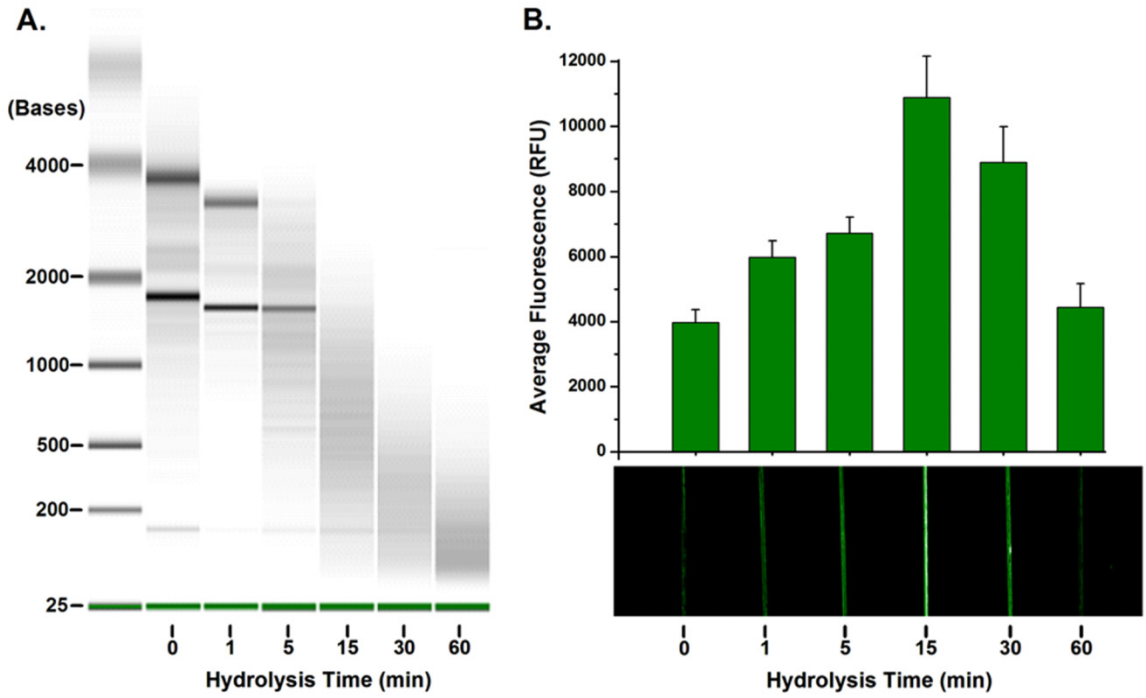

Figure 17. Effect of target RNA length on detection. A) Electropherogram verifying the hydrolysis of RNA at each of the time points. B) Average fluorescence and an image showing the effect of target RNA length on the resulting signal. At fifteen minutes the highest signal was observed.

full length genomic RNA after 15 min of hydrolysis (**Figure 17B**). These results indicate that short hydrolysis times result in decreased viral RNA lengths, making the target easier to capture and also increasing the number of target sites available for capture. However, with hydrolysis times greater than 30 min, these benefits are overcome by degradation of target sequences.

Standardization of the Beacon-Filament Assay. In order to compare these results to other diagnostics, such as ELISA, a portion of each sample was used to determine the number of PFUs in that sample. This conversion from RNA concentration to PFU was done using real-time RT-PCR (reverse transcription-

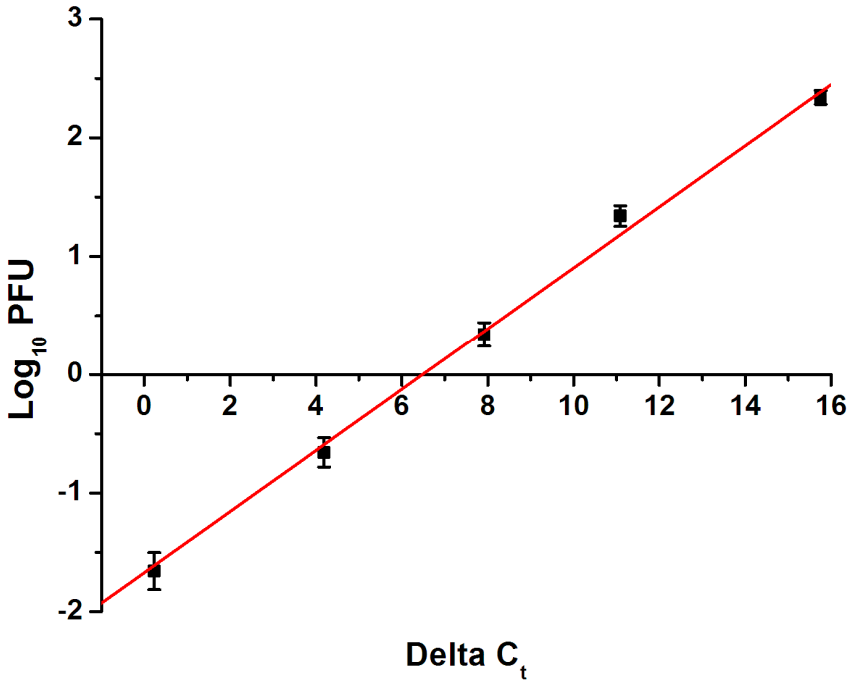

Figure 18. Conversion of delta C_t to PFU. Standard curve with an R^2 of 0.991 relating the delta C_t of RSV and GAPDH RNA to PFU.

polymerase chain reaction) to generate a standard curve relating delta (Δ) cycle threshold (C_t) of RSV RNA and GAPDH RNA to PFU. In PCR based RSV diagnostics, GAPDH has been shown to be a potential internal control when comparing samples. Therefore, samples of known PFU were processed using real time RT-PCR to determine the Ct with either RSV specific primers or GAPDH specific primers. The GAPDH Ct was then subtracted from the RSV Ct to calculate the ΔCt of the sample. When plotted against the $\log_{10}$ of PFU, a simple linear relationship was determined (**Figure 18**). This linear relationship was then used to calculate the PFU of unknown samples using only the ΔCt of the sample.

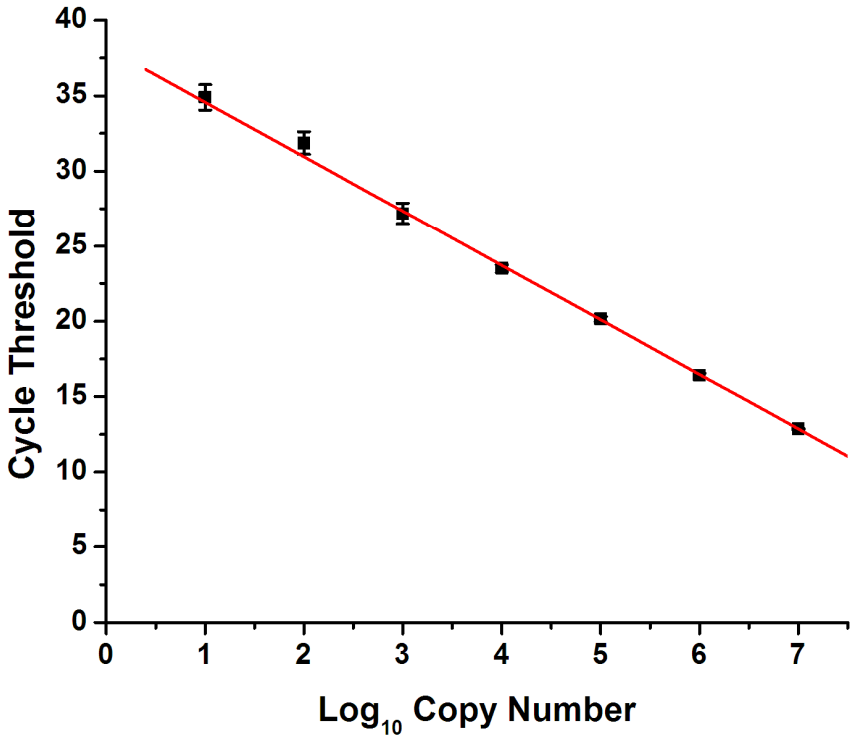

Figure 19. N-Gene copy number versus Cycle Threshold. Standard curve with an R^2 of 0.9952 relating C_t to the Log_{10} transformed number of copies of RSV RNA.

Additionally, stock of a known concentration of RSV N-gene RNA was used to calculate the number of RNA copies in the RSV samples. The RNA stock was serially diluted over 7-orders of magnitude and analyzed via RT-PCR. The dilutions allowed for the generate of a standard curve relating cycle threshold to the Log_{10} of copies of N-gene RNA (**Figure 19**). The curve was then used to calculate the number of RNA copies in each of the RSV samples tested with the beacon-filaments.

Beacon-Filament Limit of Detection. The beacon-filament lower limit of detection was approximately 200 times lower than a comparison ELISA. Filaments

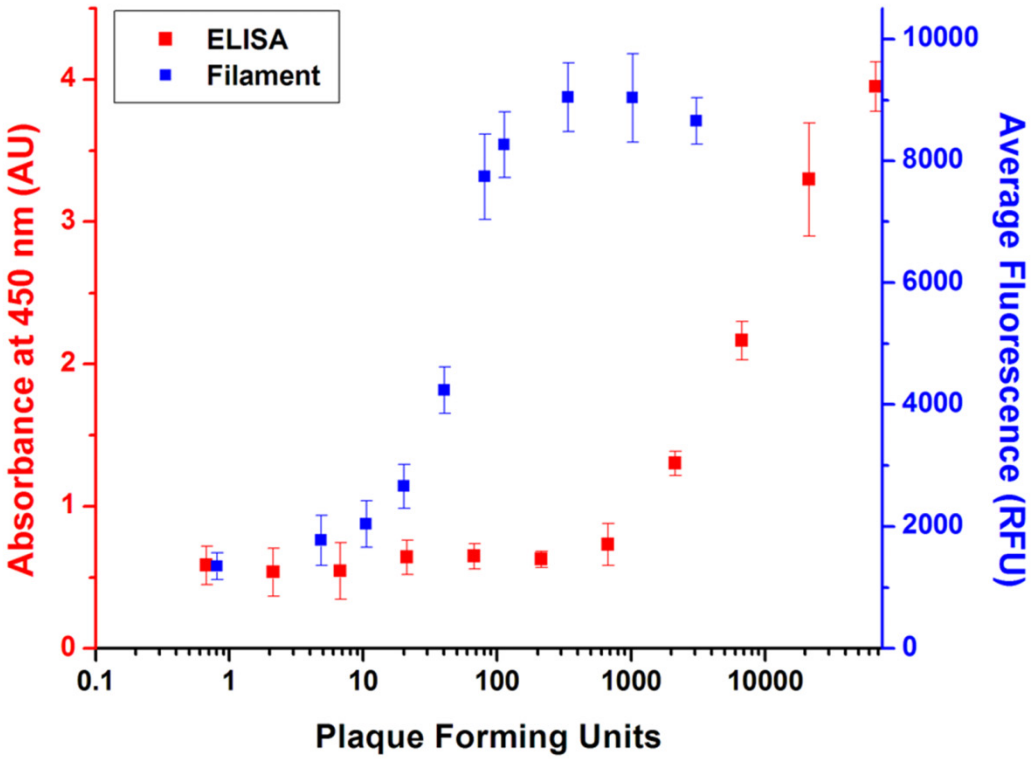

Figure 20. Comparison of the RSV detection using ELISA or the developed filament-based assay. The limit of detection using ELISA was 1750 PFU while the filament had a limit of detection of 11.9 PFU.

were incubated in solutions containing increasing amount of RNA isolated from RSV infected cells while keeping the concentration of total RNA constant at 3 ng/μL. The amount of the RNA isolated from RSV infected cells ranged from RNA isolated from uninfected cells (0 ng/μL), to that isolated from infected cells (3 ng/μL). Real-time RT-PCR was then used to convert the nanograms of RNA from infected cells to PFU. **Figure 20** compares the limit of detection of the filament-based assay and ELISA. Using a 5σ limit of detection, the filament-based assay was able to detect as few as 11.9 PFU while the limit of detection for ELISA was 1750 PFU. Using real-time RT-PCR and a stock of RSV-N gene of a known concentration, the 11.9 PFU limit of detection was calculated to be equivalent to ~5000 copies of genomic RSV viral RNA in 20 μL. This

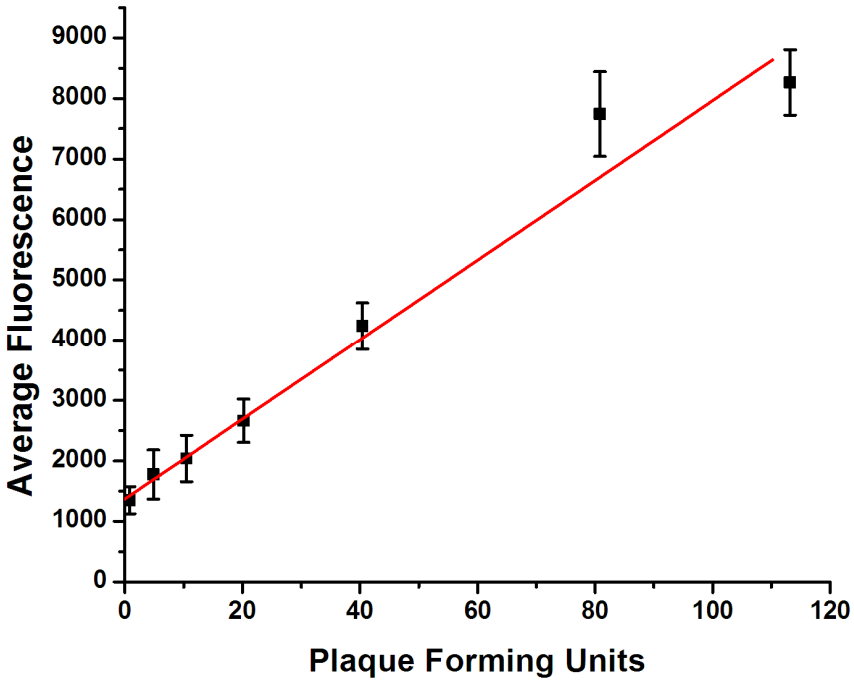

Figure 21. Linear range of the filament-based assay. A linear range up to 115 PFU can be calculated with an R^2 of 0.9717.

corresponds to a limit of detection of 4.15 x 10^{-16} M (~400 aM) RSV viral RNA. Additionally, the linear range of the filament assay was reliable up to 115 PFU (R^2 = 0.97) after which, the signal generated from the filaments saturated (**Figure 21**).

Conclusions

DNA functionalized gold-clad filaments responded only to RSV RNA, even in high concentrations of cellular RNA from uninfected HEp-2 cells. Although these studies focused on the detection of viral RNA from cultured cells, ongoing research is exploring the functionality of the filaments in clinical samples. These samples, nasopharyngeal aspirates from RSV infected children, will further demonstrate the clinical utility of the DNA functionalized filaments. The filament assays represent a core technology that has the potential to be much simpler than ELISAs, requiring only movement from one capillary to another, whereas an ELISA requires pipetting, washing, blocking and enzymes to develop the signal. Additionally, the filaments proved to be much more sensitive than ELISA, detecting as few as 12 PFU. Both the sensitivity and simplicity of DNA functionalized filaments make them a promising alternative in the development of an improved clinical diagnostic.

Bibliography

1. Perez, J. W., Haselton, F. R. and Wright, D. W., "Viral detection using DNA functionalized gold filaments", *Analyst*, 2009, **134**, 1548-1553.

2. Boivin, G., Cote, S., De Serres, G., Gilca, R., Bergeron, M. G. and Dery, P., Intersci. Conf. Antimicrob. Agents Chemother., 2003.

3. Clyde Jr., W. A., "Experimental Models for Study of Common Respiratory Viruses", *Environ. Health Perspect.*, 1980, **35**, 107-112.

4. Davidson, T., in *Gale Encyclopedia of Medicine*, eds. D. Olendorf, C. Jeryan, K. Boydon and M. K. Fyke, Gale Group, Detroit, MI, 1999, vol. 4, pp. 2478-2480.

5. Shay, D. K., Holman, R. C., Roosevelt, G. E., Clarke, M. J. and Anderson, L. J., "Bronchiolitis-Associated Mortality and Estimates of Respiratory Syncytial Virus-Associated Deaths among US Children, 1979-1997", *J. Infect. Dis.*, 2001, **183**, 16-22.

6. Tang, R. S., Spaete, R. R., Thompson, M. W., MacPhail, M., Guzzetta, J. M., Ryan, P. C., Reisinger, K., Chandler, P., Hilty, M., Walker, R. E., Gomez, M. M. and Losonsky, G. A., "Development of a PIV-vectored RSV vaccine: Preclinical evaluation of safety, toxicity, and enhanced disease and initial clinical testing in healthy adults", *Vaccine*, 2008, **26**, 6373-6382.

7. Cruz, A. T., Cazacu, A. C., Greer, J. M. and Demmler, G. J., "Performance of a Rapid Assay (Binax NOW) for Detection of Respiratory Syncytial Virus at a Children's Hospital over a 3-Year Period", *J. Clin. Microbiol.*, 2007, **45**, 1993-1995.

8. Falsey, A. R., Hennessey, P. A., Formica, M. A., Cox, C. and Walsh, E. E., "Respiratory Syncytial Virus Infection in Elderly and High-Risk Adults", *New Engl. J. Med.*, 2005, **352**, 1749-1759.

9. Sethi, S. and Murphy, T. F., "RSV Infection -- Not for Kids Only", *New Engl. J. Med.*, 2005, **352**, 1810-1812.

10. Iwane, M. K., Edwards, K. M., Szilagyi, P. G., Walker, F. J., Griffin, M. R., Weinberg, G. A., Coulen, C., Poehling, K. A., Shone, L. P., Balter, S., Hall, C. B., Erdman, D. D., Wooten, K., Schwartz, B. and for the New Vaccine Surveillance Network, "Population-Based Surveillance for Hospitalizations Associated With Respiratory Syncytial Virus, Influenza Virus, and Parainfluenza Viruses Among Young Children", *Pediatrics*, 2004, **113**, 1758-1764.

11. Shay, D. K., Holman, R. C., Newman, R. D., Liu, L. L., Stout, J. W. and Anderson, L. J., "Bronchiolitis-Associated Hospitalizations Among US Children, 1980-1996", *J. Am. Med. Assoc.*, 1999, **282**, 1440-1446.

12. Kaur, J., Tang, R. S., Spaete, R. R. and Schickli, J. H., "Optimization of plasmid-only rescue of highly attenuated and temperature-sensitive respiratory syncytial virus (RSV) vaccine candidates for human trials", *J. Virol. Methods*, 2008, **153**, 196-202.

13. Cohen, M. L., "Epidemiology of drug resistance: implications for a post-antimicrobial era", *Science*, 1992, **v257**, p1050(1056).

14. Dowell, S. F. and Schwartz, B., "Resistant pneumococci: protecting patients through judicious use of antibiotics." *Am. Fam. Physician.*, 1997, **v55**, p1647(1610).

15. Kunin, C. M., "Resistance to Antimicrobial Drugs--A Worldwide Calamity", *Ann. Intern. Med.*, 1993, **118**, 557-561.

16. Neu, H. C., "The crisis in antibiotic resistance", *Science*, 1992, **v257**, p1064(1010).

17. Dunn, J. J., Gordon, C., Kelley, C. and Carroll, K. C., "Comparison of the Denka-Seiken INFLU A·B-Quick and BD Directigen Flu A+B Kits with Direct Fluorescent-Antibody Staining and Shell Vial Culture Methods for Rapid Detection of Influenza Viruses", *J. Clin. Microbiol.*, 2003, **41**, 2180-2183.

18. Welliver, R. C., "Detection, pathogenesis, and therapy of respiratory syncytial virus infections." *Clin. Microbiol. Rev.*, 1988, **1**, 27-39.

19. Barletta, J., "Applications of real-time immuno-polymerase chain reaction (rt-IPCR) for the rapid diagnoses of viral antigens and pathologic proteins", *Mol. Aspects Med.*, 2006, **27**, 224-253.

20. Kox, L. F., Rhienthong, D., Miranda, A. M., Udomsantisuk, N., Ellis, K., van Leeuwen, J., van Heusden, S., Kuijper, S. and Kolk, A. H., "A more reliable PCR for detection of Mycobacterium tuberculosis in clinical samples." *J. Clin. Microbiol.*, 1994, **32**, 672-678.

21. LeGoff, J., Kara, R., Moulin, F., Si-Mohamed, A., Krivine, A., Belec, L. and Lebon, P., "Evaluation of the One-Step Multiplex Real-Time Reverse Transcription-PCR ProFlu-1 Assay for Detection of Influenza A and Influenza B Viruses and Respiratory Syncytial Viruses in Children", *J. Clin. Microbiol.*, 2008, **46**, 789-791.

22. Stone, G., Wetzel, J., Russ, P., Dermody, T. and Haselton, F., "Autonomous Reovirus Strain Classification Using Filament-Coupled Antibodies", *Ann. Biomed. Eng.*, 2006, **34**, 1778-1785.

23. Stone, G. P., Lin, K. S. and Haselton, F. R., "Adaptive virus detection using filament-coupled antibodies", *J. Biomed. Opt.*, 2006, **11**, 034012.

24. Stone, G. P., Mernaugh, R. and Haselton, F. R., "Virus detection using filament-coupled antibodies", *Biotechnol. Bioeng.*, 2005, **91**, 699-706.

25. Vet, J. A. M., Majithia, A. R., Marras, S. A. E., Tyagi, S., Dube, S., Poiesz, B. J. and Kramer, F. R., "Multiplex detection of four pathogenic retroviruses using molecular beacons", *Proc. Natl. Acad. Sci.*, 1999, **96**, 6394-6399.

26. Peng, X.-H., Cao, Z.-H., Xia, J.-T., Carlson, G. W., Lewis, M. M., Wood, W. C. and Yang, L., "Real-time Detection of Gene Expression in Cancer Cells Using Molecular Beacon Imaging: New Strategies for Cancer Research", *Cancer Res.*, 2005, **65**, 1909-1917.

27. Santangelo, P., Yang, L. and Bao, G., Summer Bioengineering Conference, Key Biscayne, Florida, 2003.

28. Mhlanga, M. M. and Malmberg, L., "Using Molecular Beacons to Detect Single-Nucleotide Polymorphisms with Real-Time PCR", *Methods*, 2001, **25**, 463-471.

29. Crowther, J. R., *The ELISA Guidebook*, 2nd edn., Humana Press, Totowa, NJ, 2001.

30. Lakowicz, J. R., "Radiative decay engineering 5: metal-enhanced fluorescence and plasmon emission", *Anal. Biochem.*, 2005, **337**, 171-194.

31. Neumann, T., Johansson, M. L., Kambhampati, D. and Knoll, W., "Surface-Plasmon Fluorescence Spectroscopy", *Adv. Funct. Mater.*, 2002, **12**, 575-586.

32. Du, H., Disney, M. D., Miller, B. L. and Krauss, T. D., "Hybridization-Based Unquenching of DNA Hairpins on Au Surfaces: Prototypical "Molecular Beacon" Biosensors", *J. Am. Chem. Soc.*, 2003, **125**, 4012-4013.

33. Du, H., Strohsahl, C. M., Camera, J., Miller, B. L. and Krauss, T. D., "Sensitivity and Specificity of Metal Surface-Immobilized "Molecular Beacon" Biosensors", *J. Am. Chem. Soc.*, 2005, **127**, 7932-7940.

34. Sha, M. Y., Yamanaka, M., Walton, I. D., Norton, S. M., Stoermer, R. L., Keating, C. D., Natan, M. J. and Penn, S. G., "Encoded Metal Nanoparticle-Based Molecular Beacons for Multiplexed Detection of DNA", *Nanobiotechnology*, 2005, **1**, 327-336.

35. Stoermer, R. L. and Keating, C. D., "Distance-Dependent Emission from Dye-Labeled Oligonucleotides on Striped Au/Ag Nanowires: Effect of Secondary Structure and Hybridization Efficiency", *J. Am. Chem. Soc.*, 2006, **128**, 13243-13254.

36. Fearns, R., Peeples, M. E. and Collins, P. L., "Mapping the Transcription and Replication Promoters of Respiratory Syncytial Virus", *J. Virol.*, 2002, **76**, 1663-1672.

37. Jairath, S., Brown Vargas, P., Hamlin, H. A., Field, A. K. and Kilkuskie, R. E., "Inhibition of respiratory syncytial virus replication by antisense oligodeoxyribonucleotides", *Antiviral Res.*, 1997, **33**, 201-213.

38. Xu, Z., Kuang, M., Okicki, J. R., Cramer, H. and Chaudhary, N., "Potent inhibition of respiratory syncytial virus by combination treatment with 2-5A antisense and ribavirin", *Antiviral Res.*, 2004, **61**, 195-206.

39. Player, M. R., Barnard, D. L. and Torrence, P. F., "Potent inhibition of respiratory syncytial virus replication using a 2-5A-antisense chimera targeted to signals within the virus genomic RNA", *Proc. Natl. Acad. Sci. USA*, 1998, **95**, 8874-8879.

40. Storhoff, J. J., Elghanian, R., Mirkin, C. A. and Letsinger, R. L., "Sequence-Dependent Stability of DNA-Modified Gold Nanoparticles", *Langmuir*, 2002, **18**, 6666-6670.

41. Liu, W.-T., Guo, H. and Wu, J.-H., "Effects of Target Length on the Hybridization Efficiency and Specificity of rRNA-Based Oligonucleotide Microarrays", *Appl. Environ. Microbiol.*, 2007, **73**, 73-82.

CHAPTER III

DETECTION OF RESPIRATORY SYNCYTIAL VIRUS USING NANOPARTICLE AMPLIFIED IMMUNO-PCR

The most important cause of severe respiratory illness in young children and infants is respiratory syncytial virus (RSV). RSV is the major cause of infantile bronchiolitis and the most frequent cause of hospitalization of infants and young children in industrialized countries.[1] In the United States, RSV is estimated to account for over 125,000 infant hospitalizations for bronchiolitis or pneumonia per year.[2] Although not fatal to the majority of patients, RSV can be deadly in immuno-compromised populations, and in the U.S., RSV is responsible for 10,000 deaths annually in patients over the age of 65.[3, 4] Additionally, naturally acquired immunity to RSV is not complete, and recurrent infection can be frequent.[5-7]

Early attempts at developing a formalin-inactivated RSV vaccine were hindered by an increase in disease severity upon subsequent infection of vaccinated patients.[8-10] Because of such problems, there is no approved vaccine for RSV.[11] Without a vaccine, treatment is typically limited to prophylactic passive immunization with neutralizing humanized monoclonal antibodies (palivizumab) or antivirals (ribavirin).[5, 12] The cost associated with monthly prophylactic passive immunization is expensive, so it typically is only utilized in premature or other high-risk infants.[12, 13] Additionally, these prophylactic treatments have been associated with adverse outcomes in infants with cyanotic cardiac disease.[5] Another option, antivirals, is only effective when used early in the course of infection, making early detection crucial.[14]

Although a median infective dose (ID_{50}) for RSV has not been established in humans, one clinical study showed that as few as 120 to 440 plaque forming units (PFU) in two milliliters of Hank's balance salt solution caused an infection in 83% of healthy adult volunteers.[15, 16] Another study using a temperature sensitive mutant RSV vaccine infected children with a dose as low as 27 PFU.[17] These are likely overestimates since as the RSV strain is passaged in laboratory culture, it is thought to become attenuated and that the dose of wild RSV actually required to infect an infant likely is even less than 20 PFU.[18]

With the knowledge that treatment is most effective early in the course of an infection, and that even relatively few PFUs can result in infection, it is clear that sensitive diagnostics for RSV are essential for effective treatment. Current methods for the detection of RSV include cell culture, serology and direct antigen detection. Each of these has limitations. Cell culture methods are hindered by extended observation times of up to ten days and required expertise.[19, 20] Serology based methods, which look for antibodies in response to an infection, are difficult to interpret when dealing with reoccurring infections. Many direct antigen detection strategies suffer from a lack of sensitivity; and those that are highly sensitive, such as nanoparticle magnetic resonance imaging, usually require additional, often expensive, equipment that is not typically present in a clinical setting.[21]

Direct antigen detection which detects the virus, or at least a specific protein on the virus, are often not sensitive enough to detect the early stages of infection where viral titers are expected to be low.[22] Enzyme-linked immunosorbent assays (ELISA) are an example of a rather insensitive direct antigen detection diagnostic.[23] However, ELISAs

are still common tools because of their simplicity in sample preparation and processing. Immuno-Polymerase Chain Reaction (I-PCR) offers processing similar to ELISA while coupling the sensitivity of PCR.[24] Additionally, the equipment and expertise to perform both ELISA and PCR are typically available in clinical laboratories.

To date, one of the most sensitive diagnostics available for the detection of RSV has been the use of RT-PCR to amplify and detect RSV genetic material.[25, 26] However, detection of the negative-sense RNA genome or mRNA of the virus comes with a few drawbacks. First, RNA is very sensitive to degradation by RNases and typically has a shorter half-life than proteins.[27, 28] This, in turn, places increased importance on preparation, pre-assay handling and storage of samples for RT-PCR diagnostics.[29] Secondly, studies have shown that RSV mRNA expressed during infection is cyclical and can limit the amount of mRNA present to detect at any given time; however, the surface fusion protein (F-protein) increases monotonically over time.[30] Further, the link between RT-PCR viral load and disease severity has yet to be established.[26] In contrast, an I-PCR based diagnostic for the detection of RSV comes with two inherent strengths. First, empty viral nucleocapsids can be detected because only the presence of a specific protein is required for a positive result.[31] Even fragments of cell wall that have the protein of interest expressed can be detected. Secondly, each virion contains only a single copy of RSV genomic RNA, but the protein targets are often expressed at a higher copy number, each one of which can act as a potential target.[32]

I-PCR has been modified in a number of ways to strengthen various aspects of the assay. Different antibody-DNA linking strategies have been used; from streptavidin-protein A coupling, to strictly streptavidin-biotin coupling, and even phage display

mediated I-PCR (PD-IPCR), where a single chain variable fragments are displayed on the phage and phage DNA itself acts as a DNA tag.[24, 32-34] Capture antibodies have been bound to biogenic magnetosome nanoparticles (M-IPCR) instead of protein binding plates to enhance signal generation.[35] Biotinylated DNA-streptavidin nanostructures have been used to increase the valency of the antibody binding, and in turn increase the sensitivity of I-PCR.[36] However, these studies utilized an average DNA/complex ratio of only 5, as increased DNA ratios resulted in instability of the streptavidin conjugates.[36] An I-PCR related method, the bio-barcode assay, has even been developed which utilizes nanoparticles as a scaffold to attach multiple DNA tags per antibody construct and avoids the use of PCR amplification altogether.[37]

In this work, we developed a Nanoparticle Amplified Immuno-PCR (NPA-IPCR) assay for the detection of RSV (**Figure 22**). The diagnostic assay offers amplification through two means to improve the limit of detection of a traditional ELISA. Amplification of signal is achieved both by using multivalent gold nanoparticles (AuNPs) to release multiple strands of DNA per binding event and through the use of real-time PCR to amplify released DNA. Additionally, the assay utilizes magnetic microparticles (MMPs) to capture antigen for improved washing to enable better target extraction. Our results suggest that the NPA-IPCR assay not only offers >1000-fold improvement in limit of detection over ELISA, but also a 4-fold improvement over detection via real-time RT-PCR.

Experimental

Coupling of Antibodies to Magnetic Microparticles. MagnaBind™ amine derivatized 1 μm magnetic microparticles (product #21352, Pierce Biotechnology) were activated with sulfosuccinimidyl-4-[N-maleimidomethyl]cyclohexane-1-carboxylate (Sulfo-SMCC). In a typical reaction, 200 μL of MMPs were washed three times with coupling buffer (CB) consisting of 50 mM phosphate buffer (pH 7.0), 0.15 M NaCl and 5 mM EDTA. The MMPs were then cleared from the suspension using a magnet. After 1 min, the solution became clear and MMPs were pulled to the side of the tube. When the clear supernatant and the external magnetic field were removed, the MMPs were resuspended in CB. After washing, the MMPS were activated with 20 μL of 1 mM Sulfo-SMCC. The solution was mixed and allowed to sit at room temperature for 1 hr. The MMPs were then washed 3 times to remove excess Sulfo-SMCC.

Antibody reduction was coordinated so that once the MMPs were activated, they could be immediately used. Dithiothreitol (DTT) was used to reduce anti-RSV fusion protein antibodies (clones 1269 and 1214). 15 μL of 1.2 mM DTT was added to 15 μL of purified antibodies at 30 mg/mL in phosphate buffered saline (PBS). The solution was mixed and allowed to sit at room temperature for 0.5 hr. After that time, the antibodies were separated from DTT using a NAP-5 column (product #17-0853-01, GE Healthcare Bio-Sciences Corp.). The activated MMPs were combined with the column-purified reduced antibodies and allowed to react for 1 hr at room temperature. The conjugation was quenched by the addition of β-mercaptoethanol to a final concentration of 100 μM.

After 1 hr quenching, the MMPs were washed three times with PBS and then resuspended in a final volume of 300 μL.

Coupling of Antibodies and DNA to Gold Nanoparticles. Thiolated DNA sequences (Biosearch Technologies) were received as disulfides and were activated by cleaving the disulfide bond. Cleavage was performed in 100 mM DTT, 0.1 M phosphate buffer, pH 8.3. After 0.5 hr, thiolated DNA was desalted using Microcon YM-3 centrifugal filters (product #4410, Millipore). The purified DNA was resuspended in TE buffer and stored in small aliquots at -80°C.

In a typical reaction, 35 μL of 0.2 mg/mL Synagis® antibody (humanized monoclonal antibody known to target the A antigenic site of RSV's fusion protein, product #NDC 60574-4114-1, MedImmune, Inc.) were added to 10 mL of 2.3 nM, 15 nm diameter AuNPs (product #15704-1, Ted Pella) at pH 9.3 and placed on a rotator for 0.5 hr.

Then, 50.8 μL of 107 μM activated DNA (Comp_55, **Table 2**) was added; the AuNPs were then rotated for another 0.5 hr. The solution was brought to 0.1 M NaCl, 10 mM phosphate buffer, and 0.02% Tween20 and allowed to sit for 1 hr. After this time, the concentration of NaCl was brought to 0.2 M and to 0.3 M after a third hour. Excess DNA was removed by centrifuging the solution for 20 minutes at 21,100 x gravity. The clear supernatant was then removed, and the red oily pellet was resuspended in a stock solution of 0.3 M NaCl, 10 mM phosphate buffer and 0.02% Tween20 (PB). This washing process was repeated three times. After washing, particles were resuspended, and Tag DNA (Tag_76, **Table 2**) was added to bring the molar ratio of Tag DNA:AuNPs

Table 2. Oligonucleotide sequences used in NPA-IPCR studies.

Name	Sequence 5´ → 3´
Comp_55	[C6Thiol]TTTTTTTTTTTTTTTGCTTGTCTCGTAAGTTGAGATTTCGCTATGCA CGGTCCTT
Tag_76	CTGCGACGATCTACCATCGACGTACCAGGTCGGTTGAAGGACCGTGCATAGC GAAATCTCAACTTACGAGACAAGC
Tag Primer 1	CTGCGACGATCTACCAT
Tag Primer 2	GCTTGTCTCGTAAGTTGA
RSV Primer 1	GCTCTTAGCAAAGTCAAGTTGAATGA
RSV Primer 2	TGCTCCGTTGGATGGTGTATT

to 200:1. The solution was allowed to sit at room temperature overnight. Finally, excess Tag DNA was removed using the washing method described above.

Preparation of RSV Infected Cell Lysate. HEp-2 cells (product #CCL-23, American Type Culture Collection) were cultured in OPTI-MEM media supplemented with 2% fetal bovine serum, 250 μg/mL of amphotericin-B, 10 mg/mL gentamicin and 200 mM L-glutamine and incubated at 37˚C with 5% CO_2. RSV stock was prepared by infecting a confluent T-150 flask of HEp-2 cells with RSV strain A_2. Infection was performed with rapidly thawed virus diluted to 5 mL in cell media. Following the initial infections, cells were incubated for 1 hr after which 35 mL of cell media was added to the flask. The infection was allowed to proceed for 4 days, after which cells were scraped from the surface of the T-150 flask. The supernatant containing the cells was collected in a 50 mL centrifuge tube and centrifuged for 5 min at 500 x gravity. Following removal of the supernatant, the cell pellet was resuspended to 5 mL in cell media. The cells were then frozen using a slurry of ethanol and dry ice in order to lyse cells and release virus particles. After freezing, the cells were thawed in a 37 °C water bath. The freezing/thawing cycle was repeated three times to ensure the release of virus particles from the cell wall. After the third cycle, the cells were centrifuged at 100 x gravity for 5

min to pellet large cellular debris. The supernatant was then separated into aliquots of 0.5 mL and stored at -80°C.

Antibody-Magnetic Microparticle Characterization Experiment. Pulldown experiments were performed to validate the attachment of antibodies to magnetic microparticles (MMPs). 10 µL of antibody-conjugated MMPs, 100 µL of a stock solution of RSV (1.675×10^6 PFU/mL) and 100 µL 4% bovine serum albumin (BSA, product #A3059-100G, Sigma) were mixed and placed on a rotator for 2 hr. Unbound virus was then removed from the MMPs by cleaning as previously described in the antibody-MMP coupling reaction; this was done three times. Next, the MMPs were mixed with 100 µL of 2% BSA containing 12 µg/mL of F-mix antibody with a 655 nm quantum dot (QD) attached to the antibody. The solution was stirred and placed on a rotator for 2 hr; unbound quantum dot-coupled antibodies were removed by cleaning the beads three times. After cleaning, the MMP-RSV-QD complexes were placed in a 96-well plate on a BioMag® 96-well Plate Side Pull Magnetic Separator (product #85072, Polysciences, Inc.) and imaged on a Zeiss Axiovert 200 inverted fluorescence microscope.

Validation of DNA-Gold Nanoparticle Functionalization. Antibodies and activated DNA (Comp_55, **Table 2**) were attached to AuNPs following the procedure stated above. After the removal of excess activated DNA, Tag DNA (Tag_76, **Table 2**) was added to the AuNPs. As a control, Tag DNA was also added to PB without AuNPs. The amount of complementary DNA added to 100 µL of AuNPs or PB was varied to determine the optimal molar ratio of Tag DNA:AuNPs for hybridization. After sitting at room temperature for 24 hr, the solution was centrifuged for 0.5 hr at 16,100 x gravity to

pellet the AuNPs and Tag DNA hybridized to them. 90 μL of supernatant was removed from both AuNP and PB samples. The absorbance at 260 nm of the supernatant was then obtained on an Agilent 8453 UV-Vis spectrophotometer to determine the difference between samples incubated with and without AuNPs.

To verify the release of Tag DNA upon heating, antibody-CompDNA-AuNPs prior to Tag DNA hybridization and post Tag DNA hybridization were compared. Samples were heated to 95ºC for 10 min then centrifuged at 21,100 x gravity for 15 min. The supernatant was then examined by measuring the absorbance at 260 and 280 nm.

Quartz Crystal Microbalance Validation of Antibody-Gold Nanoparticle Attachment. All quartz crystal microbalance (QCM) experiments were performed on a Maxtek, Inc. Research Quartz Crystal Microbalance with a flow rate of 30 μL/min. The crystals used were 5 MHz Ti/Au quartz crystals. After equilibrating for 0.5 hr in PBS, a 5 minute PBS baseline was obtained. A RSV stock solution containing 4.0×10^5 PFU/mL was then flowed over the crystal for 10 min, followed by an additional five minutes of PBS. After RSV binding, non-specific binding was blocked using a 1% BSA solution flow over the crystal for 10 min followed by 10 min of PBS. At this point, the flow was switched to either AuNPs functionalized with anti-RSV antibodies and DNA or, as a control, AuNPs functionalized with DNA alone.

Nanoparticle Amplified Immuno-PCR (NPA-IPCR). Pulldown experiments used 5 μL of antibody-conjugated MMPs, 100 μL of infected cell lysate at the desired dilution and 200 μL of 5% BSA. A stock solution of RSV infected HEp-2 cell lysate (8.33×10^6 PFU/mL) was serially diluted 10-fold to determine the lower limit of detection. The MMPs, virus, and BSA solution were mixed and placed on a rotator for 1 hr. Unbound

virus was then removed from the MMPs by cleaning as previously described. After three washes, the MMPs were mixed with 5 μL of 5 nM antibody-DNA functionalized AuNPs and 300 μL of 5% BSA and placed back on the rotator for 1 hr. The MMPs were then washed two times in 5% BSA followed by three additional washes in PBS. After the final wash, MMPs were resuspended in 300 μL of nuclease-free water. Solutions were then held at 95°C for 10 min followed by placement in an external magnetic field and removal of 100 μL of supernatant. The supernatant was then analyzed via PCR.

Real-time PCR was performed using a Rotor-Gene Q 5-Plex thermal cycler system (Qiagen, Alameda, CA). Reactions were done in a 25 μL volume with 12.5 μL of 2X Rotor-Gene SYBR Green PCR Master Mix (product #204074, Qiagen), 200 nM left and right primers (Tag primers, **Table 2**), nuclease-free water and 5 μL of sample. DNA polymerase activation was performed 95°C for 3 min and 40 cycles of 95°C for 15 sec to denature, 60°C for 60 sec to anneal and extend, and 72°C for 15 sec to detect fluorescence. Following amplification, a melt curve from 50°C to 99°C was performed. The limit of detection was then determined using the assay's linear range to calculate 3 standard deviations above background.

ELISA. To allow capture antibodies to bind to the Costar UV microtiter plate (product #3635, Corning), 100 μL of 10 μg/mL F-mix antibodies were added the 96-well plate and allowed to incubate at room temperature for 1 hr. After 1 hr, the wells were rinsed 3 times with PBS and blocked with 5% BSA in PBS for 1 hr. A stock solution of RSV infected HEp-2 cell lysate (8.33×10^6 PFU/mL) was serially diluted 3-fold to determine the lower limit of detection. Following blocking, BSA was removed from the wells and 100 μL of infected cell lysate at the desired dilution was added. The plate was

then incubated at room temperature for 1 hr. Following antigen binding, the wells were rinsed 3 times with PBS and 100 μL of 10 μg/mL of Synagis antibodies diluted in 5% BSA were added to each well. Once again, the plate was incubated at room temperature for 1 hr. The wells were then rinsed 3 times with PBS and 100 μL of a 1:1000 dilution in 5% BSA of goat anti-human HRP conjugated secondary antibodies (product #2010-05, Southern Biotech) were added to each well. Following 1 hr incubation at room temperature, the wells were rinsed 5 times with PBS. Next, 100 μL of TMB One Solution (product #G7431, Promega), was added to each well and the enzymatic reaction was allowed to proceed for 10 minutes, after which it was quenched with 100 μL of 2 M H_2SO_4. Finally, absorbance at 450 nm was measured using a Bio-Tek Synergy HT microplate reader. The limit of detection was then determined using the assay's linear range to calculate 3 standard deviations above background.

RNA Isolation and Real-Time Reverse Transcription PCR (Real-Time RT-PCR). An RNeasy Mini Kit (product #74104, Qiagen) was used for RNA isolation. 300 μL of cell lysate was mixed with 400 μL lysis buffer (RLT) and homogenized by passing the sample through a 20 gauge needle 8 times. 700 μL of 70% was then added to the sample, and it was bound to an RNeasy spin column. On the column, DNA was digested using an RNase-Free DNase Set (product #79254, Qiagen). The remaining RNA was then washed with the appropriate buffers (RW1 and RPE). After washing, the RNA was eluted in 50 μL of nuclease-free water, and analyzed via real-time RT-PCR.

Real-time RT-PCR was performed using a Rotor-Gene Q 5-Plex thermal cycler system (Qiagen, Alameda, CA). Reactions were done in a 25 μL volume with 12.5 μL of 2X One-Step qRT-PCR Buffer plus SYBR (product #639518, Clontech), 0.5 μL of 50X

QTaq DNA Polymerase Mix (product #639518, Clontech), 0.4 μL of 60X qRT Mix (product #639518, Clontech), 200 nM left and right primers (RSV primers, **Table 2**), nuclease-free water and 5 μL of sample. Reverse transcription was performed at 48°C for 20 min followed by an initial QTaq DNA polymerase activation step of 95°C for 3 min and 40 cycles of 95°C for 15 sec to denature, 60°C for 60 sec to anneal and extend, and 72°C for 15 sec to detect fluorescence. Following amplification, a melt curve from 50°C to 99°C was performed. The limit of detection was then determined using the assay's linear range to calculate 3 standard deviations above background.

Results and Discussion

To detect the antigen captured by MMPs, hybrid antibody-DNA probes were designed utilizing AuNPs to provide inherent amplification through antibody-tag DNA valency. The AuNP acts as a scaffold to associate antibody recognition with a multiple DNA tags of a specific sequence. Nanoparticles, specifically gold nanoparticles, were chosen because they are biologically compatible, provide a large surface area on which to couple multiple probes and allow the use of gold-thiol chemistry.[38-41] Recently, AuNPs have been co-functionalized with antibodies and DNA for a number of applications.[37, 42, 43] The 15 nm AuNPs used in this study were functionalized with Synagis® antibodies (humanized monoclonal antibodies targeted to the RSV fusion protein) to bind to antigen captured by the MMPs. The AuNPs were also functionalized with thiolated strands of DNA (Comp_55, **Table 2**) to provide a covalently attached DNA bonding site to which reporter DNA (Tag_76, **Table 2**) can be hybridized. The resulting AuNP contains both a

recognition component (Synagis®) and a signal generating component (Tag_76) which is released upon heating. In the presence of antigen, the MMPs and AuNPs form a "sandwich" which can easily be separated from unbound AuNPs and cell debris using a magnetic field (**Figure 22**). After washing, the Tag DNA of bound AuNPs is released and analyzed via PCR to detect the presence of antigen.

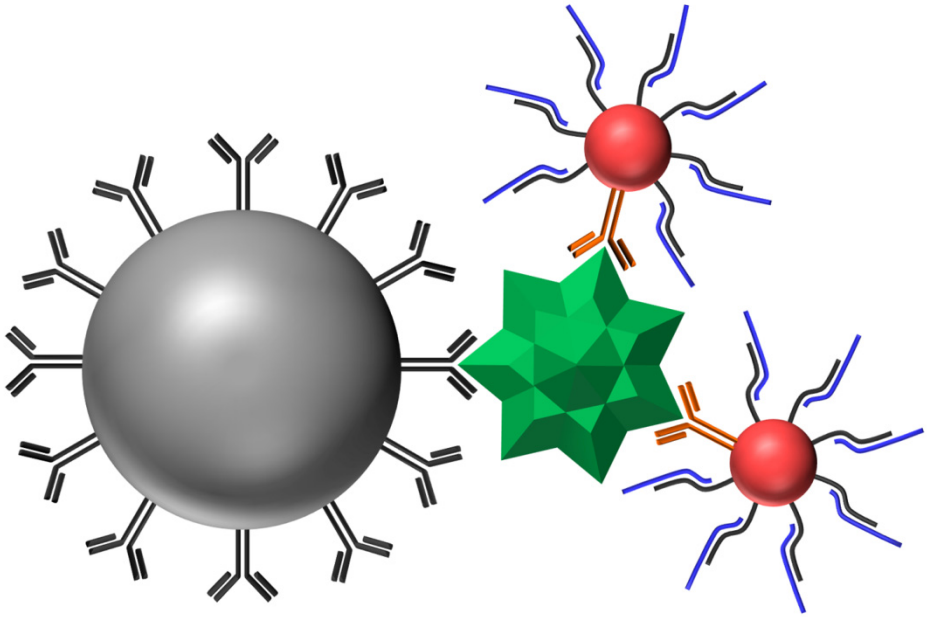

Figure 22. Illustration of the imunno-nanoparticle-PCR sandwich. RSV antigen (green) is captured and separated using antibody functionalized 1 μm magnetic microparticles (gray). The magnetic bead-antigen complex is then reacted with antibody-DNA functionalized 15 nm AuNPs (red). Upon heating, hybridized DNA (blue) is released from the AuNPs and is analyzed via real-time PCR.

The protein targeted in the designed assay, the F-protein of RSV, is a surface protein often targeted in direct antigen detection diagnostics because it is highly conserved between different strains of RSV. Published studies have shown that the F-protein of RSV has over 80% homology between different serotypes.[44] Initially, virus in the analyte solution is captured using anti-F protein antibodies functionalized to MMPs.

MMPs were chosen as the capture antibody scaffold for three reasons. First, attaching the antibodies to a microparticle as opposed to a microtiter plate allow for more thorough sampling of the analyte solution. Secondly, MMPs allow for more thorough washing of captured antigen and AuNPs to decrease non-specific binding and reduce the background signal, which tends be a major drawback of I-PCR.[45] Finally, the use of MMPs allows for ease of downstream automation in future applications.

Magnetic Microparticle Pulldown of RSV Cell Lysate. After attachment to MMPs, anti-RSV antibodies remain functional and effectively capture F-protein on RSV-infected cell lysates. To verify the functional attachment of anti-RSV antibodies to the MMPs, a pulldown experiment was performed. After conjugation of F-mix antibodies to the MMPs, the functionalized MMPs were added to RSV-infected cell lysate. An external magnetic field was used to extract captured virus. Captured RSV was labeled by the addition of F-mix antibodies coupled to fluorescent 655 nm quantum dots. Unbound quantum dots were removed by applying a magnetic field and washing. After washing, the MMPs were imaged with a fluorescent microscope (**Figure 23**). As a control, non-functionalized MMPs were exposed to RSV, followed by pulldown and addition of antibodies coupled to quantum dots. **Figure 23A** shows the fluorescence image from this experiment which contains negligible fluorescence. In **Figure 23B**, the fluorescence was generated by the presence of the fluorescent quantum dot bound to the MMP-RSV complexes. Formation of these complexes confirms that the antibodies remain functional after attachment to MMPs. Examining the average pixel intensity over the entire fluorescence images revealed that the functionalized MMPs (33.9 average pixel intensity) generated 10-fold greater fluorescence over the control MMPs (3.2 average pixel

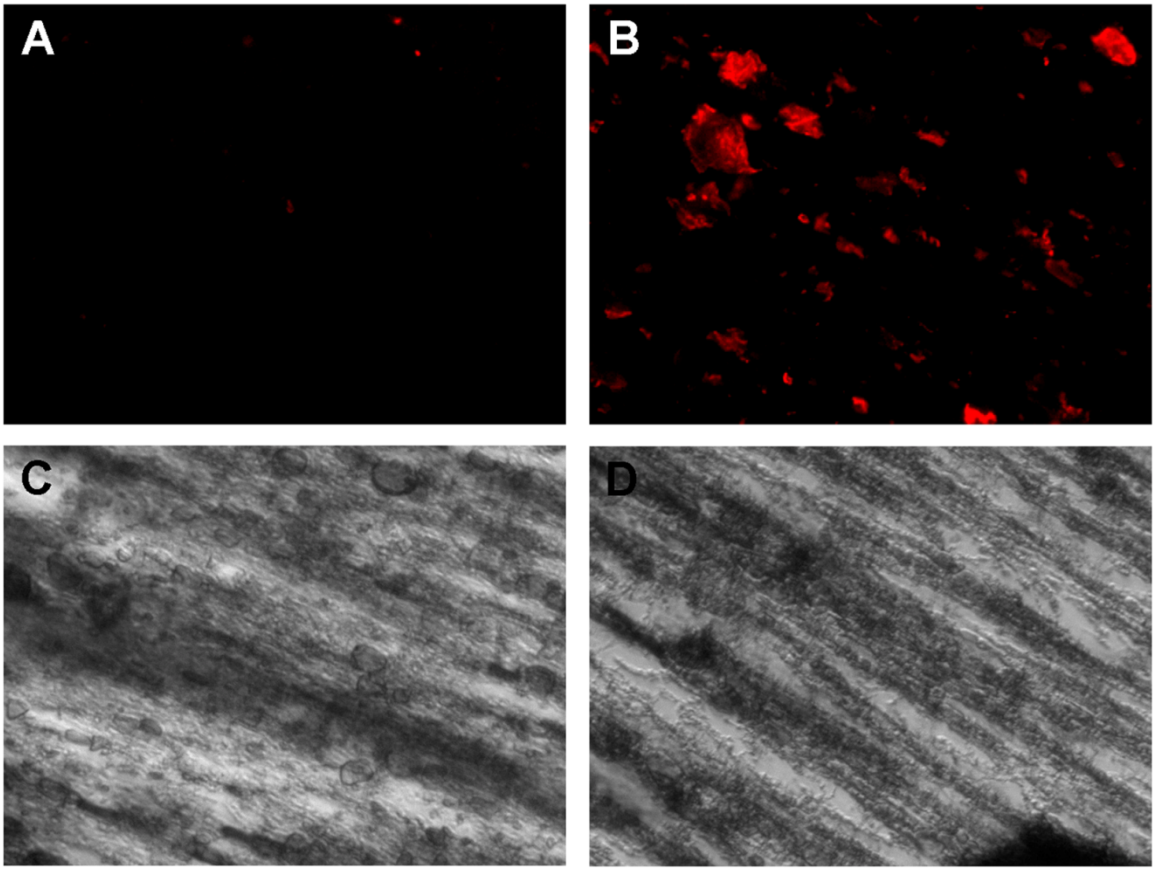

Figure 23. Images of MMP-virus-QD complexes after magnetic pulldown experiments in RSV. A mixture of MMPs unconjugated (left panels) or conjugated (right panels) to F-mix antibodies and 655 nm quantum dots conjugated to F-mix antibodies were mixed with RSV. Magnetic particles and associated complexes were extracted and washed. A) and C) Fluorescence and DIC images of unconjugated MMPs; B) and D) Fluorescence and DIC images of MMPs conjugated to F-mix antibodies. The striated patterns in the DIC images are thought to be due to the accumulation of MMPs along magnetic field lines. All images are 20x magnification.

intensity). DIC images (**Figure 23C** and **23D**) both revealed striations due to the MMPs lining up when a magnetic field was applied in the bottom right corner of both images.

Tag DNA-Gold Nanoparticle Functionalization. Cofunctionalization of tag DNA and anti-RSV antibodies on 15 nm AuNPs offer a valency of up to 70 to 1. To determine the number of Tag DNA molecules bound per AuNP, Tag DNA was incubated with samples containing antibody-CompDNA-AuNPs or a PB control. Following incubation, both the sample and control were centrifuged to pellet AuNPs and any Tag DNA

hybridized to them. The absorbance at 260 nm was then used to determine the amount of unbound Tag DNA in each supernatant. These studies revealed that saturation of the AuNPs with Tag DNA, ~70 strands per particle, occurred when Tag DNA was incubated at a molar ratio ≥ 400:1 of Tag DNA:AuNP (**Figure 24**). However, a much lower

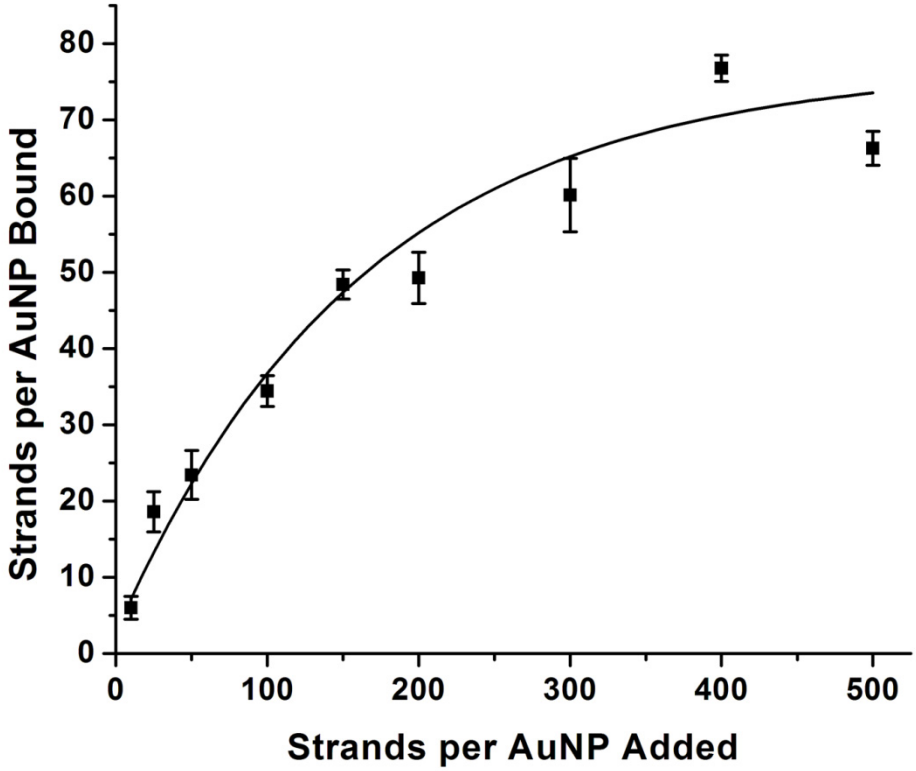

Figure 24. Number of strands of Tag DNA bound per particle versus number of strands of Tag DNA added per particle. Data shown as the mean ± S.D. (n = 3).

concentration, 200:1, still allowed for the hybridization of ~50 strands per particle, which is the concentration that was used in subsequent experiments. To verify the release of Tag DNA upon heating, antibody-CompDNA-AuNPs prior to Tag DNA hybridization and post Tag DNA hybridization were compared. The supernatant of pre-hybridized conjugates after heating revealed that a small amount of Comp DNA had been released

from the AuNP, approximately 9 ± 1.3 strands per AuNP. The post-hybridized supernatant had a much higher concentration of DNA. After subtracting out the absorbance from the Comp DNA that was released, it was determined that approximately 38 ± 0.9 strands of Tag DNA per AuNP was released upon heating. Additionally, the 260/280 absorbance ratio of the samples remained unchanged, assuring that the difference between samples was not due to the release of coupled antibodies.

QCM Validation of Antibody-Gold Nanoparticle Attachment. Upon functionalizing AuNPs with F-mix antibodies, their affinity for RSV greatly increases as compared to AuNPs conjugated to DNA alone (**Figure 25**). RSV was bound via hydrophobic interactions to the gold electrode of a quartz crystal microbalance (QCM). This was followed by washing and blocking steps. AuNPs functionalized with antibodies

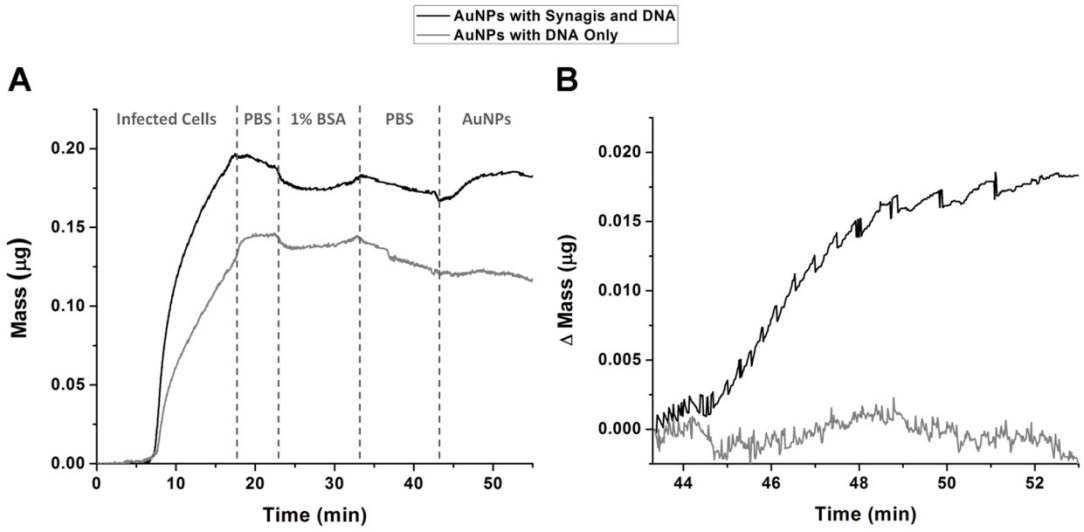

Figure 25. QCM validation of AuNP binding. Mass change of RSV exposed to AuNPs functionalized with either DNA alone (gray) or DNA and Synagis antibodies (black). A) Entire experiment showing total mass bound upon flowing RSV onto the quartz crystal, followed by a PBS wash, blocking with 1% BSA, a second PBS wash, and finally functionalized AuNPs. B) The change in mass upon flowing functionalized AuNPs over the blocked and washed RSV infected cells.

and DNA were then flowed over the crystal and into contact with any bound RSV. The binding of AuNPs to RSV resulted in a change of the crystal's resonance frequency. The degree of this change in frequency was used to determine the amount of mass bound to the crystal. When antibody-DNA-AuNPs flowed along the crystal, binding occurred and can be observed by the 0.19 μg increase in mass detected by the microbalance (**Figure 25B**). However when DNA-AuNPs which were not functionalized with antibodies were flowed along the crystal, no significant change in mass was observed (**Figure 25B**). Although the channel on which DNA-AuNPs were flowed had less binding of infected cells, this did not affect the outcome of the results. If the results are normalized to the mass of infected cells bound, the addition of antibody-DNA-AuNPs give an increase of 9.93% while DNA-AuNPs actually give a decrease of 0.26%. By comparing the addition of AuNPs with conjugated antibodies and DNA to the addition of AuNPs with DNA only, it is apparent that not only do antibodies coupled to the AuNP facilitate binding to RSV but also that AuNPs with DNA alone have very little non-specific binding to RSV, as evident by no change in mass under control conditions.

Nanoparticle amplified immuno-PCR Detection of RSV. Nanoparticle amplified immuno-PCR delivered >10,000 times more tag DNA to PCR analysis in RSV infected samples than uninfected control samples. Evaluation of the NPA-IPCR assay was performed on RSV infected HEp-2 cell lysates and compared to uninfected HEp-2 cell lysates and PBS (**Figure 26**). It is clear that there is a distinct shift in cycle threshold (C_t) between infected cells and both control samples. The RSV samples, 8.3 x 10^6 PFU/mL, had an average C_t value of 8.49 while uninfected cells and PBS were much later, 21.9 and 22.1 respectively. Additionally, it is important to note that both the uninfected cells and

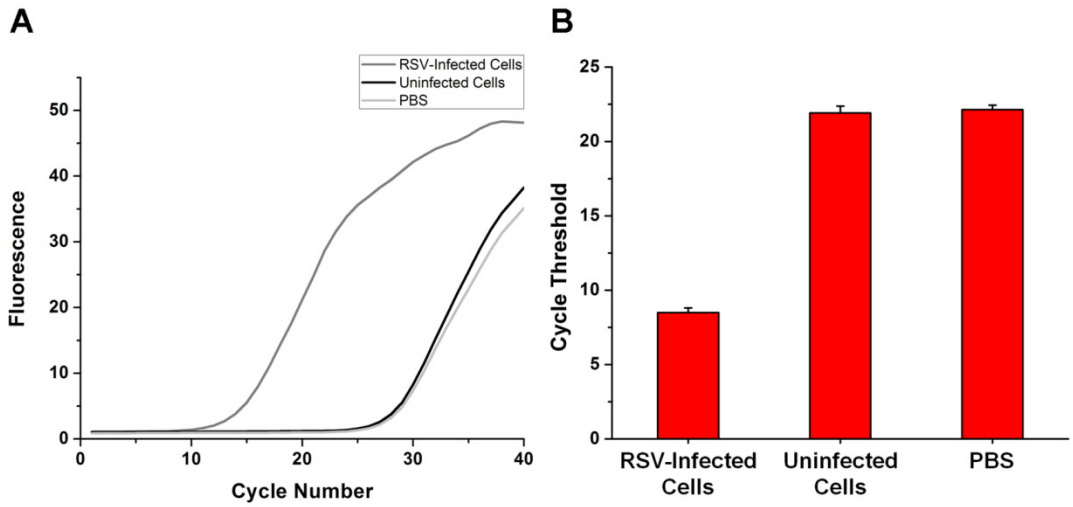

Figure 26. RSV detection via nanoparticle amplified immuno-PCR. A) Real-time PCR results of NPA-IPCR performed on RSV-infected HEp-2 cell lysates, uninfected HEp-2 cell lysates and PBS. B) Comparison of the cycle thresholds of the same experiment. Data shown as the mean ± S.D. (n = 3).

PBS have amplification; however, they cross the cycle threshold later because there is a lower initial concentration of Tag DNA present in the uninfected and PBS samples. This inherent background in I-PCR assays limits the sensitivity of this approach.[46]

To determine the lower limit of detection for NPA-IPCR, infected cells lysates were serially diluted and then assayed. The same cell lysate stock was serial diluted and assayed via RT-PCR and ELISA. ELISA was performed using the same antibodies as NPA-IPCR, to offer a direct comparison highlighting the inherent amplification potential of NPA-IPCR. RT-PCR was performed using primers that target the N-gene because it is preferentially transcribed due to its location near the promoter; resulting in higher copy numbers than other transcripts.[26] In order to compare all three methods, the signal generated from each was normalized (**Figure 27**). The normalized signal is obtained by subtracting out noise of the assay and dividing each value by the response obtained at the highest virus concentration. Both NPA-IPCR and RT-PCR have a substantially lower

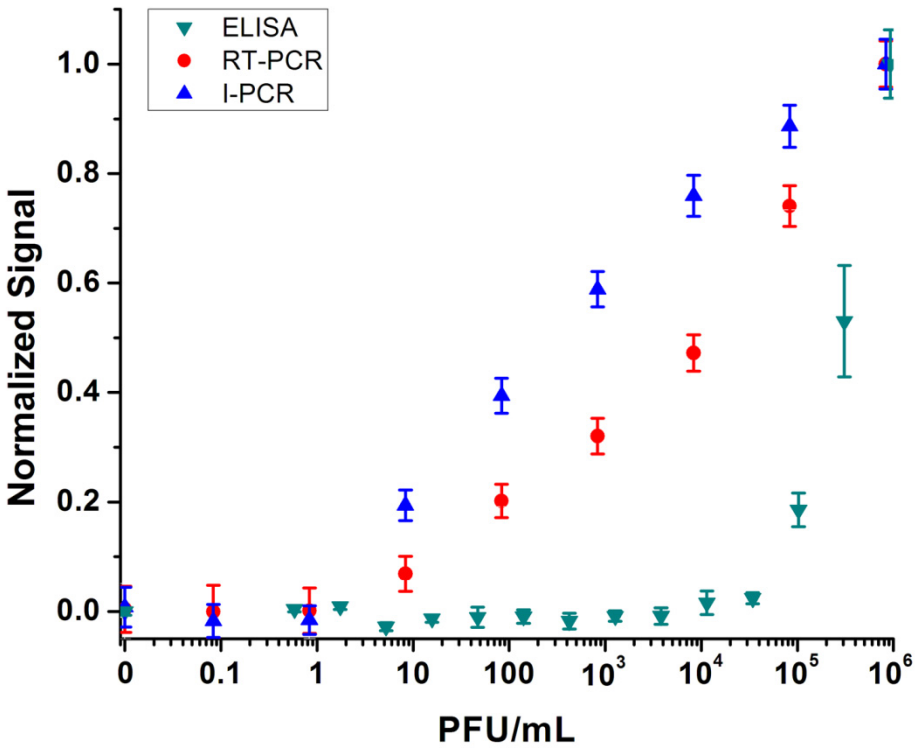

Figure 27. Detection of decreasing concentrations of RSV. Comparison of RSV detection using ELISA, real-time RT-PCR and the developed NPA-IPCR assay. Data shown as the mean ± S.D. (n = 3).

limit of detection than ELISA. The lower limit of detection for ELISA was 16,000 PFU/mL, while RT-PCR was 17.9 PFU/mL and NPA-IPCR was 4.1 PFU/mL. The limits of detection obtained for ELISA and RT-PCR in this study closely agree with previous studies and literature precedent (17,500 PFU/mL for ELISA and 14.13 PFU/mL for RT-PCR).[26, 47]

Although the dilution curves for NPA-IPCR and RT-PCR appear similar, the lower dilutions, shown in **Figure 28**, provide insight in determining why NPA-IPCR has a lower limit of detection than RT-PCR. At lower virus concentrations, ≤ 8.3 PFU/mL, RT-PCR has more variation between replicates. While both assays give an observable shift at 8.3 PFU/mL, only the NPA-IPCR is statistically above the limit of detection. The

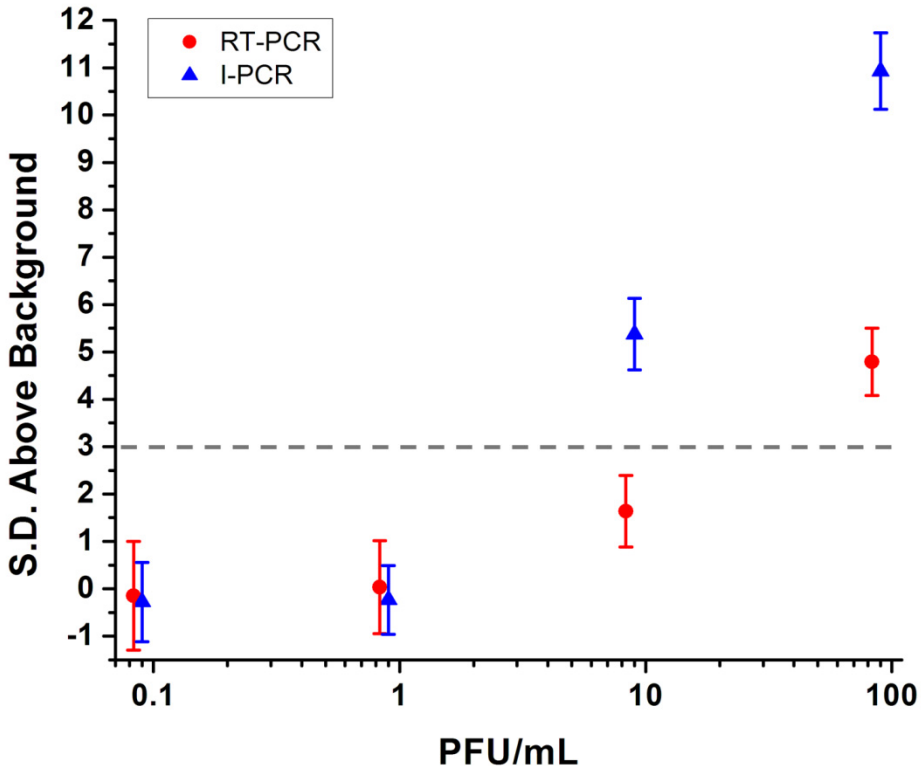

Figure 28. Detection of low concentrations of RSV. The number of standard deviations above background using both RT-PCR and NPA-IPCR at low virus concentrations. The gray dashed line shows a 3σ limit of detection. Data shown as the mean ± S.D. (n = 3). NPA-IPCR data has been shifted prevent overlapping with RT-PCR data.

variability between replicates is due in part to the amount of amplification that is required to reach the cycle threshold, but may also be due to other properties of PCR.[48] At a concentration of 8.3 PFU/mL, RT-PCR requires 29.1 cycles to reach the threshold while NPA-IPCR requires only 19.4 cycles. NPA-IPCR effectively moved the low concentration dilutions up 10 cycles, in turn reducing the amount of PCR-induced variation between replicates.

Both NPA-IPCR and RT-PCR have substantually different linear ranges than ELISA (**Figure 29**). Although the linear range of ELISA goes up to 3.1 x 10^5 PFU/mL, no response is generated at virus concentrations below 1.2 x 10^4 PFU/mL. On the other

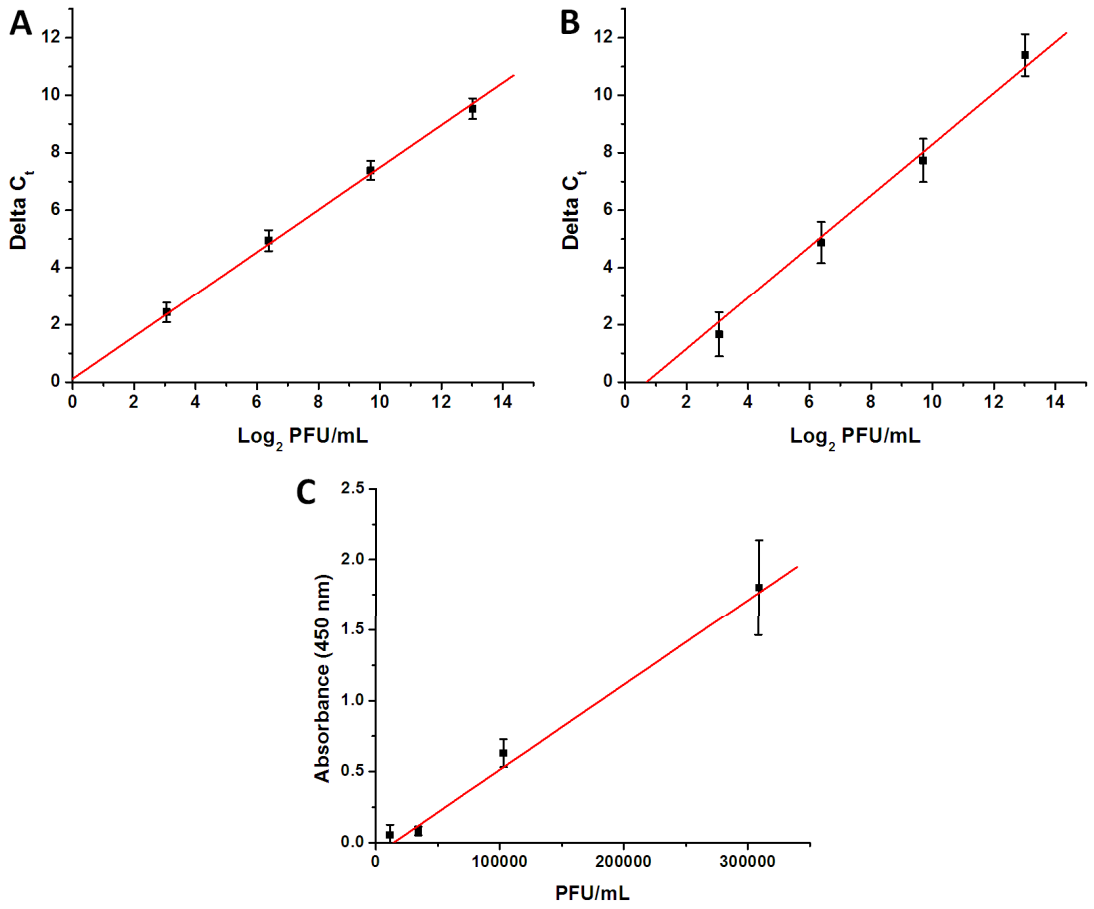

Figure 29. Linear ranges of the compared assays. Graphs showing the linear ranges of A) NPA-IPCR, B) RT-PCR, and C) ELISA.

hand, the linear ranges of NPA-IPCR and RT-PCR cover multiple orders of magnitude. NPA-IPCR is linear up to approximately 1.0 x 10^4 PFU/mL after wich saturation begins to occur. It is possible that adding higher concentrations of AuNPs could increase the viral titer at which saturation begins to occur. However, even under the current conditions, the linear range covers 4 orders of magnitiude. RT-PCR has a similar linear range to NPA-IPCR. While RT-PCR does not show saturation at high virus concentrations, the difference between C_ts at concentrations >1.0 x 10^4 PFU/mL no longer show a linear relationship with the Log_2 transformed virus concentration.

Conclusions

The nanoparticle amplified immuno-PCR assay offers highly sensitive detection of respiratory syncytial virus in HEp-2 cell lysates. The assay has a limit of detection better than RT-PCR detection of the RSV N-gene. The NPA-IPCR assay has a number of areas that could further lower the limit of detection. Larger AuNPs, such as 30 nm AuNPs, can be utilized to increase the surface area available for attaching Tag DNA. More strands of Tag DNA per AuNP would increase the number of tags released per binding event, increasing the pre-PCR amplification of the NPA-IPCR assay. Additionally, a large background signal is a significant obstacle of I-PCR assays, one that is present even in the nanoparticle-based assay.[45, 46] Steps such as stringency washes could be taken to reduce this background and further decrease the limit of detection. Although the NPA-IPCR still has room for improvement, it holds promise as a highly sensitive diagnostic.

Bibliography

1. Robert, C. W., "Review of epidemiology and clinical risk factors for severe respiratory syncytial virus (RSV) infection", *J. Pediatr.*, 2003, **143**, 112-117.

2. Shay, D. K., Holman, R. C., Newman, R. D., Liu, L. L., Stout, J. W. and Anderson, L. J., "Bronchiolitis-Associated Hospitalizations Among US Children, 1980-1996", *J. Am. Med. Assoc.*, 1999, **282**, 1440-1446.

3. Falsey, A. R. and Walsh, E. E., "Respiratory Syncytial Virus Infection in Elderly Adults", *Drug Aging*, 2005, **22**, 577-587.

4. Falsey, A. R., Hennessey, P. A., Formica, M. A., Cox, C. and Walsh, E. E., "Respiratory Syncytial Virus Infection in Elderly and High-Risk Adults", *N. Engl. J. Med.*, 2005, **352**, 1749-1759.

5. Hall, C. B., "Respiratory Syncytial Virus and Parainfluenza Virus", *New Engl. J. Med.*, 2001, **344**, 1917-1928.

6. Moore, E., Barber, J. and Tripp, R., "Respiratory syncytial virus (RSV) attachment and nonstructural proteins modify the type I interferon response associated with suppressor of cytokine signaling (SOCS) proteins and IFN-stimulated gene-15 (ISG15)", *Virol. J.*, 2008, **5**, 116.

7. Tripp, R. A., "Pathogenesis of Respiratory Syncytial Virus Infection", *Viral Immunol.*, 2004, **17**, 165-181.

8. Chin, J., Magoffin, R. L., Shearer, L. A., Schieble, J. H. and Lennette, E. H., "Field evaluation of a respiratory syncytial virus vaccine and a trivalent parainfluenza virus vaccine in a pediatric population", *Am. J. Epidemiol.*, 1969, **89**, 449-463.

9. Kapikian, A. Z., Mitchell, R. H., Chanock, R. M., Shvedoff, R. A. and Stewart, C. E., "An epidemiologic study of altered clinical reactivity to respiratory syncytial (RS) virus infection in children previously vaccinated with an inactivated RS virus vaccine", *Am. J. Epidemiol.*, 1969, **89**, 405-421.

10. Kim, H. W., Canchola, J. G., Brandt, C. D., Pyles, G., Chanock, R. M., Jensen, K. and Parrott, R. H., "Respiratory syncytial virus disease in infants despite prior administration of antigenic inactivated vaccine", *Am. J. Epidemiol.*, 1969, **89**, 422-434.

11. Kaur, J., Tang, R. S., Spaete, R. R. and Schickli, J. H., "Optimization of plasmid-only rescue of highly attenuated and temperature-sensitive respiratory syncytial virus (RSV) vaccine candidates for human trials", *J. Virol. Methods*, 2008, **153**, 196-202.

12. "Prevention of Respiratory Syncytial Virus Infections: Indications for the Use of Palivizumab and Update on the Use of RSV-IGIV", *Pediatrics*, 1998, **102**, 1211-1216.

13. Meissner, H. C., Bocchini, J. A., Jr., Brady, M. T., Hall, C. B., Kimberlin, D. W. and Pickering, L. K., "The Role of Immunoprophylaxis in the Reduction of Disease Attributable to Respiratory Syncytial Virus", *Pediatrics*, 2009, **124**, 1676-1679.

14. "Reassessment of the Indications for Ribavirin Therapy in Respiratory Syncytial Virus Infections", *Pediatrics*, 1996, **97**, 137-140.

15. Sami, I. R., Piazza, F. M., Johnson, S. A., Darnell, M. E. R., Ottolini, M. G., Hemming, V. G. and Prince, G. A., "Systemic Immunoprophylaxis of Nasal Respiratory Syncytial Virus Infection in Cotton Rats", *J. Infect. Dis.*, 1995, **171**, 440-443.

16. Kravetz, H. M., Knight, V., Chanock, R. M., Morris, J. A., Johnson, K. M., Rifkind, D. and Utz, J. P., "Respiratory Syncytial Virus", *JAMA*, 1961, **176**, 647-667.

17. Parrott, R. H., Kim, H. W., Brandt, C. D. and Chanock, R. M., "Potential of attenuated respiratory syncytial virus vaccine for infants and children", *Dev. Biol. Stand.*, 1975, **28**, 389-399.

18. Hall, C. B., Douglas, R. G., Jr., Schnabel, K. C. and Geiman, J. M., "Infectivity of respiratory syncytial virus by various routes of inoculation", *Infect. Immun.*, 1981, **33**, 779-783.

19. Falsey, A. R., Formica, M. A. and Walsh, E. E., "Diagnosis of Respiratory Syncytial Virus Infection: Comparison of Reverse Transcription-PCR to Viral Culture and Serology in Adults with Respiratory Illness", *J. Clin. Microbiol.*, 2002, **40**, 817-820.

20. Hindiyeh, M., Hillyard, D. R. and Carroll, K. C., "Evaluation of the Prodesse Hexaplex Multiplex PCR Assay for Direct Detection of Seven Respiratory Viruses in Clinical Specimens", *Am. J. Clin. Path.*, 2001, **116**, 218-224.

21. Perez, J. M., Simeone, F. J., Saeki, Y., Josephson, L. and Weissleder, R., "Viral-Induced Self-Assembly of Magnetic Nanoparticles Allows the Detection of Viral Particles in Biological Media", *J. Am. Chem. Soc*, 2003, **125**, 10192-10193.

22. Liolios, L., Jenney, A., Spelman, D., Kotsimbos, T., Catton, M. and Wesselingh, S., "Comparison of a Multiplex Reverse Transcription-PCR-Enzyme Hybridization Assay with Conventional Viral Culture and Immunofluorescence Techniques for the Detection of Seven Viral Respiratory Pathogens", *J. Clin. Microbiol.*, 2001, **39**, 2779-2783.

23. Abels, S., Nadal, D., Stroehle, A. and Bossart, W., "Reliable Detection of Respiratory Syncytial Virus Infection in Children for Adequate Hospital Infection Control Management", *J. Clin. Microbiol.*, 2001, **39**, 3135-3139.

24. Sano, T., Smith, C. L. and Cantor, C. R., "Immuno-PCR: very sensitive antigen detection by means of specific antibody-DNA conjugates", *Science*, 1992, **258**, 120-122.

25. Goodrich, J. S. and Miller, M. B., "Comparison of Cepheid's Analyte-Specific Reagents with BD Directigen for Detection of Respiratory Syncytial Virus", *J. Clin. Microbiol.*, 2007, **45**, 604-606.

26. Perkins, S. M., Webb, D. L., Torrance, S. A., El Saleeby, C., Harrison, L. M., Aitken, J. A., Patel, A. and DeVincenzo, J. P., "Comparison of a Real-Time Reverse Transcriptase PCR Assay and a Culture Technique for Quantitative Assessment of Viral Load in Children Naturally Infected with Respiratory Syncytial Virus", *J. Clin. Microbiol.*, 2005, **43**, 2356-2362.

27. Chomczynski, P., "Solubilzation in formamide protects RNA from degradation", *Nucl. Acids Res.*, 1992, **20**, 3791-3792.

28. Hargrove, J. L. and Schmidt, F. H., "The role of mRNA and protein stability in gene expression", *FASEB J.*, 1989, **3**, 2360-2370.

29. Mahony, J. B., "Detection of Respiratory Viruses by Molecular Methods", *Clin. Microbiol. Rev.*, 2008, **21**, 716-747.

30. Bentzen, E. L., House, F., Utley, T. J., Crowe, J. E. and Wright, D. W., "Progression of Respiratory Syncytial Virus Infection Monitored by Fluorescent Quantum Dot Probes", *Nano Lett.*, 2005, **5**, 591-595.

31. Adler, M., Schulz, S., Fischer, R. and Niemeyer, C. M., "Detection of Rotavirus from stool samples using a standardized immuno-PCR ("Imperacer") method with end-point and real-time detection", *Biochem. Biophys. Res. Commun.*, 2005, **333**, 1289-1294.

32. Barletta, J. and Bartolome, A., "Immuno-polymerase chain reaction as a unique molecular tool for detection of infectious agents", *Expert Opin. Med. Diagn.*, 2007, **1**, 267-288.

33. Guo, Y.-C., Zhou, Y.-F., Zhang, X.-E., Zhang, Z.-P., Qiao, Y.-M., Bi, L.-J., Wen, J.-K., Liang, M.-F. and Zhang, J.-B., "Phage display mediated immuno-PCR", *Nucl. Acids Res.*, 2006, **34**, e62.

34. Zhou, H., Fisher, R. J. and Papas, T. S., "Universal immuno-PCR for ultra-sensitive target proteindetection", *Nucl. Acids Res.*, 1993, **21**, 6038-6039.

35. Wacker, R., Ceyhan, B., Alhorn, P., Schueler, D., Lang, C. and Niemeyer, C. M., "Magneto Immuno-PCR: A novel immunoassay based on biogenic magnetosome nanoparticles", *Biochem. Biophys. Res. Commun.*, 2007, **357**, 391-396.

36. Niemeyer, C. M., Adler, M., Pignataro, B., Lenhert, S., Gao, S., Chi, L., Fuchs, H. and Blohm, D., "Self-assembly of DNA-streptavidin nanostructures and their use as reagents in immuno-PCR", *Nucl. Acids Res.*, 1999, **27**, 4553-4561.

37. Nam, J.-M., Thaxton, C. S. and Mirkin, C. A., "Nanoparticle-Based Bio-Bar Codes for the Ultrasensitive Detection of Proteins", *Science*, 2003, **301**, 1884-1886.

38. Braun, P. V., "Nanoparticles: Spontaneous ligand organization", *Nat. Mater.*, 2004, **3**, 281-282.

39. Daniel, M.-C. and Astruc, D., "Gold Nanoparticles: Assembly, Supramolecular Chemistry, Quantum-Size-Related Properties, and Applications toward Biology, Catalysis, and Nanotechnology", *Chem. Rev.*, 2003, **104**, 293-346.

40. Hurst, S. J., Lytton-Jean, A. K. R. and Mirkin, C. A., "Maximizing DNA Loading on a Range of Gold Nanoparticle Sizes", *Anal. Chem.*, 2006, **78**, 8313-8318.

41. Giulio, F. P., David, G. I. K. and Lawrence, T., "Colloidal gold nanoparticles: a novel nanoparticle platform for developing multifunctional tumor-targeted drug delivery vectors", *Drug Dev. Res.*, 2006, **67**, 47-54.

42. Qiao, F.-Y., Liu, J., Li, F.-R., Kong, X.-L., Zhang, H.-L. and Zhou, H.-X., "Antibody and DNA dual-labeled gold nanoparticles: Stability and reactivity", *Appl. Surf. Sci.*, 2008, **254**, 2941-2946.

43. Pompi, H., Buelent, C. and Christof , M. N., "Sensitive Detection of Proteins Using Difunctional DNA-Gold Nanoparticles13", *Small*, 2005, **1**, 844-848.

44. Zimmer, G., Budz, L. and Herrler, G., "Proteolytic Activation of Respiratory Syncytial Virus Fusion Protein", *J. Biol. Chem.*, 2001, **276**, 31642-31650.

45. Adler, M., Wacker, R. and Niemeyer, C. M., "Sensitivity by combination: immuno-PCR and related technologies", *Analyst*, 2008, **133**, 702-718.

46. Adler, M. and Gregory, S. M., in *Advances in Clinical Chemistry*, Elsevier, 2005, vol. Volume 39, pp. 239-292.

47. Perez, J. W., Haselton, F. R. and Wright, D. W., "Viral detection using DNA functionalized gold filaments", *Analyst*, 2009, **134**, 1548-1553.

48. Stowers, C. C., Haselton, F. R. and Boczko, E. M., "An analysis of quantitative PCR reliability through replicates using the Ct method", *J. Biomed. Sci. Engin.*, 2010, **3**, 459-469.

CHAPTER IV

THE POTENTIAL OF DNA LOGIC FOR IMPROVED IMMUNO-PCR BASED DIAGNOSTICS

In order to begin treatment of a viral infection, the virus must first be accurately and quickly diagnosed. Diagnostic methods should therefore be both sensitive and specific. Inadequate sensitivity results in false negatives,[1] while insufficient specificity results in false positives.[2, 3] Although ultra-sensitive diagnostics exist, such as I-PCR, these assays are typically limited by the high-background associated with them.[4-6] However, it is possible to use the inherent information storing nature of DNA to increase not only the sensitivity, but also the specificity of an assay.

The concept of DNA logic was first introduced by Leonard Adleman in 1994 when he demonstrated how intrinsic properties of DNA, such as base specific pairing, and the tools of molecular biology, such as PCR, could be used to solve the Hamiltonian Path Problem.[7] The Hamiltonian Path Problem is to determine if a path exists in a directed graph, starting at the beginning vertex, ending at the ending vertex, and reaching each vertex exactly once.[8] The problem is classified as NP-complete in complexity; and although with relatively few vertices, the problem appears quite simple, even a small increase in the number of vertices increases the complexity of the problem substantially.[9-11]

Adleman solved the problem by encoding each vertex with a unique 20-base DNA sequence (**Figure 30**).[7] Edges between vertices were represented by 20-base DNA

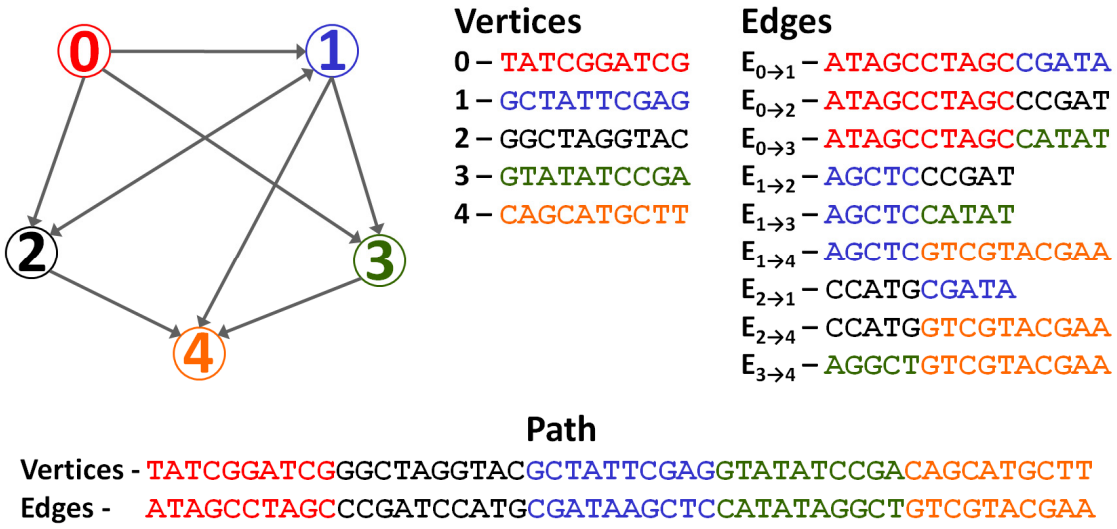

Figure 30. Truncated depiction of Adleman's use of DNA to represent a directed graph. Vertices and edges were represented by 20 base sequences. Edges connecting to and from the starting and ending vertices were the exception, and instead were represented by 30 base sequences. Edges were designed to hybridize to the two vertices that were connected by that particular edge. Extended networks of vertices and edges would form to represent possible paths.

sequences as well; these sequences were complementary to the last 10 bases of the vertex that was being departed and the first 10 bases of the vertex at which the edge arrived (unless the vertices involved were the starting or ending vertex, in which case the entire 20 base sequence was used). By mixing DNA representative of all of the vertices and edges, the edges hybridized to the vertices in such a way that all possible paths were formed. Adleman then used DNA ligase to mend the discontinuities formed along the path sequences. Primers specific to the vertices that represented the starting and ending vertices were used in PCR to amplify only routes that began and ended with the correct vertices. Gel electrophoresis was used to select only the paths that were the correct length, long enough to touch each vertex only once. Finally, affinity purification was used to select only paths that contained each vertex. In the end, Adleman's procedure

had reduced all possible paths to only those that started and ended at the correct vertex and touched each vertex only once. It had isolated the Hamiltonian Path.

Since Adleman's demonstration, the intrinsic properties of DNA have been used to build nanostructures,[12, 13] molecular computational devices,[14-16] biosensors[17-19] and DNA scaffolds.[20] Of noted interest is the development of the proximity ligation assay (**Figure 31**).[21-23] The proximity ligation assay effectively added a logical AND (Λ)

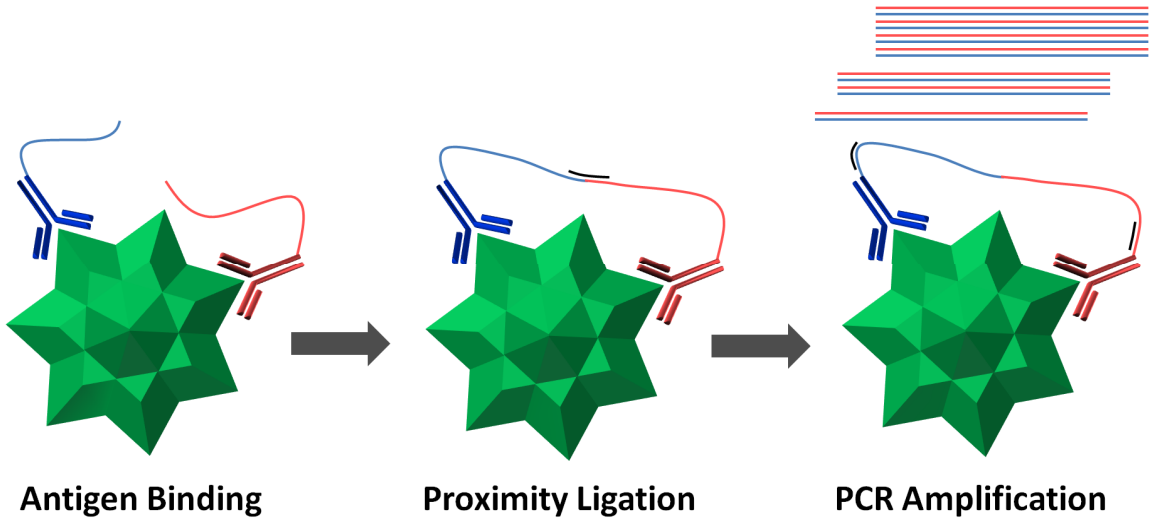

Figure 31. Proximity ligation assay. In the presence of antigen the proximity probes become spatial close, enabling the ligation and formation of the PCR template.

operation to PCR-based antigen detection.[24] The AND operation required the presence of two different antibodies or aptamers (proximity probes) binding to two different epitopes on an antigen to invoke a positive signal.[23, 25] Each proximity probe was coupled to a unique single stranded DNA tag to act as the reporter, via PCR.[21] The locations of the two epitopes were chosen such that when the two proximity probes would bind to their respective sites, they would be spatially close to each other. This, in turn, would cause the DNA tags of each probe to be spatially close. A ligation template would then be

added to the solution, and in the event that the probes were in close proximity to one another, the ligation template would ligate the two strands. DNA ligase was then added to mend the nick in the two strands.[26] This complete strand then acted as the template for PCR. Primers specific to the complete template were added and only if the two strands had been ligated together would exponential amplification occur. The assay increased specificity by requiring binding at epitope A AND binding at epitope B in order to generate a response.

Our research worked to extend this concept to create a Boolean logical NOT (¬) operation, which could effectively reduce the effects of nonspecific binding on ultra-sensitive assays, such as I-PCR. DNA logic tag sequences were hybridized to DNA covalently bound to gold nanoparticles (AuNPs, **Figure 32**). Each DNA logic sequence is associated with a particular antibody through mutual attachment to the same AuNP. In the presence of an antigen, the AuNPs functionalized with specific antibodies will bind to the desired epitope on the antigen. A second construct, an antibody functionalized MMP is also added to the analyte solution in order to form a MMP-antigen-AuNP complex which can be separated from the rest of the analyte solution using an external magnetic field.

The DNA logic tags are used as reporters, via PCR, of a binding event and designed to enable the performance of a Boolean logic NOT operation. The NOT operation is designed to subtract the effects of non-specific binding prior to PCR amplification. In doing so, the logic tags ensure that the resulting signal is a function of specific binding, NOT non-specific interactions.

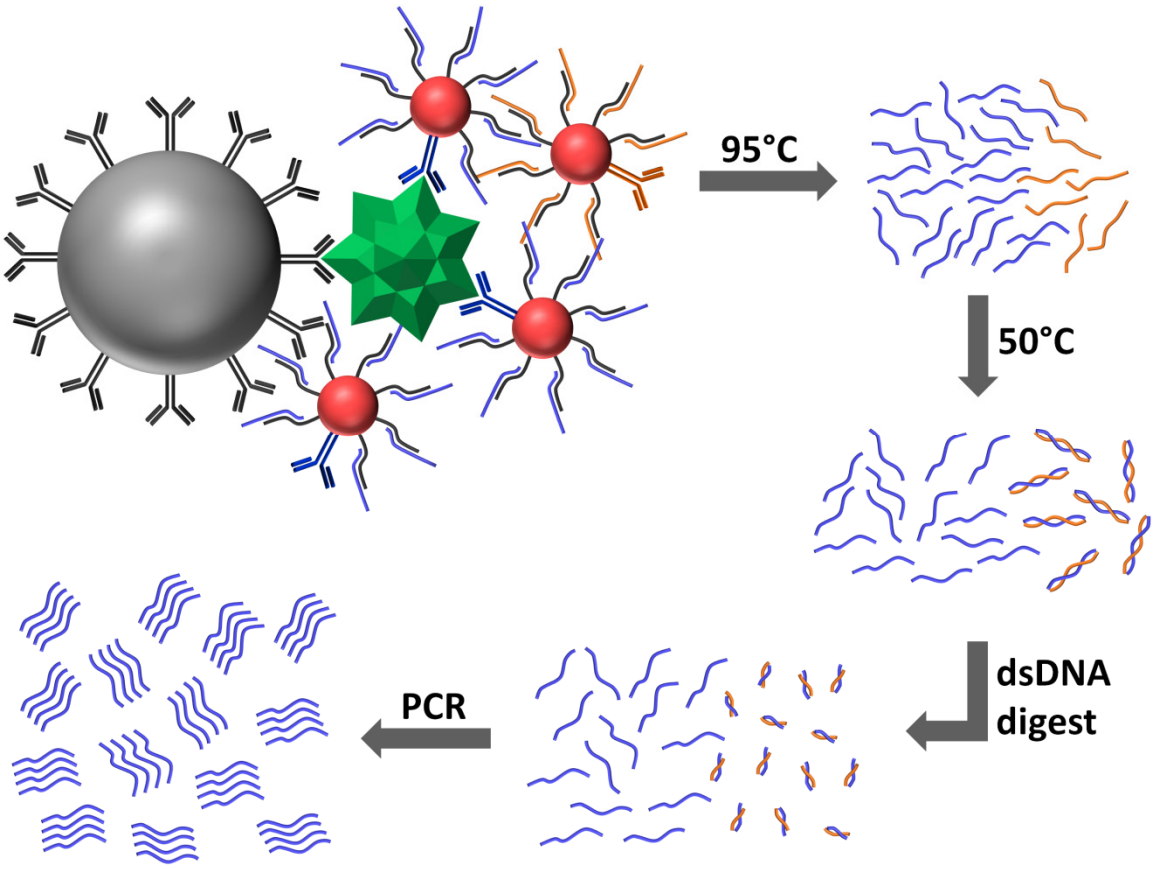

Figure 32. DNA logic NOT operation. The NOT operation requires the use an antigen-specific probe (blue AuNP) and a non-specific probe (orange AuNP). During antigen detection a number of AuNPs become non-specifically entrapped, represented by one orange and one blue AuNP not bound via an antibody interaction. Upon heating, hybridized DNA is released and dsDNA is formed equivalent to the amount of non-specific binding. A restriction enzyme is used to cut the dsDNA, and only the remaining DNA is available for PCR amplification.

To perform the NOT operation, two types of AuNPs were added to the analyte solution. The first type of AuNP was functionalized with an antigen specific antibody and tag DNA (TagA, **Table 3**) that can be amplified using PCR. The second type of AuNP was functionalized with an isotype matched non-specific antibody and tag DNA (TagA´, **Table 3**), which contained a restriction site that is complementary to TagA. During separation, a certain number of AuNPs become entrapped in complexes without actually binding to an epitope, resulting in a non-specific signal. With the second AuNP added,

Table 3. Oligonucleotide sequences used in DNA logic studies.

Name	Sequence 5´ → 3´
TagA	CTGCGACGATCTACCATCGACGTACCAGGTCGGTTGAAGGACCGTGCATAGCGAAATCTCAACTTACGAGACAAGC
TagA´	TTCGCTATGCACGGTCCTTCAACCGACCTGGTACGTATCGACAGTTGACCGTACTTTACGTGGAGTACGCTTTACC
Comp_TagA	[C6Thiol]TTTTTTTTTTTTTTTGCTTGTCTCGTAAGTTGAGATTTCGCTATGCACGGTCCTT
Comp_TagA´	[C6Thiol]TTTTTTTTTTTTTTTGGTAAAGCGTACTCCACGTAAAGTACGGTCAACTGTCGAT
Comp_A*	[C6Thiol]TTTTTTTTTTTTTTTGGTAAAGCGTACTCCACGTAAAGTACGGTCAACTGTCGAT
Primer 1	GCTTGTCTCGTAAGTTGA
Primer 2	CTGCGACGATCTACCAT

the number of non-specifically trapped AuNPs should be roughly equal between both types of AuNPs. Prior to PCR detection, the DNA was released from the AuNP and then annealed, forming double-stranded DNA (dsDNA) of TagA/TagA´. Since TagA´ is essential for the formation of dsDNA, the amount of dsDNA formed was directly proportional to the number of non-specific AuNPs trapped during the pulldown. A restriction enzyme that cleaves at the TagA/TagA´ restriction site was used to degrade the formed dsDNA. Once degraded, the DNA no longer serves as a template for PCR. In turn, the NOT operation removed the effects of non-specific binding on the final signal; and the remaining DNA, which is excess TagA (in the event an antigen is present) is amplified and detected using real-time PCR.

Experimental

Coupling of Antibodies to Magnetic Microparticles. MagnaBind™ amine derivatized 1 μm magnetic microparticles were activated with sulfosuccinimidyl-4-[N-maleimidomethyl]cyclohexane-1-carboxylate (Sulfo-SMCC). In a typical reaction, 200 μL of MMPs were washed three times with coupling buffer (CB) consisting of 50 mM phosphate buffer (pH 7.0), 0.15 M NaCl and 5 mM EDTA. The MMPs were then cleared from the suspension using a magnet. After 1 min, the solution became clear and MMPs were pulled to the side of the tube. When the clear supernatant and the external magnetic field were removed, the MMPs were resuspended in CB. After washing, the MMPs were activated with 20 μL of 1 mM Sulfo-SMCC. The solution was mixed and allowed to sit at room temperature for 1 hr. The MMPs were then washed 3 times to remove excess Sulfo-SMCC.

Antibody reduction was coordinated so that once the MMPs were activated, they could be immediately used. Dithiothreitol (DTT) was used to reduce anti-RSV fusion protein antibodies (clones 1269 and 1214). 15 μL of 1.2 mM DTT was added to 15 μL of purified antibodies at 30 mg/mL in phosphate buffered saline (PBS). The solution was mixed and allowed to sit at room temperature for 0.5 hr. After that time, the antibodies were separated from DTT using a NAP-5 column. The activated MMPs were combined with the column-purified reduced antibodies and allowed to react for 1 hr at room temperature. The conjugation was quenched by the addition of β-mercaptoethanol to a final concentration of 100 μM. After 1 hr quenching, the MMPs were washed three times with PBS and then resuspended in a final volume of 300 μL.

Coupling of Antibodies and DNA to Gold Nanoparticles. Thiolated DNA sequences were received as disulfides and were activated by cleaving the disulfide bond. Cleavage was performed in 100 mM DTT, 0.1 M phosphate buffer, pH 8.3. After 0.5 hr, thiolated DNA was desalted using Microcon YM-3 centrifugal filters. The purified DNA was resuspended in TE buffer and stored in small aliquots at -80°C.

In a typical reaction, 35 μL of 0.2 mg/mL Synagis® antibody (humanized monoclonal antibody known to target the A antigenic site of RSV's fusion protein) or an isotype matched (human IgG1κ) antibody was added to 10 mL of 2.3 nM, 15 nm diameter AuNPs at pH 9.3 and placed on a rotator for 0.5 hr. Then, 50.8 μL of 107 μM activated DNA (Comp_TagA or Comp_TagA´, **Table 3**) was added; the AuNPs were then rotated for another 0.5 hr. The solution was brought to 0.1 M NaCl, 10 mM phosphate buffer, and 0.02% Tween20 and allowed to sit for 1 hr. After this time, the concentration of NaCl was brought to 0.2 M and to 0.3 M after a third hour. Excess DNA was removed by centrifuging the solution for 20 minutes at 21,100 x gravity. The clear supernatant was then removed, and the red oily pellet was resuspended in a stock solution of 0.3 M NaCl, 10 mM phosphate buffer and 0.02% Tween20 (PB). This washing process was repeated three times. After washing, particles were resuspended, and Tag DNA (TagA or TagA´, **Table 3**) was added to bring the molar ratio of Tag DNA:AuNPs to 200:1. The solution was allowed to sit at room temperature overnight. Finally, excess Tag DNA was removed using the washing method described above.

Preparation of RSV Infected Cell Lysate. HEp-2 cells were cultured in OPTI-MEM media supplemented with 2% fetal bovine serum, 250 μg/mL of amphotericin-B, 10 mg/mL gentamicin and 200 mM L-glutamine and incubated at 37˚C with 5% CO_2.

RSV stock was prepared by infecting a confluent T-150 flask of HEp-2 cells with RSV strain A_2. Infection was performed with rapidly thawed virus diluted to 5 mL in cell media. Following the initial infections, cells were incubated for 1 hr after which 35 mL of cell media was added to the flask. The infection was allowed to proceed for 4 days, after which cells were scraped from the surface of the T-150 flask. The supernatant containing the cells was collected in a 50 mL centrifuge tube and centrifuged for 5 min at 500 x gravity. Following removal of the supernatant, the cell pellet was resuspended to 5 mL in cell media. The cells were then frozen using a slurry of ethanol and dry ice in order to lyse cells and release virus particles. After freezing, the cells were thawed in a 37°C water bath. The freezing/thawing cycle was repeated three times to ensure the release of virus particles from the cell wall. After the third cycle, the cells were centrifuged at 100 x gravity for 5 min to pellet large cellular debris. The supernatant was then separated into aliquots of 0.5 mL and stored at -80°C.

Restriction Enzyme Digest. To test the NOT operation, TagA was hybridized with TagA´ and cleaved by the HpyCH4V restriction enzyme. The reaction was prepared by adding various units of HpyCH4V (or NEB's Diluent B for no enzyme controls) to 1 μM TagA and 2 μM TagA´ in incubation buffer (50 mM potassium acetate, 20 mM Tris-acetate, 10mM magenesium acetate, 1mM dithiothreitol, at pH 7.9) from New England Biolabs. This mixture was then incubated at 37°C for 1 hour, followed by a heat inactivation step of 72°C for 25 minutes. In order to verify the results, the samples were then examined using agarose gel electrophoresis and/or PCR.

Agarose Gel Electrophoresis. In order to verify the results from PCR and restriction enzyme digestion, agarose gels were run. 10 μL of samples from either

reaction was mixed with 2 µL 10X SYBR Gold in dimethylsulfoxide (DMSO), and 0.5 µL 10X loading buffer. The mixtures along with 4 µL EZ load 20 base pair DNA ladder combined with 2 µL SYBR Gold were run on a 4% agarose with Tris-Borate-EDTA gel for 30 minutes to 1 hour at 120 V. The gels were then visualized under 254 nm ultraviolet light using the BioDoc-It Gel Documentation System.

Real-Time Polymerase Chain Reaction (PCR). Real-time PCR was performed using a SmartCycler II thermal cycler system. Reactions were performed in a 25 µL volume with 12.5 µL of iTaq SYBR Green Supermix with ROX (0.4 mM dATP, 0.4 mM dCTP, 0.4 mM dGTP, 0.8 mM dUTP, iTaq DNA polymerase, 50 units/ml, 6 mM Mg^{+2}, SYBR Green I dye, 1 µM ROX reference dye, and stabilizers), 200 nM left and right primers, and nuclease-free water. The optimized protocol was a three-step PCR, beginning with an initial iTaq DNA polymerase activation step of 95°C for 3 minutes followed by 40 cycles of 95°C for 30 s to denature, 56°C for 30 s to anneal and extend, and 78°C for 6 s to detect fluorescence.

Results and Discussion

RSV was used as a model to test the potential of the DNA Logic NOT operation on non-specific binding. MMPs were functionalized with anti-RSV antibodies and used to capture RSV virions and infected cells. After capture, two types of functionalized AuNPs were added to the solution. The first type of AuNP was functionalized with RSV specific antibodies, covalently attached DNA (complementary to TagA), and TagA DNA hybridized to the covalently bound strand. The second type of AuNP was functionalized

with isotype matched non-specific antibodies, covalently attached DNA (complementary to TagA´), and TagA´ DNA hybridized to the covalently bound strand. After magnetic separation of the MMP-RSV-AuNP complex, the solution was heated to 95ºC to release both TagA and TagA´ entrapped in the complex. The released DNA was allowed to hybridize to form TagA/TagA´ dsDNA, and then digested with a restriction enzyme (HpyCH4V). The digested DNA was then analyzed via real-time PCR (**Figure 33**).

Upon performing the NOT operation, it was clear that the shift in cycle threshold (C_t) indicative of DNA cleavage occurring was not present (**Figure 33**). The C_t values of samples before and after the restriction enzyme digest were too similar to conclude that the dsDNA had been cut. However, pertinent information still existed in the experiment.

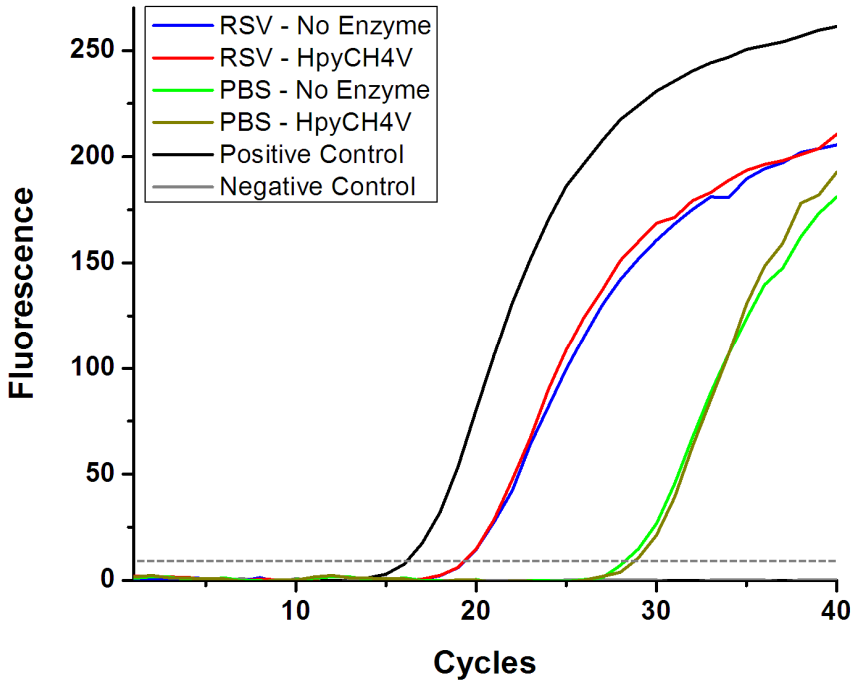

Figure 33. PCR analysis of an initial attempt at the NOT operation. Samples incubated with RSV (blue & red) had a distinctive shift when compared to samples incubated in PBS (green & gold). The PBS samples represent the high background associated with I-PCR, which the NOT operation seeks to reduce. Samples incubated with the restriction enzyme HpyCH4V (red & gold), had no distinguishable shift when compared to no enzyme control samples (blue & green).

First, it was clear that in the presence of infected cell lysates, the C_t shifted approximately 10 cycles earlier indicating that substantially more TagA DNA was present than when the reaction was performed in PBS. Second, non-specific binding occurred, which was observed by the fact that the PBS control samples have an earlier C_t than no template controls (negative control). It is this inherent background that the NOT operation seeks to reduce. The background signal, present because TagA DNA is added to all samples, even RSV negative samples, limits the sensitivity of I-PCR.[27, 28]

To determine whether the problem with the NOT operation was in the antigen-complexing steps or in the actual restriction enzyme digestion and subsequent PCR, stock solutions of TagA and TagA´ were used to validate digestion and PCR detection. Femtomolar concentrations of TagA and TagA´ were directly combined at room temperature and allowed to hybridize. The sample was diluted in incubation buffer and then split in half. Restriction enzyme was added to one sample, and the other served as a no enzyme control and Diluent B was added. Both samples were incubated at 37°C and then heat-inactivated prior to PCR analysis. PCR analysis showed no shift in samples treated with restriction enzyme when compared to a no enzyme control (**Figure 34**).

High concentrations (uM) were used to optimize and visualize the restriction digest via gel electrophoresis. The first factor evaluated was hybridization temperature. Hybridization temperature was significant because dsDNA formation is essential in DNA cleavage occurring. In order for the logic operation to occur, TagA and TagA´ must anneal to become dsDNA. Only then will the restriction enzyme cut the DNA and subtract out the non-specific binding. Gel electrophoresis was used to verify dsDNA formation (**Figure 35**). As **Figure 35** shows, annealing is sensitive to temperature and

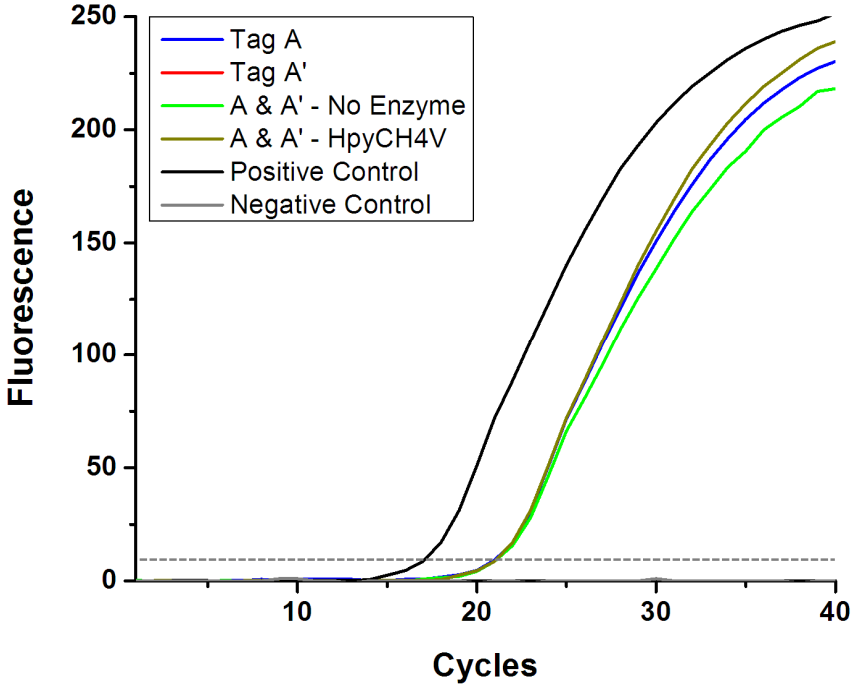

Figure 34. NOT operation controls. Femtomolar concentrations of TagA and TagA´ directly combined showed no shift in C_t upon incubation with the restriction enzyme HpyCH4V. Additionally, TagA´ alone did not amplify during PCR (red).

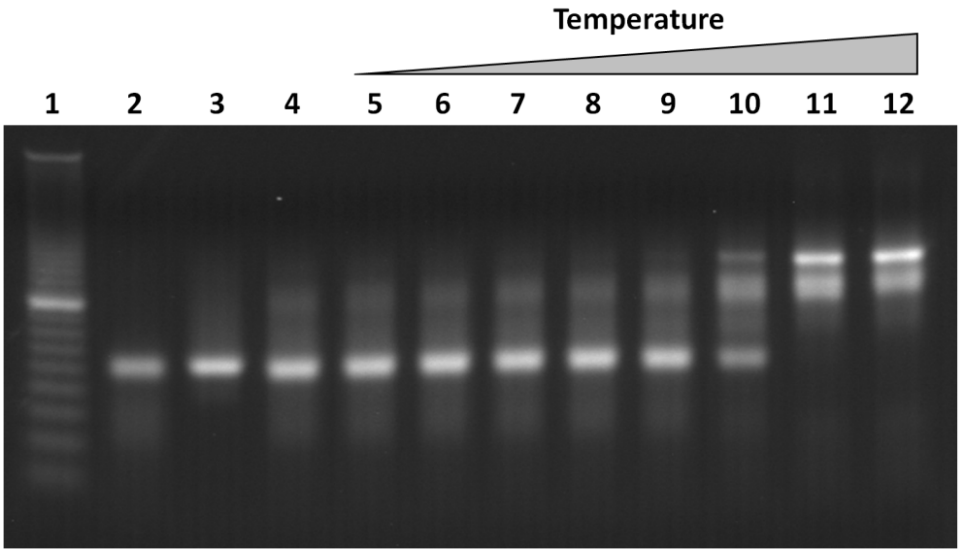

Figure 35. dsDNA formation of TagA/TagA´. Lane 1: 10-bp ladder. Lane 2: Single stranded TagA DNA. Lane 3: Single stranded TagA´ DNA (TagA complement). Lane 4: Equal molar ratios of TagA and TagA´ at room temp. Lanes 5 through 12: Equal molar ratios of TagA and TagA´ annealed for 20 minutes at increasing temperatures (60 – 95 °C).

increased temperature is needed to completely anneal equimolar ratios of TagA and TagA´. When TagA and TagA´ were combined at room temperature, no shift in electrophoretic mobility is observed. Not until 20 min at 80°C does the TagA/TagA´ band begin to shift, indicating formation of dsDNA. It took 20 min at 90°C, for the band to completely shift. With this information it was determined that an annealing of 20 minutes at 90ºC (lane 11) was required prior to enzymatic digestion.

Using the optimized annealing temperature, the restriction digest was repeated at a high concentration to allow visualization via gel electrophoresis instead of PCR. **Figure 36** shows, at high concentrations, cleavage of the dsDNA occurs. Lane 4 verifies that prior to the restriction digest, TagA/TagA´ is double stranded. Although time does

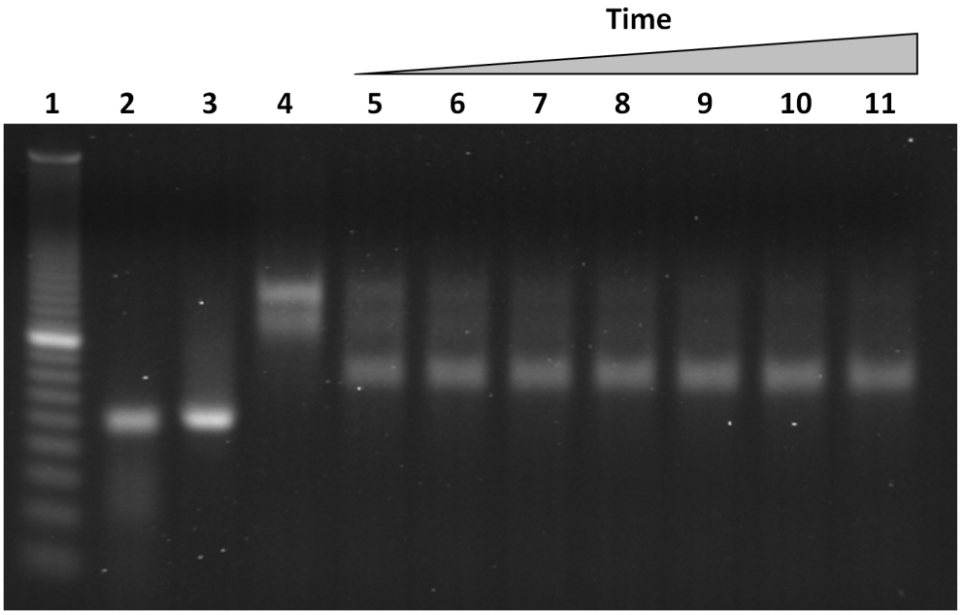

Figure 36. Time dependant cleavage of dsDNA. Lane 1: 10-bp ladder. Lane 2: Single stranded TagA DNA. Lane 3: Single stranded TagA´ DNA (TagA complement). Lane 4: dsDNA after cleavage conditions for 60 min without restriction enzyme present. Lanes 5 through 11: dsDNA after increasing cleavage times (1, 5, 15, 30, 60, 120, 240 mins) in the presence of HpyCH4V.

have some effect on the extent of cleavage, the vast majority of cleavage is accomplished in the 1st minute (lane 5). These same samples were diluted to PCR acceptable concentrations and a shift in C_t can be seen (**Figure 37A**). **Figure 37B** shows that after 1 min of cleavage, a shift of approximately 3.5 cycles is observed which is equivalent to approximately 91% less template available for PCR. After 240 min of cleavage, which by visualization on the gel can serve as an endpoint of the reaction, a shift of approximately 5 cycles is observed, equivalent to approximately 97% cleavage.

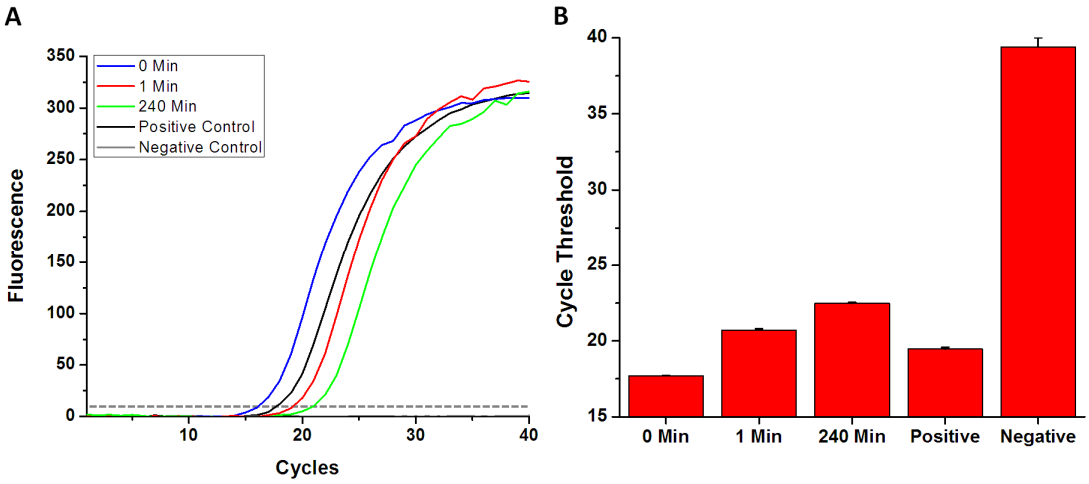

Figure 37. Shift in C_t generated by extended cleavage times. A) Samples annealed and cleaved at micromolar concentrations show a shift upon dilution and PCR analysis. B) The vast majority of cleavage occurs in the first min with a shift of 3.5 cycles. However, extended times, 240 min, increased the shift to 5 cycles.

These results make it apparent that PCR is effective at detecting cleavage of dsDNA; however when the optimized restriction digest conditions were used to repeat the experiment shown in **Figure 34**, no shift was observed post-cleavage (data not shown). The only difference between the gel-based studies and the repeated experiment was the DNA concentration at which the restriction digest was performed. To enable the gel-

based studies to be visualized, the reaction was performed at μM concentrations and then diluted for PCR analysis. However, for the PCR-based experiments the restriction digest was performed at fM concentrations.

In order to test the DNA concentration dependence of the restriction digest, the digest was repeated at decreasing concentrations and analyzed via PCR. **Figure 38** shows that as the concentration at which the restriction digest is performed decreases the ΔC_t, which represents the amount of cleavage that has occurred, also decreases. At concentrations above 10 nM, the PCR analysis becomes problematic because the

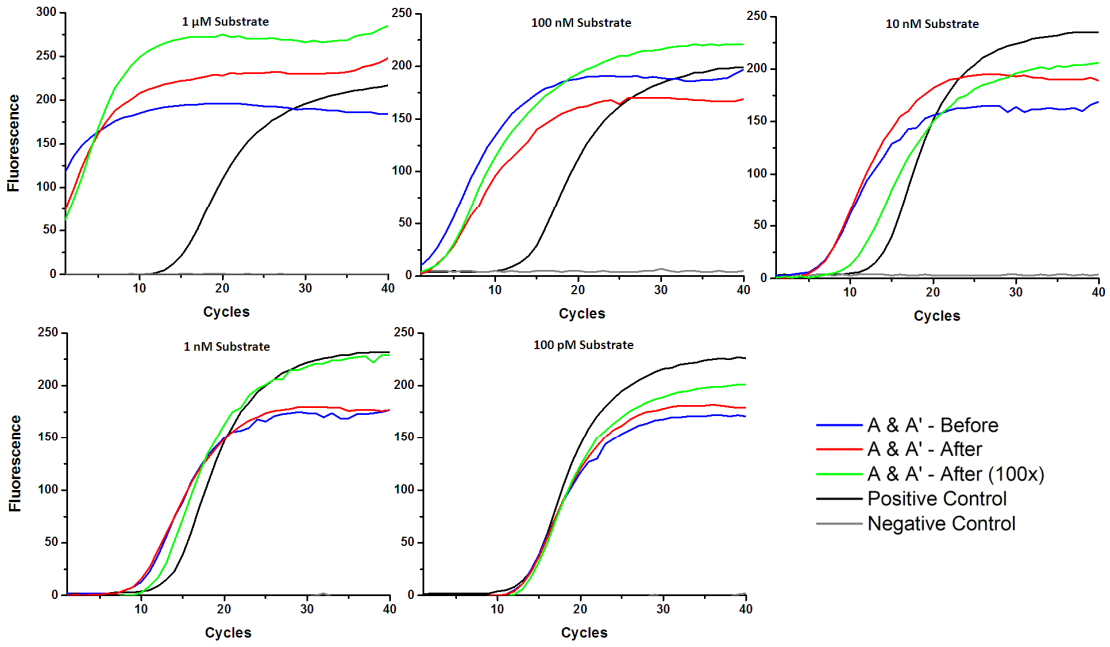

Figure 38. dsDNA concentration dependence of the restriction digest. At micromolar and high nanomolar concentration of dsDNA, a shift between before and after enzyme digested samples is observed. However, at low nanomolar concentrations the restriction enzyme needs to be present at 100-fold excess to observe a shift. When the concentration of dsDNA is picomolar, even a 100-fold excess of restriction enzyme does not generate as shift.

concentration of template DNA is too high to obtain a 5 cycle baseline. Although quantitation at these concentrations is difficult, it is easy to observe that a shift in C_t does

occur after the restriction digest. At 1 μM and 100 nM dsDNA concentrations, restriction enzyme at both a 1x concentration and a 100x concentration effectively cut the dsDNA (**Figure 39**). However, at lower concentrations (10 nM to 1 nM dsDNA) cleavage only

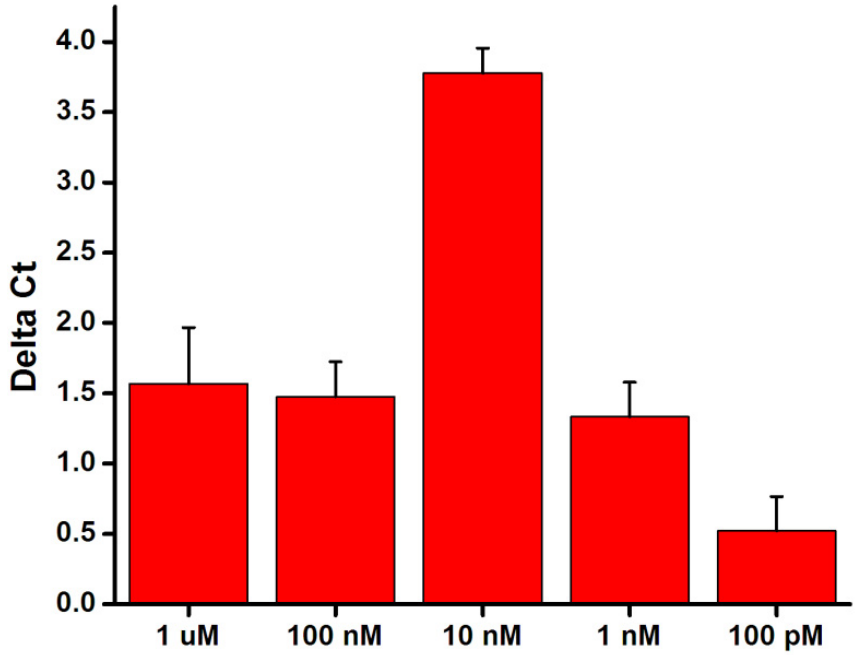

Figure 39. Delta C_t at decreasing dsDNA concentrations. Micromolar and high nanomolar concentrations of dsDNA must be considered with the knowledge that they are too high for accurate quantitation via PCR. However, examining 10 nanomolar and less concentrations reveals that the shift in C_t decreases as dsDNA concentration decreases.

occurs in extreme excess of restriction enzyme (100x). After the concentration of dsDNA is ≤10 pM, no cleavage is observed even in the presence of 100x restriction enzyme. It was clear that as very low concentrations of TagA/TagA´ dsDNA, no feasible concentration of restriction enzyme would facilitate the NOT operation. The pertinent question then was what would be the concentration of DNA in a cleavage reaction for an actual pull down experiment. **Figure 40** shows that a positive control sample results in a concentration of ~5 pM TagA. A PBS control sample, which represents the

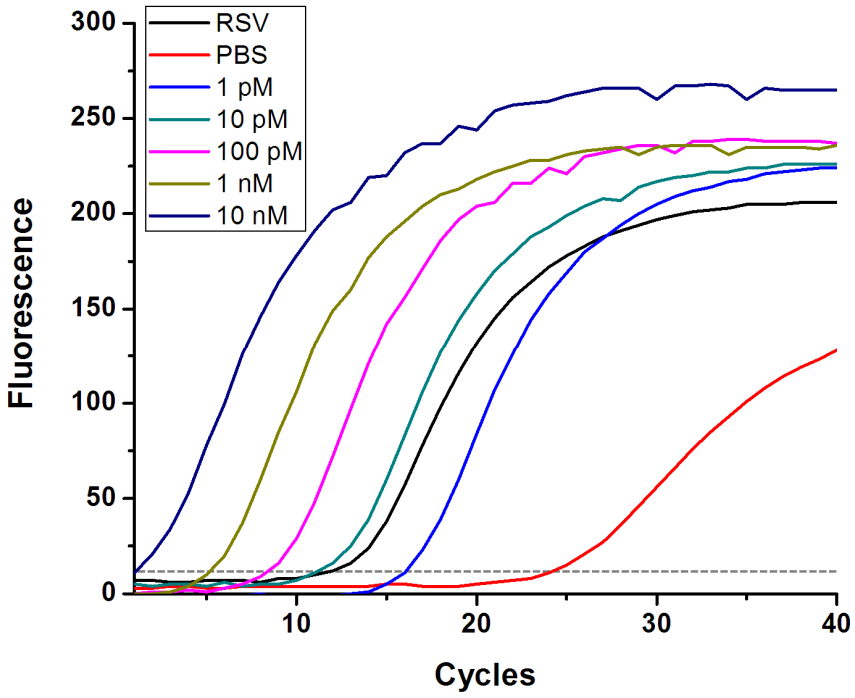

Figure 40. TagA DNA concentrations generated via antigen pulldown. The concentration of TagA pulled down in an RSV positive reaction (black) is ≤ 5 pM. The background signal generated in a PBS reaction (red) is much less, in the femtomolar range.

concentration that would actually be subtracted, is in the fM range. Unfortunately, this is below the limit at which the restriction reaction seems to function properly.

The possibility remains that the kinetics we have been working with are unique to the HpyCH4V enzyme we have been using, and that a different enzyme might be more amicable to the NOT operation. Fortunately, TagA and TagA´ were designed to have a second Rsa1 restriction site. The restriction digest was repeated at µM concentrations, using HpyCH4V, Rsa1, or a combination of both (**Figure 41**). It is clear from lanes 6 and 9 that in the presence of both enzymes, the TagA/TagA´ dsDNA gets cut into smaller fragments. However, **Figure 42A** reveals that this doesn't have an effect on the PCR results. An equivalent shift in C_t is achieved from using only HpyCH4V as compared to

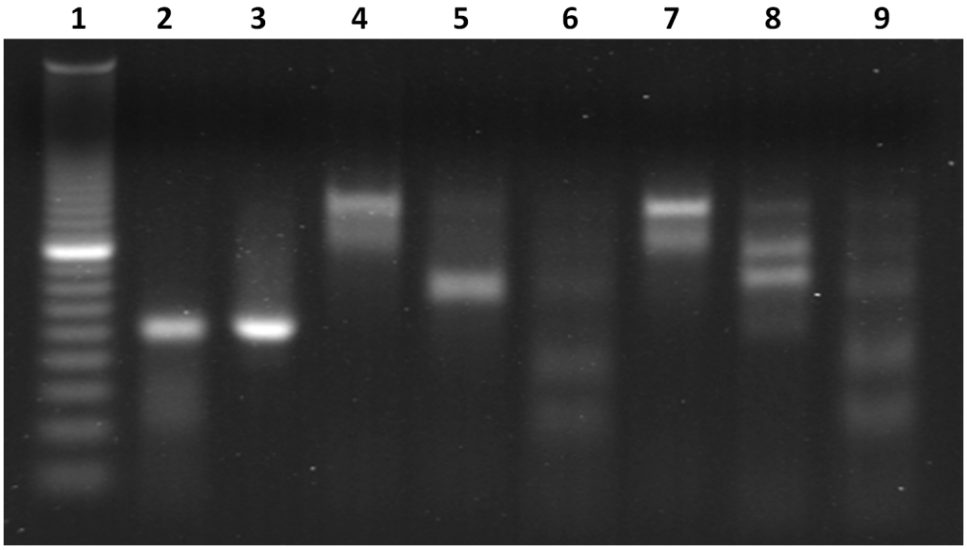

Figure 41. Gel electrophoresis of dsDNA cleaved with multiple restriction enzymes. Lane 1: 10-bp ladder. Lane 2: Single stranded TagA DNA. Lane 3: Single stranded TagA´ DNA (TagA complement). Lane 4: dsDNA after digest for 240 min in HpyCH4V-specific buffer (no enzyme present). Lane 5: dsDNA after digest for 240 min with HpyCH4V in HpyCH4V-specific buffer. Lane 6: dsDNA after digest for 240 min with HpyCH4V and Rsa1 in HpyCH4V-specific buffer. Lane 7: dsDNA after digest for 240 min in Rsa1-specific buffer (no enzyme present). Lane 8: dsDNA after digest for 240 min with Rsa1 in Rsa1-specific buffer. Lane 9: dsDNA after digest for 240 min with Rsa1 and HpyCH4V in Rsa1-specific buffer.

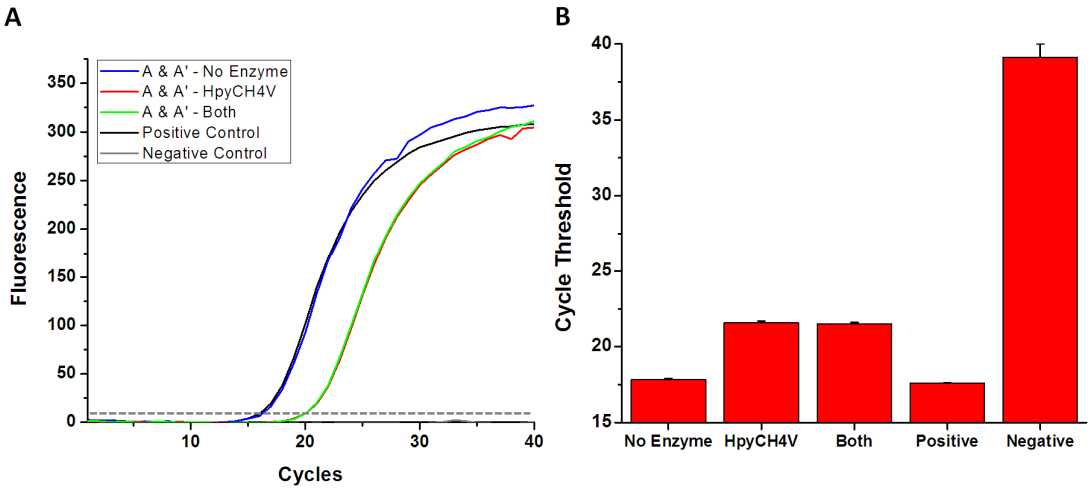

Figure 1. PCR analysis of multiple enzyme cleavage. A) When performed at micromolar concentrations and then diluted for PCR analysis, a shift is observed after dsDNA cleavage. B) However, the shift generated from using both HpyCH4V and Rsa1 (both) is no greater than the shift generated by only cleaving with HpyCH4V.

a combination of HpyCH4V and Rsa1 (**Figure 42B**). The smallest shift in C_t resulted from using only Rsa1 to digest the dsDNA (data not shown).

Therefore, non-enzymatic means of subtracting out non-specific binding were explored. One of the promising methods explored was the use of functionalized AuNPs to specifically capture dsDNA. Following capture, the AuNPs were then centrifuged to remove the non-specific binding prior to PCR amplification. In these experiments, AuNPs were functionalized with DNA (A*) which was used to capture dsDNA (**Figure 43**). A* was designed to be complementary to the 3′ end of TagA′. In the event of non-specific binding, TagA′ would hybridize to TagA as shown earlier. After the formation of TagA/TagA′ dsDNA, AuNPs functionalized with A* are added to the sample and

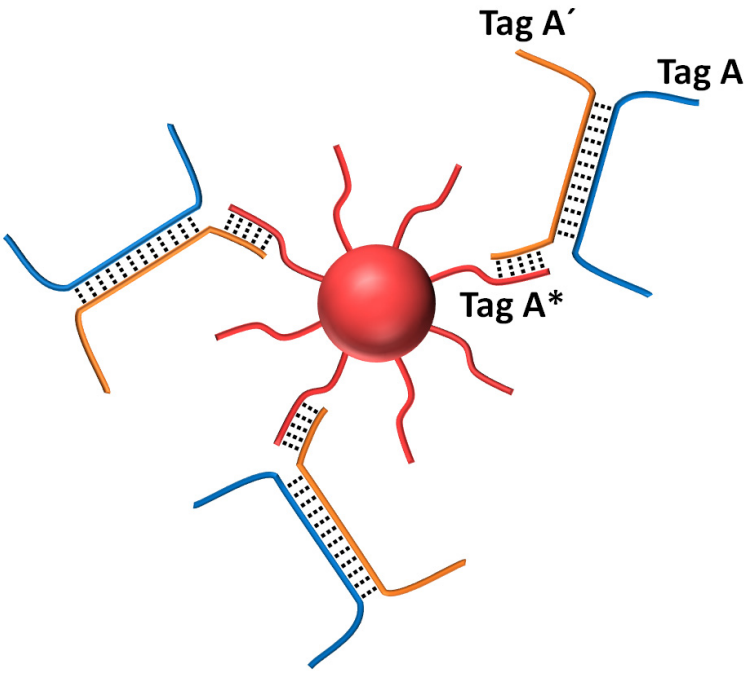

Figure 43. Representation of using A* AuNPs to remove dsDNA. Upon formation of dsDNA, the 3′ end of TagA′ is used to hybridize to A* which is functionalized to a 15 nm AuNP. After hybridization with A*, centrifugation is used to remove the AuNPs, and in turn, dsDNA.

allowed to hybridize to the free 3′ end of TagA′. The AuNPs were then centrifuged and pulled down any hybridized DNA with them. The supernatant was then removed and analyzed via PCR.

As **Figure 44** shows, the use of A* functionalized AuNPs resulted in significant ΔC_ts, even at low fM concentration. In these experiments the concentration of A* AuNPs used to pulldown dsDNA was 5 pM. At this concentration of AuNPs, 1 fM of

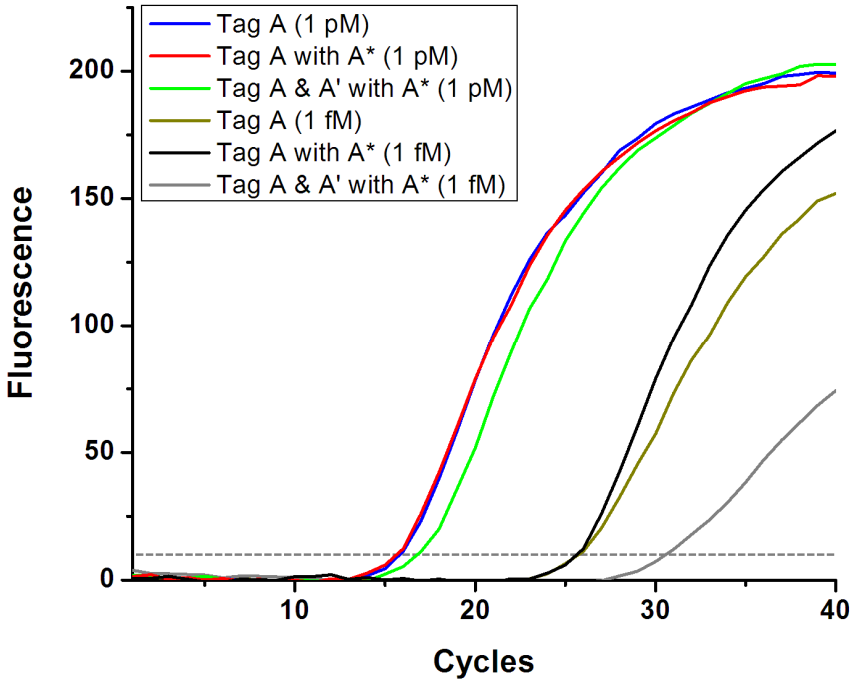

Figure 44. Removal of dsDNA using A* AuNPs. At femtomolar concentrations of dsDNA, the A* AuNPs effectively removed 97% of the dsDNA (black & gray). However, at picomolar concentrations the AuNPs removed only 50% of the dsDNA (red & green). In both cases, the presence of TagA′ was required to result in a shift in C_t.

dsDNA was shifted 5 cycles, indicating a 97% decrease in TagA. At higher concentrations of dsDNA (1 pM), the shift was less significant, but still present. It is possible that excess concentrations of AuNPs are required to capture the dsDNA,

therefore more AuNPs may be needed to capture pM concentrations of dsDNA. In either case, the pulldown is specific to TagA/TagA´ complexes because no shift is observed when A* AuNPs are incubated directly with TagA. In an attempt to pulldown higher concentrations of dsDNA, 1 nM A* AuNPs was used in the pulldown (**Figure 45**). It is apparent that the variation between replicates becomes quite large in the presence of 1 nM concentrations of AuNPs. It is possible that at these concentrations not all of the AuNPs are being removed prior to PCR, and they are then interfering with the PCR. Even the TagA/A* AuNP control sample becomes noisy, which indicates that the variation is not due to variable amounts of dsDNA being pulled down, but rather, a

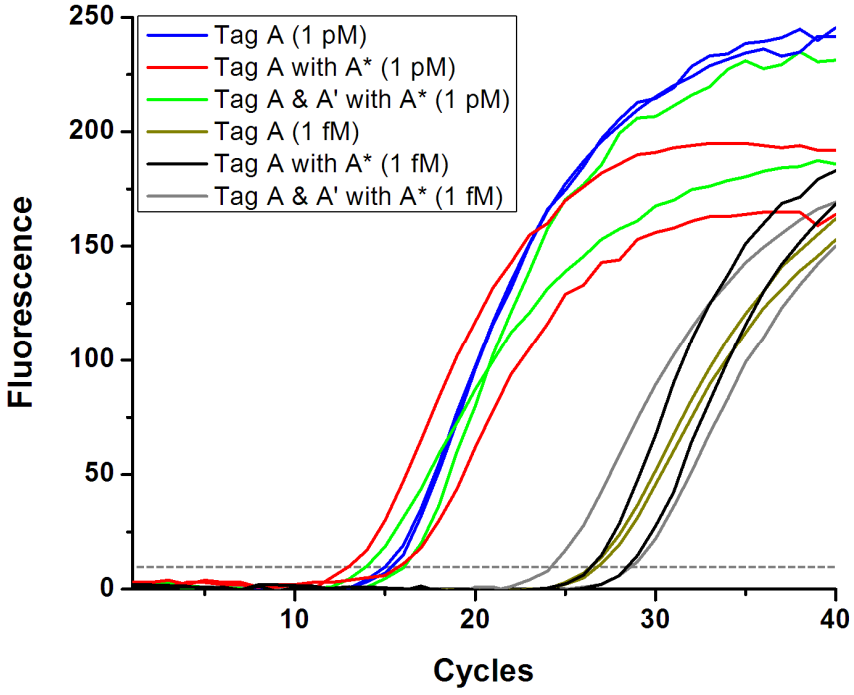

Figure 45. Using nanomolar AuNPs to remove dsDNA. The use of nanomolar concentrations of A* AuNPs results in increased noise during the PCR analysis.

variation in the PCR. It is possible that centrifuging the AuNPs at higher speeds than 16,100 x gravity (as used in this experiment) might reduce the variation.

Conclusions

The use of DNA logic, specifically a Boolean NOT operation, offers the potential to reduce the effects of non-specific binding in certain protein detection assays. DNA logic can be utilized in assays such as immuno-PCR where an antigen is detected via a protein interaction, and then the detection is reported via a DNA probe. The logic operation uses the information stored in unique DNA sequences to perform a NOT operation on the DNA prior to the detection being reported. The simplest approach to removing non-specific DNA is to force the DNA from non-specific binding into a double stranded formation, and then remove the dsDNA. Although an enzymatic based NOT operation proved unsuccessful, the principle remains: removing non-specific reporter DNA prior to PCR. Other methods such as physically removing the DNA via centrifugation can result in the desired effect without using enzymes. The use of DNA functionalized AuNPs effectively removed 97% of dsDNA, which in an I-PCR assay would be representative of non-specific binding. If the AuNP removal was optimized, it is possible that even more dsDNA could be removed prior to amplification. However, even reducing the background signal 97% could substantially increase of the sensitivity of an I-PCR based assay.

Bibliography

1. Myrmel, H., Navaratnam, V. and Åsjø, B., "Detection of antibodies to hepatitis C virus: False-negative results in an automated chemiluminescent microparticle immunoassay (ARCHITECT® Anti-HCV) compared to a microparticle enzyme immunoassay (AxSYM HCV Version 3.0)", *J. Clin. Virol.*, 2005, **34**, 211-215.

2. Johnson, Dwight R. and Kaplan, Edward L., "False-Positive Rapid Antigen Detection Test Results: Reduced Specificity in the Absence of Group A Streptococci in the Upper Respiratory Tract", *J. Infect. Dis.*, 2001, **183**, 1135-1137.

3. Saah, A. J. and Hoover, D. R., "Sensitivity and Specificity Reconsidered: The Meaning of These Terms in Analytical and Diagnostic Settings", *Ann. Intern. Med.*, 1997, **126**, 91-94.

4. Adler, M., Wacker, R. and Niemeyer, C. M., "Sensitivity by combination: immuno-PCR and related technologies", *Analyst*, 2008, **133**, 702-718.

5. Barletta, J., "Applications of real-time immuno-polymerase chain reaction (rt-IPCR) for the rapid diagnoses of viral antigens and pathologic proteins", *Mol. Aspects Med.*, 2006, **27**, 224-253.

6. Sims, P. W., Vasser, M., Wong, W. L., Williams, P. M. and Meng, Y. G., "Immunopolymerase Chain Reaction Using Real-Time Polymerase Chain Reaction for Detection", *Anal. Biochem.*, 2000, **281**, 230-232.

7. Adleman, L. M., "Molecular computation of solutions to combinatorial problems", *Science*, 1994, **266**, 1021-1024.

8. Garey, M. R. and Johnson, D. S., *Computers and Intractability: A Guide to the Theory of NP-Completeness*, W. H. Freeman & Co., 1979.

9. Bertossi, A. A., "The edge Hamiltonian path problem is NP-complete", *Inform. Process. Lett.*, 1981, **13**, 157-159.

10. Baumgardner, J., Acker, K., Adefuye, O., Crowley, S., DeLoache, W., Dickson, J., Heard, L., Martens, A., Morton, N., Ritter, M., Shoecraft, A., Treece, J., Unzicker, M., Valencia, A., Waters, M., Campbell, A. M., Heyer, L., Poet, J. and Eckdahl, T., "Solving a Hamiltonian Path Problem with a bacterial computer", *J. Biol. Engin.*, 2009, **3**, 11.

11. Karp, R. M., Miller, R. E. and Thatcher, J. W., in *Complexity of Computer Computations*, Plenum Press, 1972, pp. 85-103.

12. Storhoff, J. J. and Mirkin, C. A., "Programmed Materials Synthesis with DNA", *Chem. Rev.*, 1999, **99**, 1849-1862.

13. Taton, T. A., Mucic, R. C., Mirkin, C. A. and Letsinger, R. L., "The DNA-Mediated Formation of Supramolecular Mono- and Multilayered Nanoparticle Structures", *J. Am. Chem. Soc.*, 2000, **122**, 6305-6306.

14. Mao, C., LaBean, T. H., Reif, J. H. and Seeman, N. C., "Logical computation using algorithmic self-assembly of DNA triple-crossover molecules", *Nature*, 2000, **407**, 493-496.

15. Benenson, Y., Paz-Elizur, T., Adar, R., Keinan, E., Livneh, Z. and Shapiro, E., "Programmable and autonomous computing machine made of biomolecules", *Nature*, 2001, **414**, 430 - 434.

16. Wang, Y., Sun, J., Cui, G., Zhang, X. and Zheng, Y., "Basic Logical Operations Using Algorithmic Self-Assembly of DNA Molecules", *J. Nanoelectron. Optoe.*, **5**, 30-37.

17. Fang, Y., Xu, Y. and He, P., "DNA Biosensors Based on Metal Nanoparticles", *J. Biomed. Nanotechnol.*, 2005, **1**, 276-285.

18. Mascini, M., Palchetti, I. and Marrazza, G., "DNA electrochemical biosensors", *Fresenius J. Anal. Chem.*, 2001, **369**, 15-22.

19. Zhai, J., Cui, H. and Yang, R., "DNA based biosensors", *Biotechnol. Adv.*, 1997, **15**, 43-58.

20. Yan, H., Park, S. H., Finkelstein, G., Reif, J. H. and LaBean, T. H., "DNA-Templated Self-Assembly of Protein Arrays and Highly Conductive Nanowires", *Science*, 2003, **301**, 1882-1884.

21. Fredriksson, S., Gullberg, M., Jarvius, J., Olsson, C., Pietras, K., Gústafsdóttir, S. M., Östman, A. and Landegren, U., "Protein detection using proximity-dependent DNA ligation assays", *Nat. Biotechnol.*, 2002, **20**, 473-477.

22. Gullberg, M., Gustafsdottir, S. M., Schallmeiner, E., Jarvius, J., Bjarnegard, M., Betsholtz, C., Landegren, U. and Fredriksson, S., "Cytokine detection by antibody-based proximity ligation", *Proc. Natl. Acad. Sci.*, 2004, **101**, 8420-8424.

23. Gullberg, M., Fredriksson, S., Taussig, M., Jarvius, J., Gustafsdottir, S. and Landegren, U., "A sense of closeness: protein detection by proximity ligation", *Curr. Opin. Biotechnol.*, 2003, **14**, 82-86.

24. Yasubumi, S., "DNA-based algorithms for learning Boolean formulae", *Nat. Comput.*, 2003, **2**, 153-171.

25. Green, L. S., Jellinek, D., Jenison, R., Ostman, A., Heldin, C.-H. and Janjic, N., "Inhibitory DNA Ligands to Platelet-Derived Growth Factor B-Chain", *Biochemistry*, 1996, **35**, 14413-14424.

26. Rossi, R., Montecucco, A., Ciarrocchi, G. and Biamonti, G., "Functional characterization of the T4 DNA ligase: a new insight into the mechanism of action", *Nucl. Acids Res.*, 1997, **25**, 2106-2113.

27. Adler, M., Wacker, R. and Niemeyer, C. M., "A real-time immuno-PCR assay for routine ultrasensitive quantification of proteins", *Biochem. Biophys. Res. Commun.*, 2003, **308**, 240-250.

28. Adler, M. and Gregory, S. M., in *Advances in Clinical Chemistry*, Elsevier, 2005, vol. Volume 39, pp. 239-292.